UNIVERSITÀ DEGLI STUDI DI CATANIA

Dipartimento di Scienze Biologiche, Geologiche e Ambientali
Sezione Scienze della Terra

DOTTORATO DI RICERCA IN GEODINAMICA E SISMOTETTONICA

XXV CICLO

SEISMIC CHACTERIZATION OF VULCANO ISLAND AND AEOLIAN AREA BY TECTONIC AND SEISMO-VOLCANIC EVENTS

Dott. Vincenzo Milluzzo

Coordinatore
Prof. Carmelo Monaco

Tutor

Prof. Stefano Gresta

Co-tutor

Dott. Salvatore Alparone
Dott. Salvatore Gambino

DICEMBRE 2012

Al piccolo grande Fisico

Contents

Chapter 1

Introduction, key aims and organization of the thesis

Volcanic unrest is often recorded as variations in a number of physical parameters. Different geophysical techniques are used to monitor these parameters (seismology, deformation analyses, remote sensing, electromagnetic studies, gravimetry, infrasound analyses, etc…). The seismology gives useful information about the location of magma bodies/hydrothermal fluids in depth, their dynamics and composition and the plumbing system geometry (e.g. Kumagai and Chouet, 1999; Chouet et al., 2003; Patanè et al., 2006). Moreover, most of the volcanic eruptions have been preceded by an increase in earthquake activity beneath or near the volcano (McNutt, 1996).

The multi-disciplinary approaches are proven to be the best way to improve our knowledge about volcano dynamics. However, monitoring active volcanoes to

forecast major eruption still remains a serious problem. In fact, although measurable changes in geophysical and geochemical data are observed at many volcanoes before eruptions, no unique simple laws of prediction can be determined.

Volcanic seismology is the branch of seismology in which the seismological techniques are applied to understand the physical conditions and dynamic status of volcanic systems. For many years it was the principal instrument to observe both the active and quiescent volcanoes. The main goal of volcanic seismology is the identification of variations in volcanic activity by observation of changes in behaviour of seismic parameters, in order to predict eruptions or, in the event of eruptions in progress, the evolution of these for short and medium term (Neuberg et al., 2006). The volcanic seismology has developed strongly over the past 10-15 years, by using sophisticated broadband seismic equipment and application of new techniques of observation and analysis (Kawakatsu et al., 2000).

Active volcanoes are source of a great variety of seismic signals. Traditionally, seismo-volcanic signals have been classified into five different types: high-frequency (HF) also called volcano-tectonic (VT); low-frequency (LF) earthquakes also called long period (LP); volcanic tremor; hybrid events and volcanic explosions also called explosion-quakes (e.g. Minakami, 1974; Lahr et al., 1994; McNutt, 1996; Zobin, 2003; Ibanez et al., 2003).

Based on this premise, the aim of this thesis is twofold: 1) to analyze the seismo-volcanic events of Vulcano, defined as seismic events linked to the dynamics of the shallow hydrothermal system (Alparone et al., 2010); 2) to study the tectonic earthquakes, linked to the main structures of the Aeolian area, in order to better understand the seismogenic characteristics of the area. The two categories of events will be analyzed at first separately and only in the final phase of the project will look for a relationship between them and the volcanic activity at Vulcano.

The island of Vulcano is part of the Aeolian archipelago located in the southern Tyrrhenian basin. After the last eruption in 1888-1890 **(fig. 1.1)**, the only

activity on the island is associated with hydrothermal systems and the fumaroles of La Fossa area, where seismo-volcanic events originates.

Fig. 1.1 Representation of the eruption of 1888-1890, taken from: "The eruptions of Vulcano" by O. Silvestri, 1891.

In the first part of the thesis we report the results of the study on seismo-volcanic events that characterize the area of La Fossa of Vulcano. This particular type of earthquakes, with very local character due to low energy associated, shows different morphological and spectral characteristics compared to the tectonic events recorded on the same island, which will be analyzed in the second part of the thesis.

The microseismicity of Vulcano involved since the 60s a number of researchers, some of which have provided an interpretation of the mechanism of genesis of these events, based mainly on the study of the waveforms.

The results achieved by these authors can be summarized as:

Latter (1971)

- √ There are "Unusually perfect sinusoidal tremors" and events with a strong affinity to small tectonic shock;

- √ The first impulse is followed by a train of sine waves showing no dispersion;
- √ The magnitude of these event is negative;
- √ The source is a mechanism of resonance, probably caused by gaseous explosions in cavity above the magma chamber;

Blot (1971)

- √ The events show regular wave train after the arrival of the first phase;
- √ Sometimes two phases are distinguishable: Rayleigh and S;
- √ We propose a classification based on the frequency content of seismic events: 1st class = 20 Hz, 2nd class = 13 ± 3 Hz, 3 rd class = 8 Hz;
- √ The events are interpreted as an explosion inside a resonant tube below the crater between 500 and 1000 m depth;

Del Pezzo (1981, 1983)

- √ The seismicity presents: a dominant low-frequency (2 Hz), the absence of clear phases in the seismogram and a marked monochromaticity;
- √ The source mechanism probably related to degassing;
- √ From a classification based on both the frequency content that the hypocentral depth can be distinguished: high-frequency shallow events and low frequency deep events;

Neri (1981)

- √ There are "Volcanic-tectonic" and "Volcanic" events;
- √ Those volcanic show a very smooth swing and suggest a mechanism of resonance in a cavity;

Falsaperla e Neri (1986)

- √ The microseismicity is associated with both degassing and fracturing phenomena;

Luongo e Vulcano (1989)

- √ The shallow seismicity of La Fossa is explained by "wave tube" generated by explosive sources in columns of fluids;

Godano e Vilardo (1991)

- √ The events are generated by excess pressure in the fracture filled by magmatic fluids;

Bottari et al. (1992)

- √ There are two classes of events: high frequency with a first arrival pulse and a clear S phase; low-frequency monochromatic events, very shallow and located on the main fumarolic fields;

Montalto (1994, 1996)

- √ There are two main categories M-shocks and N-shocks events, respectively monochromatic events related to a mechanism of resonance and N-type events "not monochromatic" related to mechanisms of hydrothermal alteration of material;

The proposed classifications and interpretations on the genesis of seismo-volcanic events of Vulcano, confirmed that the island's volcanic system is complex and time-varying. Although most authors interpret microseismicity of La Fossa generated by processes such as degassing or micro fracture, but the apparent lack of a model does not allow to give a robust interpretation.

In this thesis, a detailed analysis was conducted on the waveforms and frequency content of seven thousand of seismo-volcanic events recorded from January 2004 to December 2009. Based on the results obtained, in the **chapter 4** we propose a new classification of local seismic events of Vulcano, which did not presume to replace the previous ones, but that simply identifies in detail the most recent seismicity. This classification is also reflected by the results of a detailed analysis of cross-correlation.

We investigated also the relationship between volcano-seismic events, recorded at La Fossa crater of Vulcano during 2004-2009, and the dynamics of the

hydrothermal system. Thanks to the use of powerful tools such as time-frequency analysis of Fourier and Wavelet, we analyze the temporal variations of the frequency content of seismic events, in order to have more information about the properties, evolution and current status of the volcanic island.

In detail, **chapter 4** regards the time variations of long period events occurring in the time period 2004-2009 at Vulcano and **chapter 5** regards the analysis and the time variation of the tornillos events occurring in the same period at Vulcano island. We decided to better analyze this two classes of seismo-volcanic events because the long period events have increased in number during the first three years analyzed while the tornillos events have increased in number during the last years analyzed. In fact while only 15 tornillos were recorded during 2004–2006, one thousand of tornillos occurred in 2007–2009 time period. So we chose to study in detail this two class of events (LP and TR) to better characterize the whole studied period and with the aim of investigating their source mechanism and their relationship with hydrothermal activity.

In **chapter 6** we compared different geophysical and geochemical data sets and the time relations among the different time series are discussed. The objective of this phase of the project was the quantitative study on the relationship between the time series of temperature (both on the ground that the fumaroles), earthquakes (near the island of Vulcano), CO_2 dataset and seismo-volcanic events. At the end of this part of the thesis, based on the results obtained on the analysis of the seismo-volcanic events and on their features, we can infer that such events at Vulcano are related to two different source mechanisms: (1) fracturing processes of rocks and (2) resonance of cracks (or conduits) filled with hydrothermal fluid.

After careful analysis of the seismo-volcanic events of the Aeolian area, in the **chapter 7** the attention was paid to the tectonic events, in order to find possible relationships with the volcanic activity in the area. The aim of this part of the thesis is to identify spatial clusters of earthquakes, locate active seismogenic zone and their relationships with the volcanic activity in the Aeolian Archipelago.

To recognize possible spatial clusters and identify active seismogenic zones and structures in the Aeolian Archipelago, in the south of Italy, we analyzed the spatial pattern of seismicity between 1993 and 2010 in a selected area comprising Vulcano, Lipari, Salina and Filicudi and calculated 22 fault plane solutions (FPSs) for shocks with magnitude greater than 2.7. First, we computed a 1-D velocity model for this area including information from recorded earthquakes by a joint hypocenter-velocity inversion (Kissling et al., 1994). Successively, we applied the double-difference approach of Waldhauser and Ellsworth (2000), finding that a certain part of the scattered epicenter locations collapse in roughly linear features.

A detailed discussion is focused on a seismogenic structure, NE–SW oriented, 3–8 km deep, located in the northern area of Vulcano island. This recognized element could represent a link between magma accumulation zones, thus representing a possible preferential pathway along which magma may intrude.

In the **chapter 8** we tried to summarize the obtained results and we proposed a new interpretative model on the genesis of the seismo-volcanic events, their time variation and the tectonic activity of the Aeolian area.

This work can provide useful suggestions for not only the results, but because it goes to pay attention on a volcanic system, whose activity in the last two decades has increased significantly, showing signs of a potential reactivation.

This is evidenced by the numerous crises characterized by large variations in temperature, chemical and isotopic composition of fumarolic fluids and thermal waters (Chiodini et al., 1992; Montalto, 1996).

Chapter 2

Geological and structural overview of the Aeolian islands

The presence of both constant seismic activity and active volcanism in Aeolian Arc is the evidence that this area is characterized by high geodynamic activity. Several authors have suggested various models on the origin and evolution of the Tyrrhenian Basin:

- √ The first proposed models are based on the mechanism of oceanization (Van Bemmelen, 1969; Morelli, 1970; Selli e Fabbri, 1971) or on the expansion mechanism. On the base of this mechanism, the retroarch expansion generates the Tyrrhenian Basin as a marginal basin (Barberi et al., 1973; Boccaletti et al., 1976);
- √ Other hypotheses suggest that the opening of the western Mediterranean basin and the origin of the Tyrrhenian Sea during the Late Miocene, are due to a "split" between Alps and the Apennines orogenesis, followed by creation of new lithosphere. In this model, the "split" is accompanied by

a counterclockwise rotation of the Italian peninsula, with a consequent compression of the central region and a strong distortion of the Calabro-Peloritano Arc *(Scandone, 1979; Gasparini et al., 1982);*

- √ A model of Mantovani et al. (1982) proposed that the structural evolution of central and western basins of the Mediterranean and of the Calabro-Peloritano Arc, have been determined by a left lateral collision between Europe and Africa and by a counterclockwise rotation of the Adriatic plate;
- √ A migration process of backarc is assumed by *Malinverno and Ryan (1986);*
- √ *Locardi (1988)* correlates the genesis of the Tyrrhenian Sea with the development and growth of a diapiric mantle structure;
- √ *Patacca et al. (1990)* associate the formation of the Tyrrhenian Sea with a passive subduction of the Ionian lithospheric slab;
- √ Another model suggests instead a mechanism of passive ascent of the mantle due to post-collisional phase of the plates *(Ventura et al., 1999).*

What seems certain is that the Tyrrhenian Basin was located in a series of blocks parallel to the margin of the basin, in accordance with the Apennines trend. However all authors seem to agree in assuming a general process of opening with kinematics in southeast direction **(fig. 2.1)**.

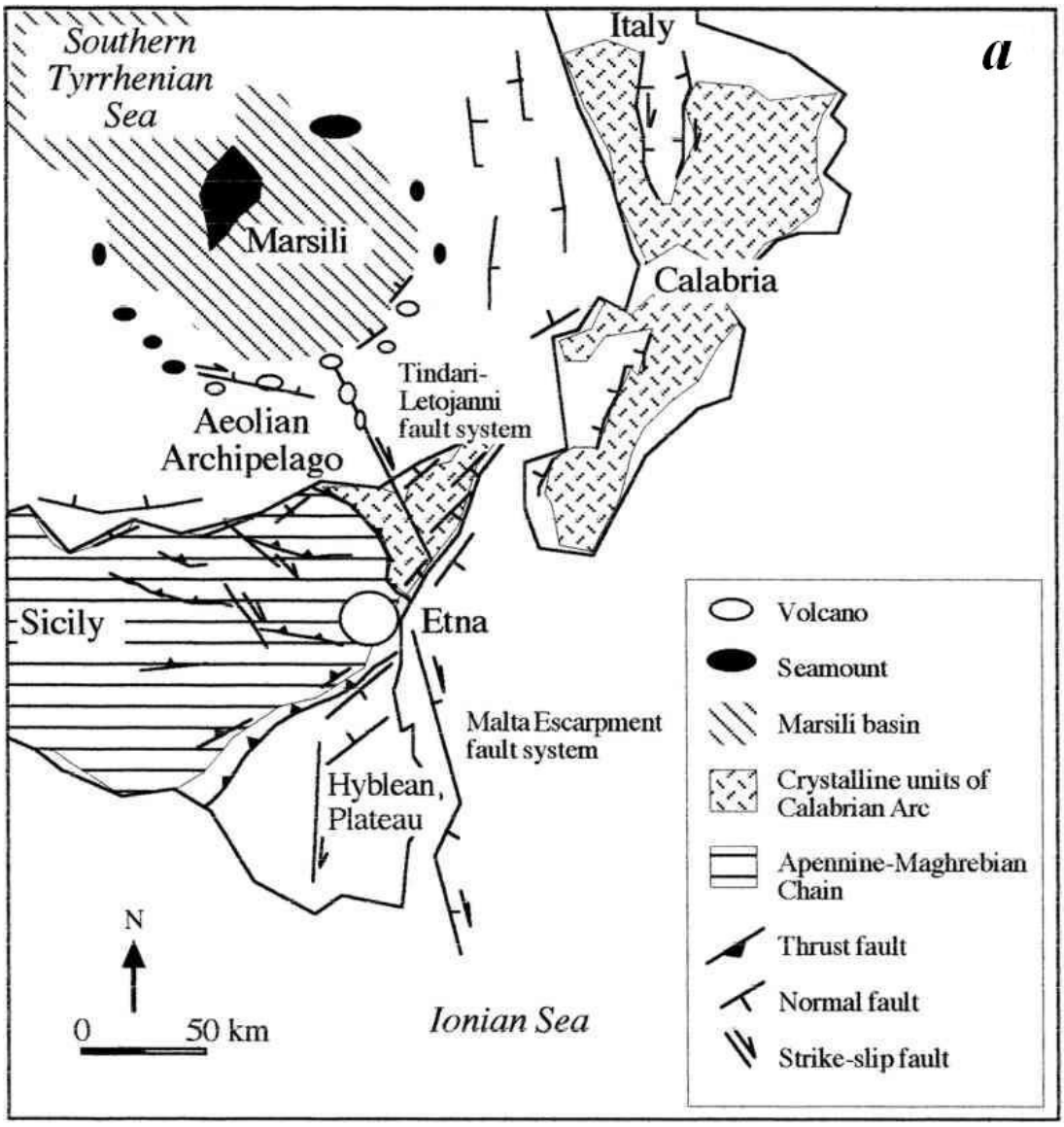

Fig. 2.1: Structural scheme of the south-tyrrhenian Basin (Ventura et al., 1999)

In the Aeolian area are present several variations in the direction of the fault systems: in fact the faults show a NS trend in northern Calabria, a NE-SW trend in the southern Calabria and EW in northern Sicily (Ghisetti e Vezzani, 1981).
A relocation of deep earthquakes in this area and some studies based mainly on the focal mechanisms of shallow and deep earthquakes, led Gasparini et al. (1982) to hypothesize a Benioff spoon-shaped plan, laterally extended from the Gulf of Naples to Ustica island, which reaches a depth of 500 km.
In south-eastern margin of the Tyrrhenian Sea, a few tens of kilometres from the northern coast of Sicily, in addition to the numerous seamounts, we find the volcanic arc of the Aeolian Islands. The archipelago consists of seven islands surrounded by several rocks, among which that of Basiluzzo. Five of these islands: Alicudi, Filicudi, Salina, Panarea and Stromboli form a ring structure that extends for 80 km with N-NW concavity, while the other two: Lipari (the largest with its 37.3 km^2) and Vulcano (the southernmost island of the archipelago is just 22 km from the shores of Capo Milazzo), are located along a NW-SE trend that obliquely intersects the arc just near the island of Salina. The archipelago is made up of volcanic islands whose complex morphology can be explained, in addition to the eruptive activity, with the action of sea and tectonic activity. The three islands still volcanically active are: Stromboli, with a persistent eruptive activity, Vulcano, famous for its numerous explosive eruptions in historical times, the last of which dates from 1888-1890, and Lipari, whose last eruption is dated about 1400 years before Christ. The Aeolian volcanism highlights a wide compositional range consists of calcalin, shoshonitic and potassic alkaline products, it also notes that moving counterclockwise from NW to SE along the arc, the corresponded volcanic activity is progressively younger (Barberi et al. , 1973; Keller, 1980).
The Aeolian Islands are located thus in a region of low crustal thickness: according to Morelli et al. (1975) the thickness varies from 18 to 25 km, but the Moho becomes deeper probably reaching the 35 km southward under Peloritani and eastward in Calabria.

From a structural standpoint, the area of the north-eastern Sicily shows a "tectonic alignment" that connects the Aeolian islands with the Maltese-Ibleo escarpment, NNW-SSE oriented and with right movements (Barbano et al., 1979). In particular we highlighted major dislocations with a lithospheric character like "Aeolian-Tindari-Giardini", capable of influencing in a decisive way the seismic activity in the area and to play a key role in the development of the volcanic structures **(see chapter 7)** (Barbano et al. , 1979; Ghisetti and Vezzani, 1981, Frazier et al., 1982). Another structure with WNW-ESE direction, is located in the western sector, near the seamount of Sisifo and affects Alicudi and the area near Vulcano Island **(fig. 2.2).**

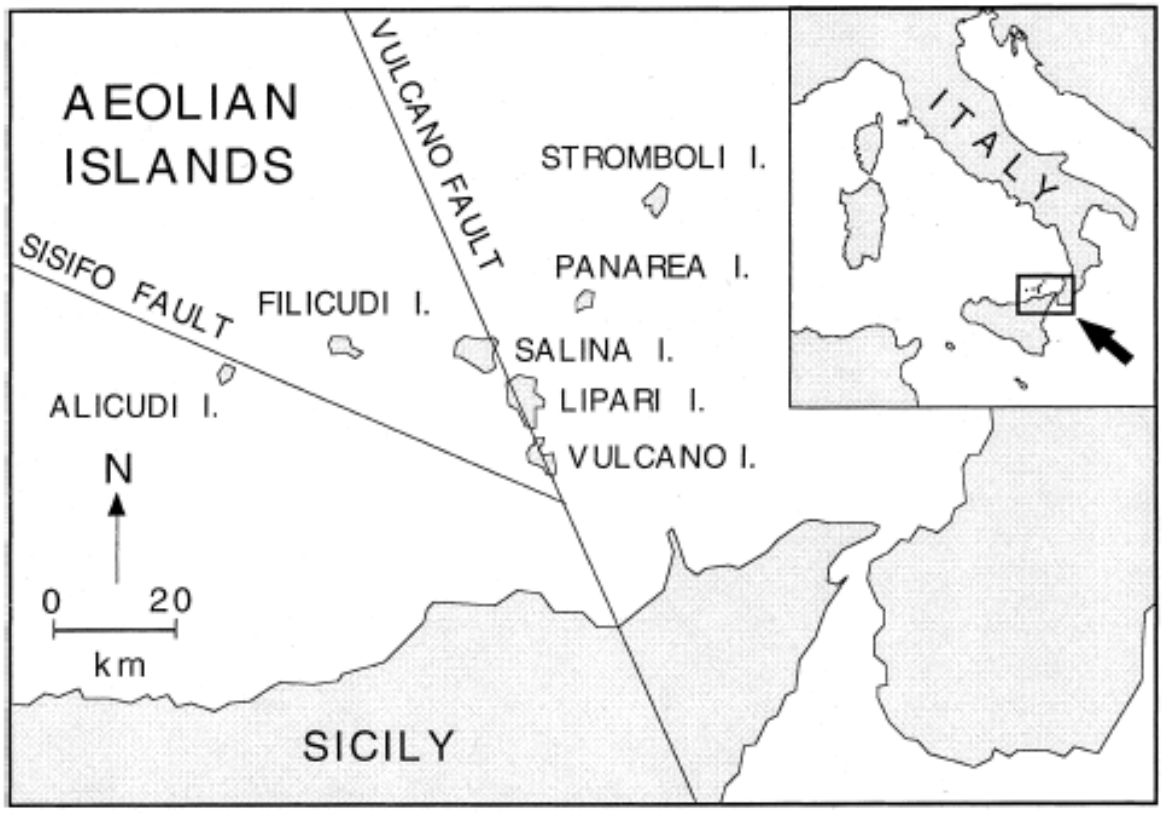

Fig. 2.2: Aeolian archipelago with the two main structures in the area: Vulcano (Aeolian-Tindari-Giardini) and Sisifo fault (Bolognesi, 1999).

In the region of the Aeolian islands, the release of seismic energy presents variability in seismic styles **(fig. 2.3; 2.4)**. In the Gulf of Patti, for example, are recorded sequences like "mainshock-aftershock"; near to Vulcano there is a clear dominance of seismic swarms; while to the west of Lipari and Vulcano coexist the two different phenomena with modest release of energy. On the basis of tectonic structures that are activated, the recorded seismic events in the Aeolian area are divided into two classes:

I. In a first class “local seismicity" are grouped the shocks generated by local structures. The small magnitude values that distinguish this class could be due to the presence of active volcanism that would not allow the accumulation of very high stress and the subsequent release of large amounts of energy (Del Pezzo and Martini, 1981);

II. Belong instead to the second class "regional seismicity” mainly the tectonic earthquakes related to tectonic phenomena and generally characterized by values greater than magnitude 2.5 (Falsaperla and Blacks, 1986). The most energetic seismic event, belonging to this class, in recent decades, it is certainly the earthquake of April 15, 1978, with magnitude 5.5. This event, located in the Gulf of Patti, was followed by a sequence of “aftershocks”, characteristic of areas with homogeneous medium where the stresses are concentrated in the space.

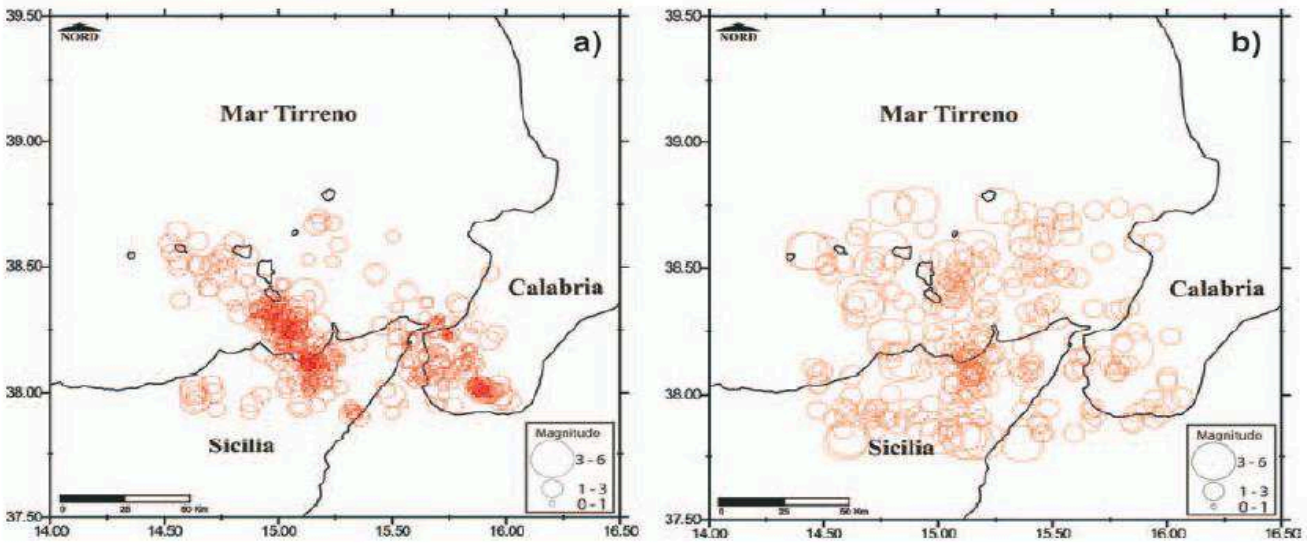

Fig. 2.3: Seismicity recorded by INGV from: (a) 1978 to 2000; (b) from 2001 to 2003 *(Mattia et al., 2006).*

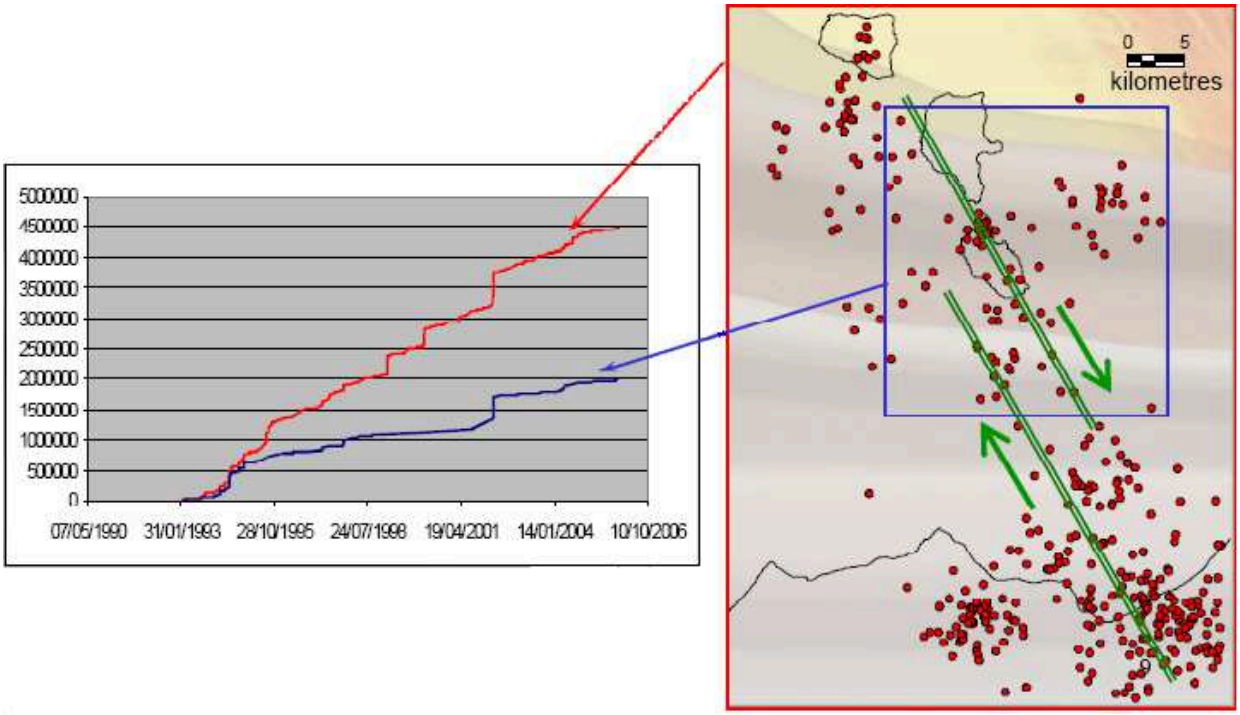

Fig. 2.4: Seismicity recorded in the Tyrrhenian Basin (inset in red) by INGV in the period 1993 to 2006, compared with the seismicity recorded in area of Lipari-Vulcano (inset in blue) at the same time interval *(Puglisi et al. 2007).*

The Aeolian area compared to neighbouring seismically active areas, presents different geological and seismotectonic features. The Etna region, located about 100 km south of the Aeolian Islands, is characterized by a basaltic volcanism and earthquakes with moderate magnitude; the Strait of Messina, on the eastern edge of the arc of islands, can be described as graben structure (Bottari et al., 1992) characterized by earthquakes with low frequency of occurrence and high magnitude, as witnessed by the strong magnitude 7.2 event of 1908 that devastated the city of Messina.

The earthquake of Messina is one of the most devastating events that have affected the Italian territory in the last centuries. All authors agree that the focal mechanism was of normal type, however there is no convergence of views regarding the determination of the position and geometry of the tectonic structure that generated the aforementioned earthquake (Bottari et al., 1986; Valensise and Pantosti, 1992).

Chapter 3

Vulcano island: geological e structural framework

Vulcano is the southernmost of the Aeolian Islands, a volcanic arc lying on the south eastern side of the Tyrrhenian Sea in the south of Italy. The island of Vulcano, has been known since the ancient ages for its intense volcanic activity. In antiquity the island was sacred to Hephaestus, the god of volcanoes and endogenous forces of nature and was known as Hiera (the sacred) or Hierà Ephaestus (the island sacred to Hephaestus). The entire island has an area of 22 Km^2 and has an irregular shape, roughly similar to a parallelogram elongated NW-SE direction with an appendix in the northern part constituted by of Vulcanello. At Vulcano, we can distinguish three zones with different characteristics (**fig. 3.1**). A great mass formed by the SE Old Vulcano (Caldera del Piano), a middle part consisting of the current cone of La Fossa and the

northern extreme part of Vulcanello consisting of circular shape with a diameter of 1300 meters.

From the geological point of view **(fig. 3.2)**: *Old Vulcano* is formed by a crater of few kilometers in diameter, which forms the southern frame of the island. It is characterized by an alternation of pyroclastic scoria and basaltic lava flows associated with sandy pyroclastite that have given rise to a Strombolian cone type with a height, from mean sea level, of about 1000 meters (Frazier and La Volpe, 1987; Gioncada et al., 2003). The truncated cone has a very large bottom base; radiometric surveys have determined for this old crater, an age of just over 100,000 years (Frazier and La Volpe, 1987). Subsequently the island's volcanic activity has migrated northward and the old cone, remained inactive, it has been partially filled by effusive material and / or exploded during subsequent eruptions. The second main part of the island is formed by the current volcano of *La Fossa,* in the northern-central part of the island. La Fossa consists of a cone of 390 meters above sea level surrounded by the remains of the previous cones, and has a base diameter of 2 km. The present cone of La Fossa, always subaerial, was born on a basaltic lava flow of the old volcano and is made up mainly of ash and lapillus compacted together. Here, there is intense fumarolic activity that defines an ideal alignment from south to north that joins the main crater of the current volcano to Vulcanello fumarols. *Vulcanello* has nearly perfect conical shape and stands 123 meters above sea level. Originally, it was more detached from the island, but in 1550, the date on which dates the last eruptive period of Vulcanello, it was joined by an isthmus formed by volcanic ash erupted from Vulcanello itself or the cone of La Fossa.

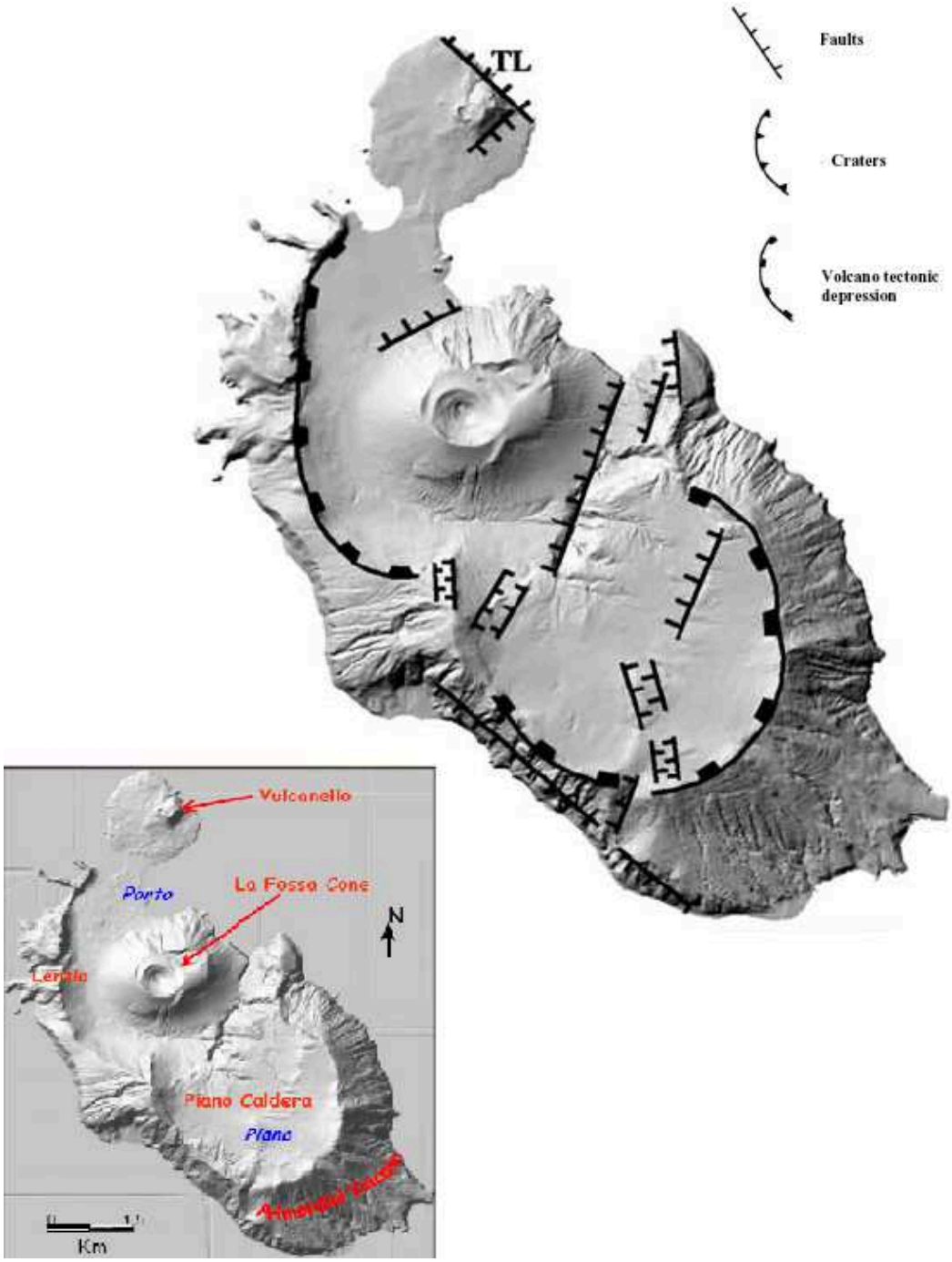

Figure 3.1: Structural map of Vulcano island, showing the shallow evidence of the "Aeolian-Tindari-Giardini" structures (Gioncada et al., 2003).

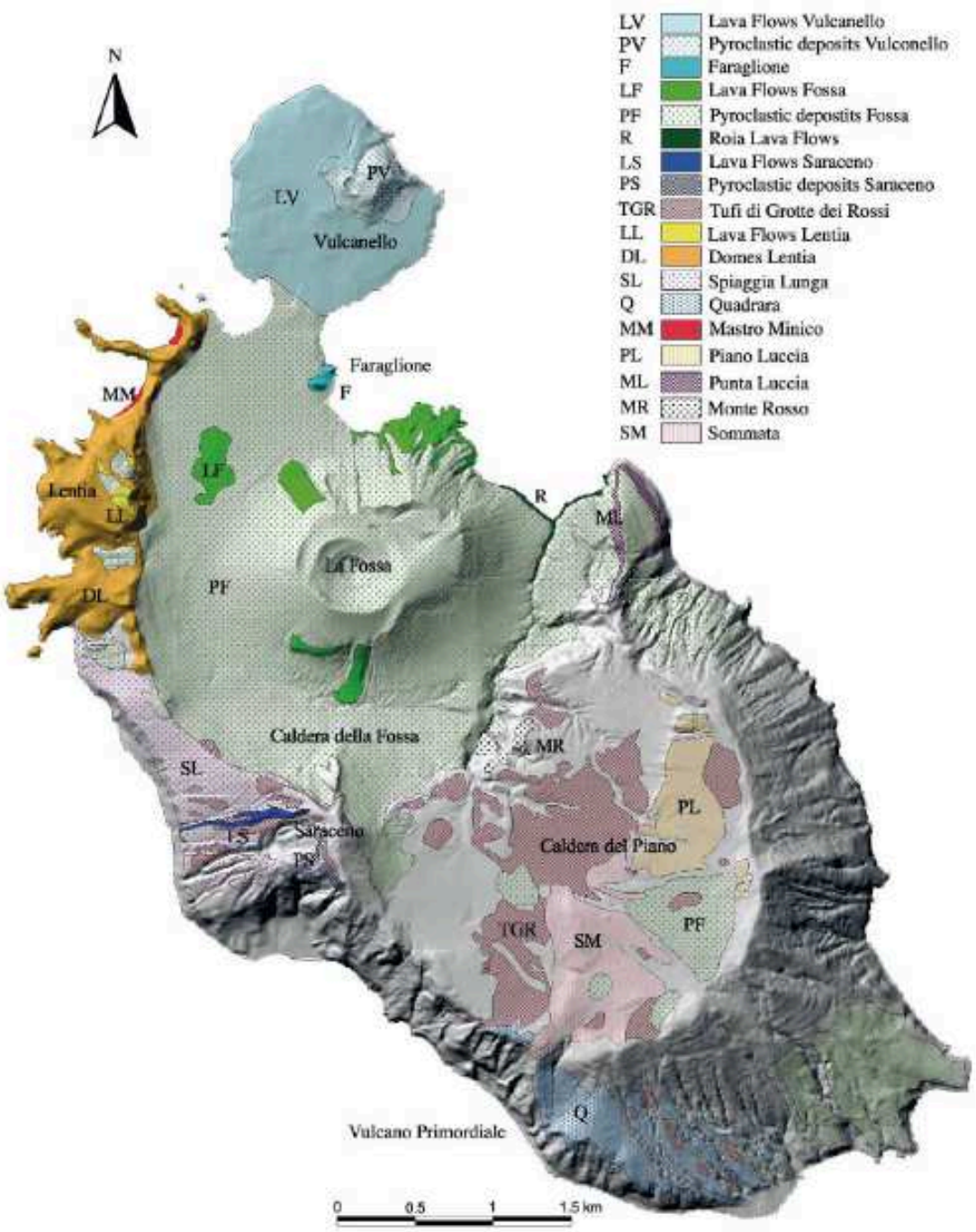

Figure 3.2: Schematic geological superimposed an image of the island of Vulcano (DEM Gioncada et al., 2003).

A structural study of the Vulcano island conducted by Ventura (1994) has identified two main systems of strike slip faults oriented NW-SE along the north-eastern and south-western coasts. These structures seem to be the shallow expressions of major regional crustal structures and are accompanied by a series of normal faults with NE-SW and NS trend. The geometric relationships between the different fault systems, as well as the presence of two calderas within the island, would consist according to Ventura (1994) with the structural association observed in pull-apart basins **(fig. 3.3)**.

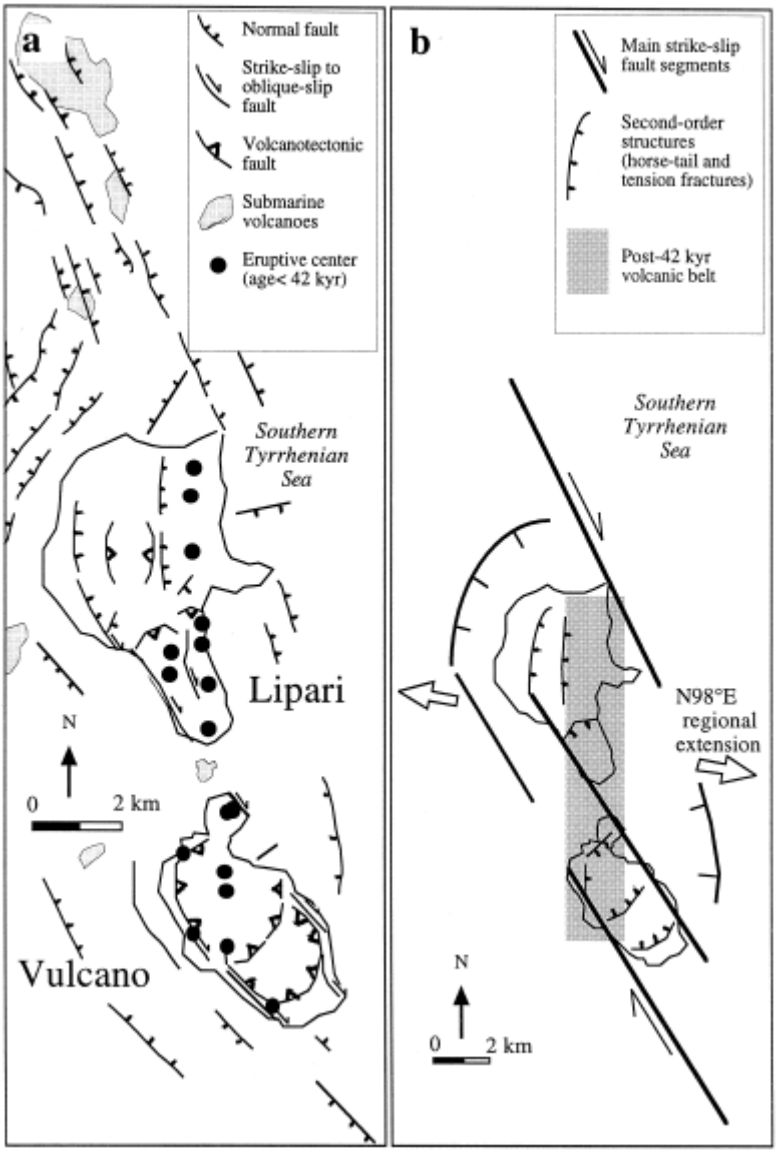

Figure 3.3: (a) Structural map of Lipari and Vulcano, and sector of surrounding sea; (b) structural model of Lipari and Vulcano: pull-apart basin (Ventura, 1994).

Vulcano has been active in the last few centuries, erupting calc-alkaline and shoshonitic products (Barberi et al., 1974) and showing an explosive nature with frequent transitions from phreato-magmatic to magmatic activity (Mercalli and Silvestri, 1890; Barberi et al., 1988). A magmatic body was identified at a depth of 2-3 km below La Fossa crater by geophysical and geochemical studies (Ferrucci et al., 1991; Clocchiatti et al., 1994; Nuccio and Paonita, 2001). Researchers also agree on the presence of an hydrothermal system below the La Fossa cone (Chiodini et al., 1993 and 1995; Nuccio et al., 1999; Paonita et al., 2002), whose thermodynamic conditions (temperature, pressure and composition) can show large temporal variations (Di Liberto et al., 2002). Since the last eruption in 1888-1890, volcanic activity produces fumarolic emissions varying in intensity and temperature over time. The fumaroles are mainly concentrated at La Fossa crater **(fig. 3.1)**, where the fumarole fields, as well as the steam heated areas, have significantly expanded in the last 20 years (Bukumirovic et al., 1997; Boyce et al., 2007). Based on geochemical studies (Chiodini et al., 1993; Nuccio et al., 1999), the fumarolic emissions of La Fossa crater are fed by fluids coming from both the magmatic and the hydrothermal system.

Apart from regional earthquakes, recognizable by the high duration (60-150 s) and difference S-P variable from 3 to 16 s, the seismic activity recorded at Vulcano is distinguishable in two main categories **(fig. 3.4**):

I. *"Volcano-tectonic"(VT)* events for brittle fracturing. Similar to the VT earthquakes defined in other classifications (e.g. Wassermann, 2009), they are originated by shear failure caused by stress buildup and resulting in slip on a fault plane.
II. *"Seismo-volcanic"* events associated with the fluid dynamics in the conducts of fumarolic field, which constitute the background microseismicity almost constantly recorded on the island (Latter, 1981; Montalto, 1994)**;**

The *"volcano-tectonic"* earthquakes with local nature show these main features:

√ evident P-S phases;

- √ hypocentral depth usually <4.5 km;
- √ magnitude on average <2.5;
- √ polychromatic nature with high content of high frequency (10-25 Hz);
- √ duration of 10-80 seconds;
- √ first impulsive arrival;
- √ low variability of the signal to the various stations;
- √ higher energy values compared to "volcanic" events ;
- √ they can occur in seismic swarms;

Several studies have also confirmed that the occurrence of these events can lead to changes:

- √ on the chemical composition of the fumaroles (Chiodini et al., 1992);
- √ on the heat flow (Barberi et al., 1991; Alparone and Aubert, 2000);
- √ on the phases of ground deformation (Falsaperla et al., 1989, Barberi et al., 1991);

Considering instead the *"seismo-volcanic"* earthquakes it is clear that are characterized by:

- √ absence of P or S phases clearly identifiable (elliptic-circular particle motion);
- √ hypocentral depth less than 2 km;
- √ average duration of 20 s.;
- √ magnitude usually <1.5 (even negative);
- √ amplitudes 10^{-6}-10^{-5} m/s (Luongo et al., 1989);
- √ diffuse monochromaticy (typical of events related to fluid dynamics);
- √ low detection at the stations: are mainly detected at "Vulcano crater" station (IVCR) on the northern slopes of the volcano;
- √ high heterogeneity of the waveforms;

The events belonging to this second category represent a quantitatively important percentage and provide useful information on the mechanisms of earthquake generation connected to the fluid dynamics inside the volcano.

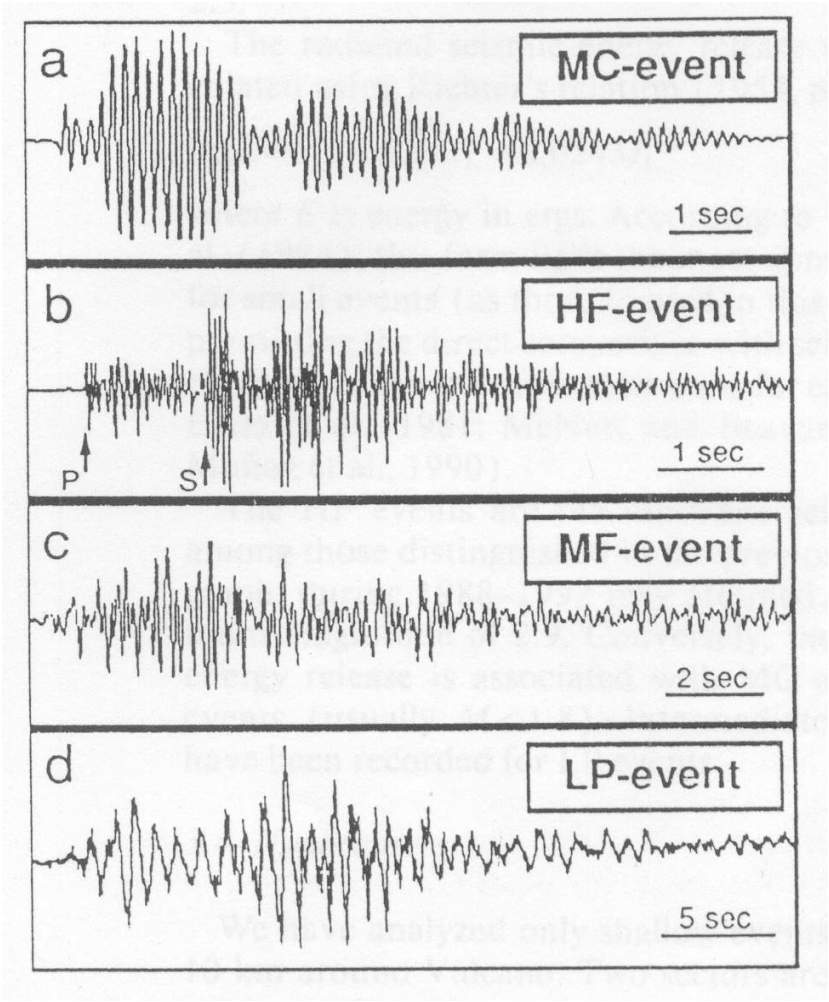

Figure 3.4: Typical examples of waveforms of events: *"seismo-volcanic"* a) c) d); *"volcano-tectonic"* b), recorded at the station of Vulcano Cratere "IVCR" (Montalto, 1994).

Increases in the temperatures of the fumaroles and changes in the chemical composition of their emissions (mainly an increase in the CO_2 flux and concentration), called temperature and geochemical anomalies, respectively, occur at the same time as the number of seismo-volcanic events increases at La Fossa of Vulcano **(fig. 3.5)** (Alparone et al., 2010; Aubert et al., 2008; Granieri et al., 2006; Inguaggiato et al., 2008). The most recent anomalies were observed in the period 2004-2009. There is broad agreement among researchers about the fact that both seismic and geochemical anomalies are related to increased inputs of magmatic fluids into the fumarolic system, whereas their relationship to unrest processes leading up to eruptions is still being debated (Barberi et al., 1991; Italiano and Nuccio, 1992; Bukumirovic et al., 1997; Granieri et al., 2006; Nuccio et al., 1999; Nuccio and Paonita, 2001).

Figure 3.5: Photos of "La Fossa"crater in the north of Vulcano island, in the background it can see Lipari and Salina: the other two islands in the Aeolian archipelago.

Chapter 4

Time-space variation of volcano-seismic events at La Fossa of Vulcano

4.1 Introduction

Three distinct areas can be recognised at Vulcano: the southern area, called Caldera del Piano, the central area, known as La Fossa crater, and Vulcanello, located in the northernmost part of the island **(fig. 4.1)**. A magmatic body was identified by geophysical and geochemical studies at a depth of about 2–3 km below La Fossa crater (Ferrucci et al. 1991; Clocchiatti et al. 1994; Nuccio and Paonita 2001).

Since the last eruption in 1888-1890, volcanic activity has been characterised by fumarolic emanations of variable intensity and temperature, mainly concentrated at La Fossa crater.

According to the chemical and isotopic signatures, the fumarolic fluids have been interpreted as a mixture of two components whose proportions vary with time: (1) a magmatic component, which is deep and released from a magma body; (2) a hydrothermal component which is shallower and formed by the

evaporation of fluids of marine origin entering the zone near the conduits where deep hot fluids rise (Chiodini et al. 1995; Granieri et al. 2006). In particular, the magmatic component is richer in CO_2, N_2 and He than H_2O (Chiodini et al. 1995). The development of the fumarolic field and the hydrothermal areas has significantly expanded in the last 20 years (Boyce et al. 2007).

The fumarolic fields are currently sited in different areas, as shown in **fig. 4.1**. Temperature increases and changes in the fumarolic gases chemistry, mainly consisting of an increase in CO_2 and He flux, were observed in 1979-1981, 1985, 1996, 2004, 2005, 2006, 2007, 2008 and 2009. Such changes, mainly geochemical and geothermal anomalies, have been interpreted as an increase in the concentration of the magmatic component of the fumarolic fluid (Granieri et al. 2006). However, it is still uncertain whether these anomalies could lead to eruptions (Barberi et al. 1991; Italiano and Nuccio 1992; Bukumirovic et al. 1997; Granieri et al. 2006).

These geochemical and geothermal anomalies are often accompanied by increases in seismic energy release. However, few seismological studies have been performed at Vulcano (e.g. Blot 1971; Latter 1971; Del Pezzo and Martini 1981; Falsaperla and Neri 1986; Montalto 1994a, b). Seismic activity originating in the area of Vulcano is associated with double-couple sources and fluid dynamics that generate earthquakes and volcano-seismic events, respectively. Double-couple sources are related to the activity of tectonic structures; they typically occur in swarm-like sequences of low magnitude (generally, $M \leq 2.5$), and show clear P and S phases. Generally, they are clearly recorded at all the stations of the Aeolian seismic network. Conversely, the volcano-seismic events are related to fluid dynamics within the hydrothermal system at shallow depth, are characterised by poorly defined P and S phases and can only be detected in very narrow areas (Aubert and Alparone 2000). The main features of the volcano-seismic events at Vulcano, as well as their source mechanisms, are still not well known. Montalto (1994a) invokes two different processes for the volcano-seismic events: brittle fracturing of hydrothermally altered materials and resonance of the plumbing system. The first process gives

rise to the socalled N-shocks, characterised by broad-band spectra, the second to the so-called M-shocks, showing a monochromatic spectral content (Montalto 1994a).

The aim of this work is the study of the volcano-seismic events occurring at Vulcano during 2004-2009, in order to identify events with similar features and infer their source mechanisms. In addition, we analyse the time variation (if any) of the seismic events, which may provide information on the evolution of the hydrothermal system.

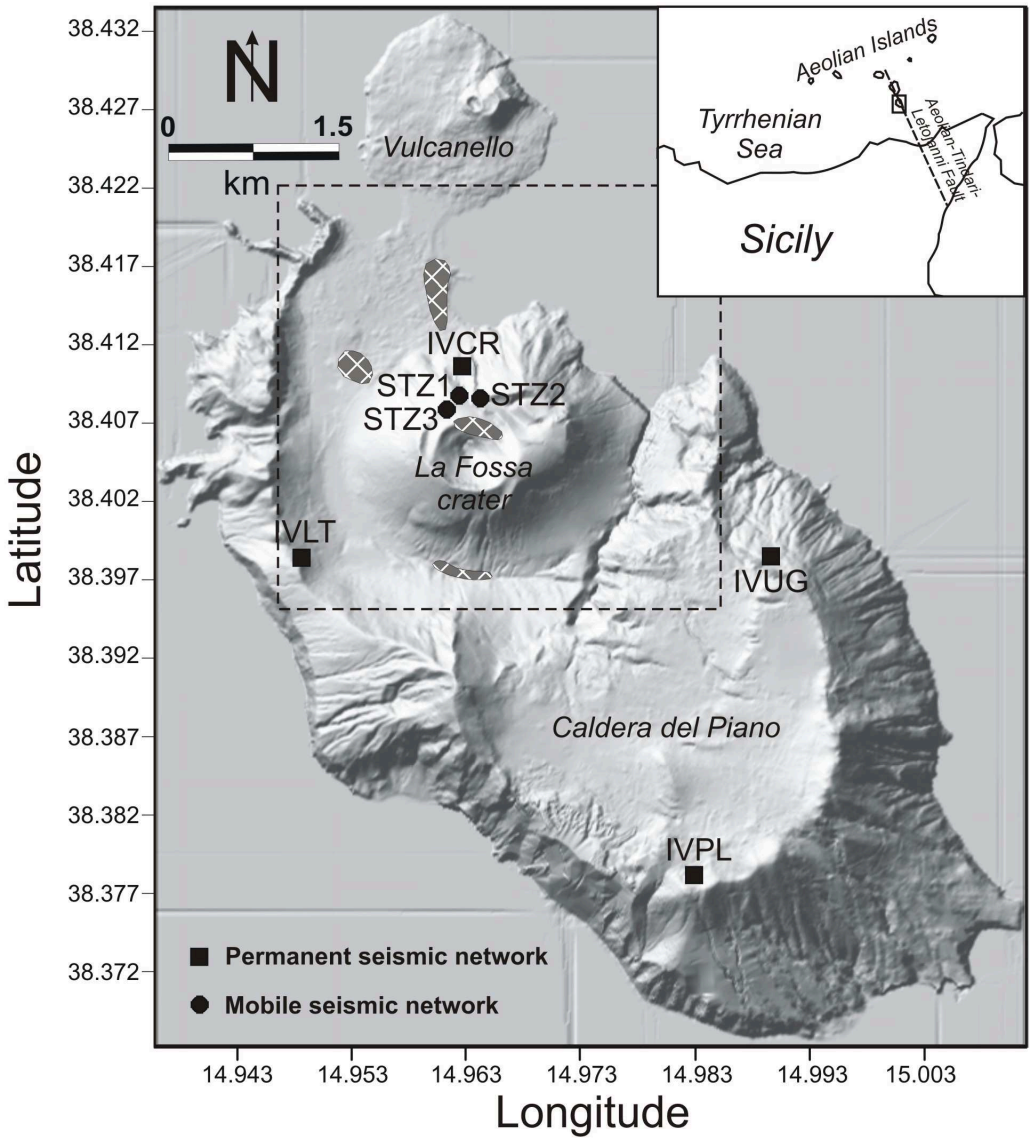

Fig. 4.1 Map of Vulcano island showing the location of the seismic stations used in this work. The dashed rectangle highlights the region shown in **fig. 4.11**. The cross-hatched areas indicate the main fumarolic fields (Harris and Maciejewski, 2000; Diliberto et al., 2002).

4.2 Instrumental topics and data set

During 2004-2009, seismic monitoring at Vulcano was performed by a permanent seismic network **(fig. 4.1)** run by the Catania section of INGV. It was composed of four stations, equipped with three-component, analogue, short period (1 s cut-off period) geophones (Geotech S13) with seismic signal acquired at a sampling rate of 100 Hz. A mobile seismic network, run by the University of Catania and by the Catania INGV, was installed at the end of 2005; it comprised three digital 24-bit seismic stations, equipped with broadband Lennartz LE-3D 20 s, and was located on the northern rim of La Fossa **(fig. 4.1)**. The seismic signal was acquired at a sampling rate of 125 Hz.

Fourteen thousand and five hundred volcano-seismic events, occurring between January 2004 and December 2009, were analysed.

The very few double-couple earthquakes (the most powerful ones occurred in September 2005 and were located near La Fossa crater; Gambino et al. 2007) were neglected. Six increases in seismic activity (**fig. 4.2a**; seismic sequences) were identified during the analysed period. These sequences coincided with geochemical and geothermal anomalies and took place approximately during November 2004-April 2005, September 2005-January 2006, July-October 2006 (Diliberto et al. 2007), July-November 2007, August-December 2008 and May-December 2009 **(fig. 4.2)**. The third seismic sequence is not as clear as the others and, as illustrated in the following paragraphs, is characterised by an increasing number of hybrid (HB) events, a type of volcano seismic event.

In order to study the features of seismic events, we performed (1) spectral analysis by Fast Fourier Transform (FFT), continuous wavelet transform (CWT) and Sompi method; (2) cross-correlation analysis by a bridging technique and using the method described by Green and Neuberg (2006); (3) hypocentral location of the most powerful events.

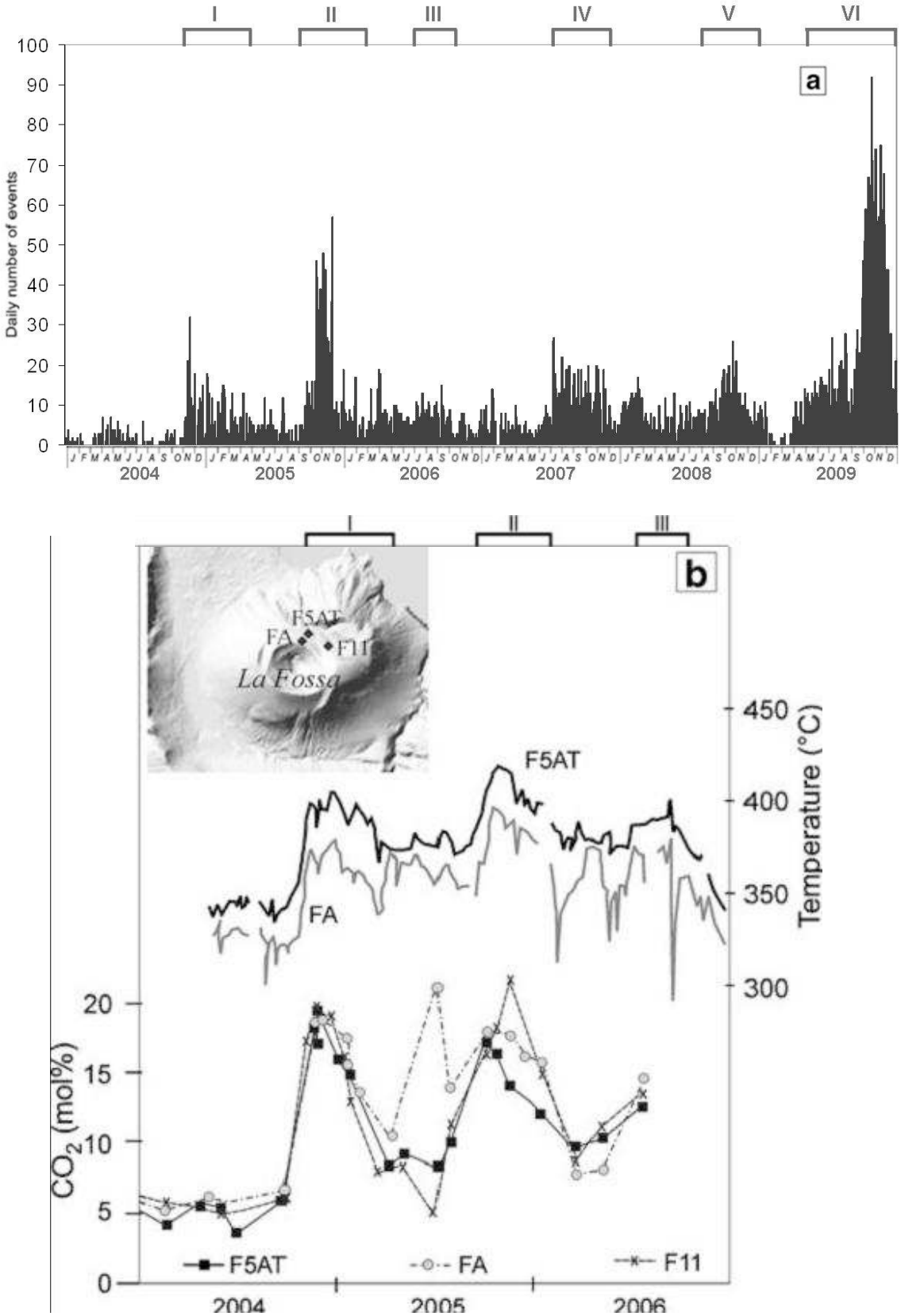

Fig. 4.2 (a) Daily number of seismic events at Vulcano during 2004-2009. The brackets and roman numerals at the top indicate the periods characterised by the six main seismic sequences. **(b)** Time variation of the temperatures and CO_2 concentration at the crater fumaroles (see inset for location) for the 2004-2006 period (redrawn from INGV-PA (2006a,b)

4.3 Classification

Among the roughly 14500 volcano-seismic events recorded from 2004-2009 at La Fossa of Vulcano, we selected 7037 events that exceed a specified amplitude threshold. All these events are characterised by magnitude lower than 1, and poorly defined P and S phases.

These 7037 volcano-seismic events were classified on the basis of visual inspection, spectral and time-frequency analyses. In particular, the time-frequency analysis was performed by means of Short Time Fourier Transform (STFT) and Continuous Wavelet Transform (CWT). While the classic Discrete Fourier Transform (DFT) is suited to stationary signals and is completely insensitive to the changes in coupling over time, the STFT and CWT are applied in order to represent signal variability in time-frequency space. The former represents a time-frequency analysis with fixed resolution, the latter transforms the signal into a multi-resolution time-scale with high frequency resolution at low frequencies and high temporal resolution at high frequencies. The simultaneous use of several time-frequency methods greatly improves the description of the recorded phenomena (Lesage et al. 2002).

Three classes of events were recognised **(fig. 4.3; Tables 4.1 and 4.2)**:

- Long period events, which are characterised by a spectral content mainly ranging between ~ 0.5 and 5 Hz, and are similar to the long period events observed in most volcanoes (Chouet 1996). Their waveforms are generally composed of phases with slightly different frequency following each other. Two distinct subclasses can be recognised within this class: i) hybrid (HB) events, that, similarly to the hybrid events described by Lahr et al. (1994), are characterised by a first phase with higher frequency (~ 4 Hz) and changing amplitude during the studied period, and a tail with lower frequency (~ 2 Hz); ii) mixed (MX or M2) events, characterised by a monochromatic first phase with duration of 1-2 s and frequency of 4 Hz, tail showing low amplitude and frequency ranging between 4 and 10 Hz.

- High frequency (HF) events, that are the most powerful among all the studied classes and are characterised by wide frequency range and by seismic energy between 5 and 25 Hz. Regarding their spectral content, these events resemble the typical volcano-tectonic (VT) earthquakes recorded in most of the volcanic areas and are interpreted as resulting from brittle failure of the rocks (e.g. Lahr et al. 1994). However, the emergent onset, the poorly defined P and S phases and the narrow areas where these events can be detected, make them different from VT earthquakes.
- Monochromatic (MC) events, which show a single frequency peak at 6 or 8 Hz and generally last about 10-15 seconds. Other events belonging to this class show a much longer duration (30-50 seconds) and a very slow amplitude decay **(fig. 4.4a,b,c)**. These features make them highly similar to the "tornillos", recorded at a small number of volcanoes, such as Galeras (Seidl and Hellweg 2003), Tongariro (Hagerty and Benites 2003), Tatun Volcano Group (Lin et al. 2005). Consequently, we also call tornillos (TR) these particular monochromatic events of Vulcano. Many different models have been proposed for the physical source of tornillos: fluid-filled cracks (Gil-Cruz and Chouet 1997; Hagerty and Benites 2003), lumped-parameter models (Julian 1994), self-excited eddy shedding and turbulent slug flow oscillations (Hellweg 2000). Moreover, according to Seidl and Hellweg (2003), tornillos can be interpreted as the free vibration response of a fluid-filled cavity to a pressure pulse (linear model) or as the initial transient leading into a tremor sequence generated by a non linear, self-excited oscillator (non-linear model) **(see chapter 5)**.

Events belonging to high frequency and monochromatic classes showed an almost steady spectral content for their entire duration. Conversely, the long period events were characterised by successive seismic phases with different dominant frequency **(fig. 4.3)**. It is worth noting that we did not find very long period events (characterised by period in the range 2-100 s; Ohminato et al. 1998), at least in the acquisition frequency band of the sensors (period lower than 20 s).

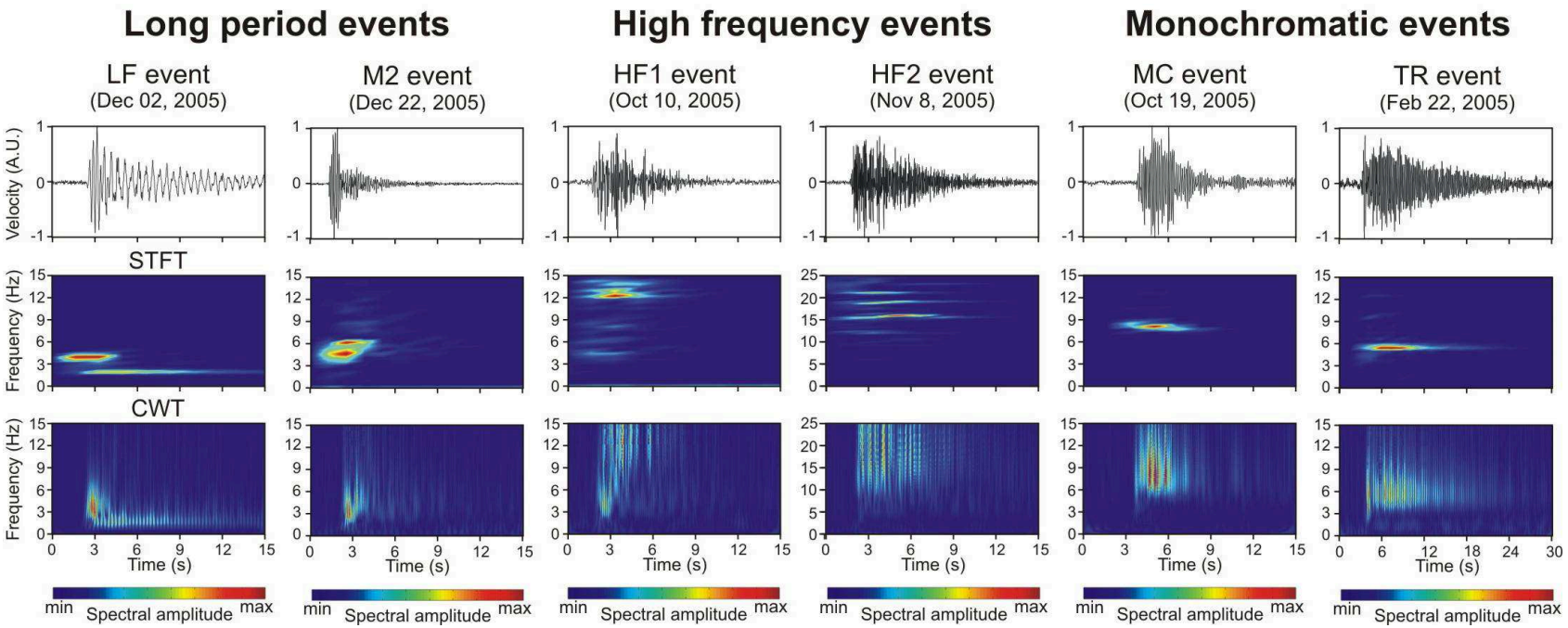

Fig. 4.3 From top to bottom: waveforms, Short Time Fourier Transform (STFT) and Continuous Wavelet Transform (CWT) of examples of the classes of seismic events recorded at the vertical component of IVCR station. The STFT was obtained by splitting the seismic signal in 2.56-second-long windows with 50% overlap. The CWT was calculated with frequency resolution of 0.1 Hz.

Table 4.1 Classification scheme of the volcano-seismic events recorded at La Fossa of Vulcano

Classes		**Features**
Long period events	HB – Hybrid events	First phase with frequency of ≈ 4 Hz and amplitude changing during the studied period, and a tail with frequency of ≈ 2 Hz
	MX – Mixed events	Monochromatic first phase with duration of 1-2 s and frequency of 4 Hz, and tail showing low amplitude and frequency ranging between 4 and 10 Hz
High frequency events	HF events	Wide frequency range generally from 5 to 25 Hz, high values of energy
Monochromatic events	MC events	Single frequency peak generally equal to 6 or 8 Hz and duration mostly ranging between 10 and 15 s. A small number of MC events (tornillos) show a longer duration (30-50 s)

Table 4.2 Classification results of the volcano-seismic events recorded at La Fossa of Vulcano in the period 2004-2009

	MC	HF	HB	MX	TR	Tot.
2004	48	81	8	24	3	164
2005	95	240	99	69	10	513
2006	55	111	72	25	1	264
2007	132	171	3	144	358	808
2008	315	470	23	191	409	1408
2009	1404	1613	195	383	285	3880
Tot.	2049	2686	400	836	1066	7037

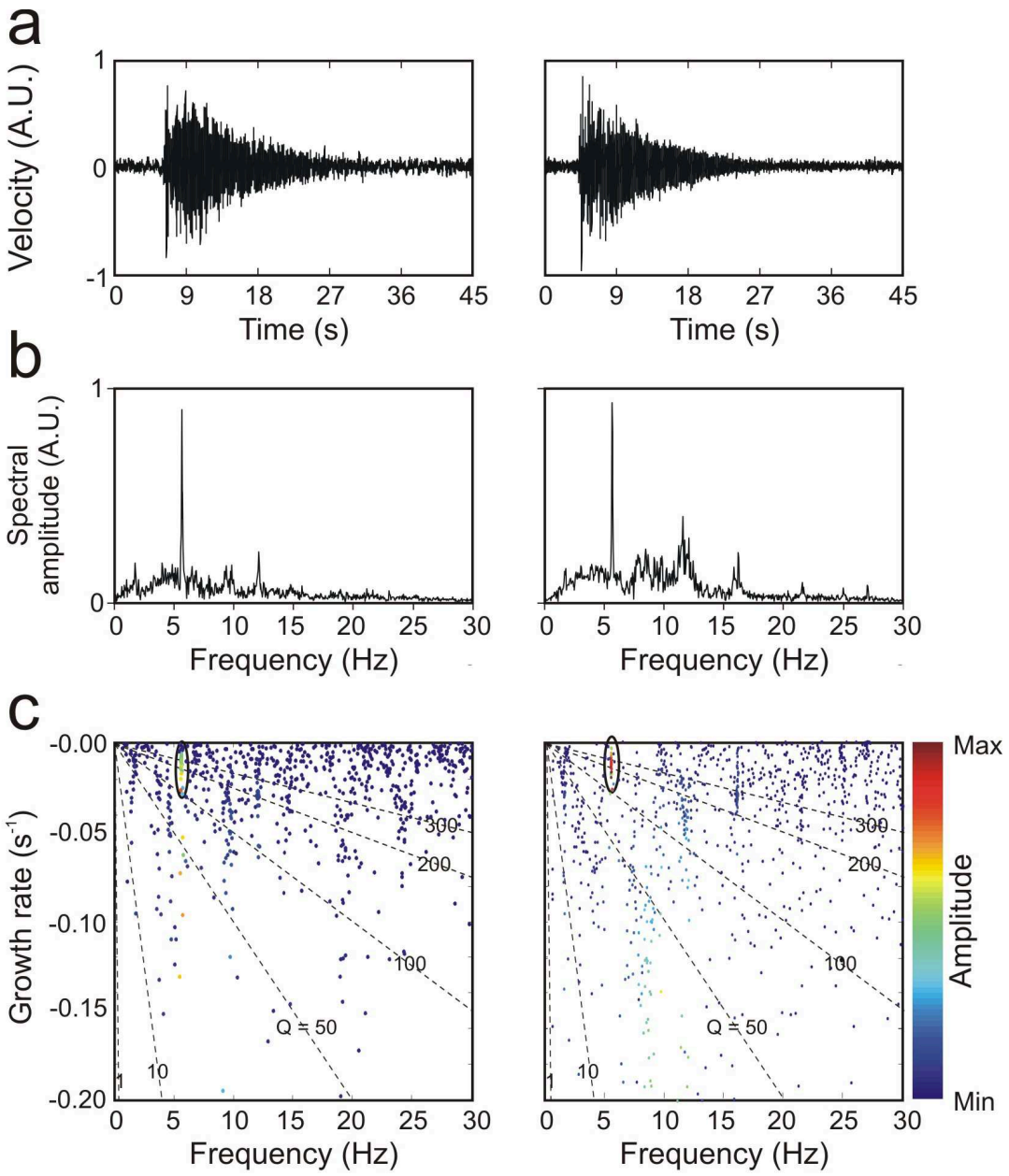

Fig. 4.4 (a) Two examples of waveforms of TR events, recorded by the vertical component of IVCR station, and corresponding **(b)** STFT, obtained by splitting the seismic signal in 2.56-second-long windows with 50% overlap, **(c)** amplitude spectra and **(d)** *f-g* diagrams, obtained for all the trial AR orders (4-60). Dot colours indicate the amplitude values of the wave elements (see colour scale). The dashed lines represent lines along which the quality factor (Q) is constant. Clusters of points (encircled with solid ellipses) indicate dominant spectral components of the signal, scattered points represent noise.

We performed cross correlation analysis on the events of each class recorded by the vertical component of IVCR station, by using the bridging technique (Barani et al. 2007). If two pairs of correlated events, (A, B) and (B, C) share a common event (B), then all the events are attributed to the same family, even if the cross correlation coefficient between A and C is lower than the chosen threshold. Therefore, event B represents the "bridge event" between these couples. The cross correlation function was calculated on windows with length ranging from 1 to 2.5 s, and beginning with the onset of the events. The events of each class and subclass were grouped into families by a threshold value of cross correlation coefficient. Then, for each threshold value the total number of events composing all the families with at least 2 events was taken into account and the percentage with respect to the total number of the events of the class and subclass (in the case of MX and HB events) was calculated. Multiple trials were performed with values of cross correlation threshold ranging from 0.7 to 0.9 with step of 0.05. This procedure was followed to evaluate the repeatability and stationarity of the seismic source. Some results of this analysis are reported in **fig. 4.5**. We observed that the events exhibit different degrees of waveform similarity, according to their class or subclass. In fact MC, HB and MX events showed a high degree of waveform similarity inside each group, whereas HF events were characterised by very variable waveforms.

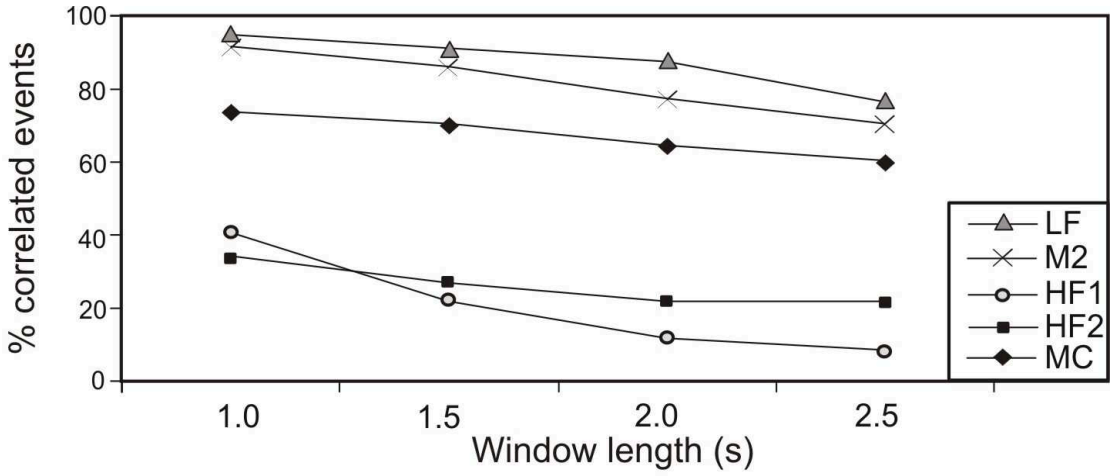

Fig. 4.5 Percentage of correlated HB (LF) , MX (M2), HF and MC events versus window length, obtained by threshold of cross correlation coefficient of 0.8.

4.4 Time variations

We investigated the time variations of the monthly number, waveform and spectral content of the events belonging to the seismic classes.

The monthly number of events was calculated for each class (and subclass in the case of MX and HB events). Then this number was transformed into a percentage with respect to the total number of events belonging to the same group **(fig. 4.6)**. For example, in November 2005, 37 HB events were recorded; since we detected 400 HB events during the whole 6-year-long period, the percentage of HB events during November 2005 was 9,25%. This time distribution suggests that the number of events of all the classes increases during the first and second seismic sequences, while the third sequence is characterised by an increase only in the number of the HB events. Moreover, taking into account the six-year-long investigated period, HB events were recorded for the first time during the first seismic sequence, disappeared in the fourth and fifth seismic sequence and reappear at the end of 2009. Moreover, it is worth noting that while many TR events were observed in 2007-2009, only 15 TRs were recorded during the previous three years, 2004 – 2006. This topic will be analyzed in detail in **chapter 5**.

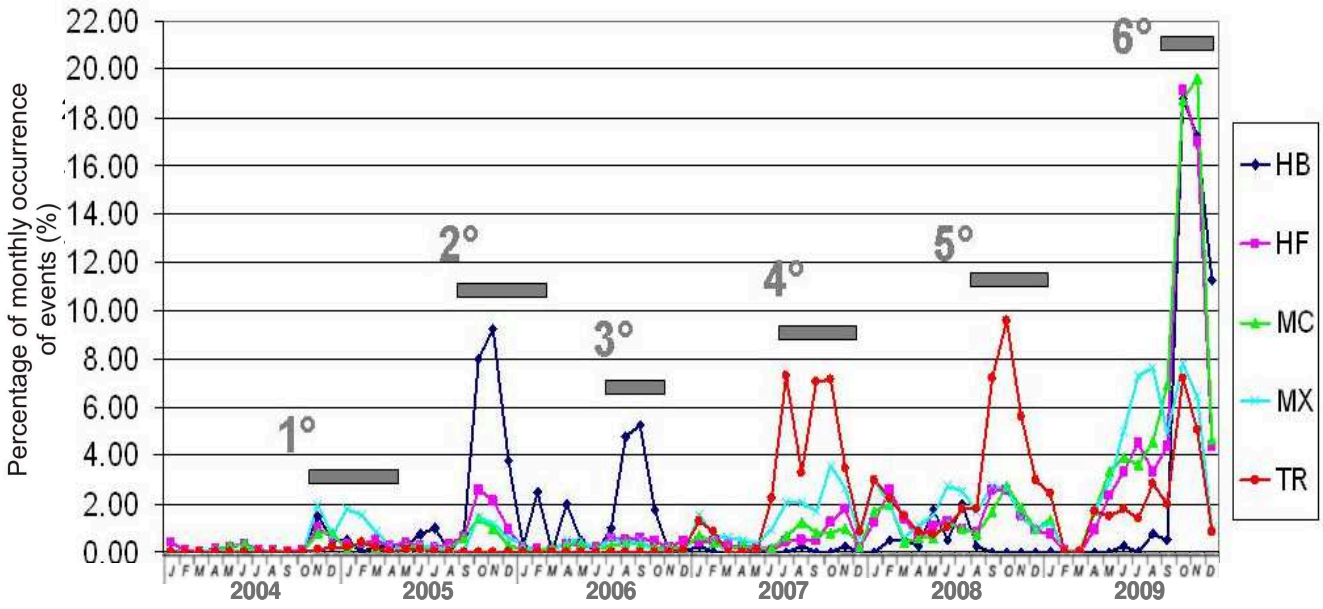

Fig. 4.6 Monthly distribution of HB, MX, HF, MC and TR events. Numbers and gray rectangles indicate the periods characterised by the seismic sequences.

As a second step, we studied the time evolution of the waveform by using the cross correlation function (Green and Neuberg 2006). This method entails the following steps: i) the signals, recorded by the vertical component of station IVCR, were filtered according to the spectral features of the considered class; ii) a cross correlation matrix was obtained for each class by using 5-second-long windows of signal, beginning with the onset of the events; iii) a master event was selected as the event with the largest number of values of cross correlation coefficient above the threshold of 0.7; iv) an average waveform of the family was found by stacking all events that were well-correlated with the master event (cross correlation coefficient > 0.7); v) this stacked waveform was then cross-correlated with the original seismic records, and all events with a cross correlation coefficient greater than the threshold were grouped into a waveform family; vi) the steps iii)-v) were repeated until the entire matrix was classified into distinct groups. In this procedure, the overlap between clusters was not allowed. Once an event was assigned to a given group, it was removed from the correlation matrix. Unlike the aforementioned bridging technique, this method allows identifying of gradual waveform variations because of the lack of "bridge events".

The most striking waveform variations were observed for HB events, as shown by the cross correlation matrix in **fig. 4.7a**. In particular, two sequential families of HB events (hereafter called HB1 and HB2) were found, with a third smaller family (HB1_2) briefly occurring between the two main families. The variation from HB1 to HB2 occurred at the end of the second seismic sequence (January 26, 2006). Family HB1 was composed of events characterised by a monochromatic first phase with duration of 1-2 s and frequency of 4 Hz, and a tail showing frequency of 2 Hz and duration of about 10 s. Family HB2 comprises events with frequency ranging between 2.4 and 3.1 Hz. Families HB1 and HB2 mainly characterised the second and third seismic sequences, respectively. Family HB1_2 was noted in the period between the occurrence of HB1 and HB2. In **fig. 4.7a** inset, the time distribution of the cross correlation coefficient, obtained by comparing the first HB event with all the other HB

events, is reported. This distribution suggests that the time variation of the waveform was gradual and mainly occurred during the periods between the seismic sequences. It is worth noting that this cross correlation analysis was also performed by using 8-second-long windows and gave the same results. With the aim of highlighting the average features of the three families, we obtained a stacked waveform for each family **(fig. 4.7b)**.

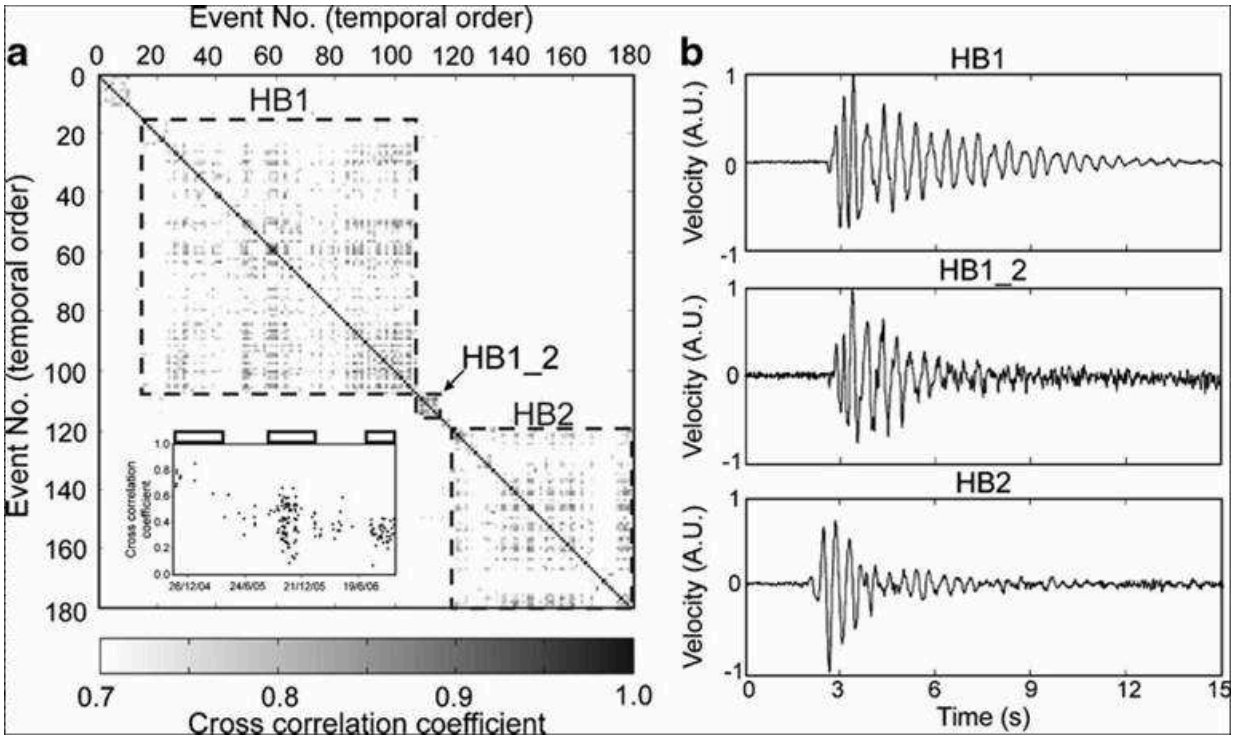

Fig. 4.7 (a) Correlation matrix for HB events showing the three families (indicated as HB1, HB1_2 and HB2) following each other. The inset in the lower left corner indicates the time variation of the cross correlation coefficient values, obtained by comparing the first HB event with all the other HB events (the top empty rectangles indicate the periods characterised by the seismic sequences). **(b)** Waveforms obtained by stacking the correlated events.

In order to study the time variation of the spectral features of MC, HF, HB and MX events, we performed two different frequency domain analyses: FFT and Sompi method (Kumazawa et al. 1990, and references therein). With FFT we calculated one spectrum for each event by using 10-second-long windows, whose onset coincided with onset of the event. Then, we normalised and averaged the spectra of the events occurring during 10-day-long time spans and

the obtained average spectra were visualised as pseudo-spectrograms. By using this method, we noted that HB events showed the most striking time variations of the spectral content. As depicted in the pseudo-spectrogram of **fig. 4.8a**, the HB events were composed of two main components at frequencies at ~ 2 and 4 Hz. It is worth noting that these two components gradually shifted toward higher frequencies during the two 6-month-long periods between the seismic sequences, and remained steady in the seismic sequence intervals. Moreover, the spectral amplitude of the first phase at about 4 Hz, the dominant component of HB events observed during the first sequence, diminished during the second sequence and almost disappeared by the third.

Many types of volcano-seismic signals, such as the long period events observed at most volcanoes, are characterized by simple waveforms and consist of a superposition of decaying harmonic oscillations, which may represent the impulsive response of a resonator system (Nakano and Kumagai 2005). In order to obtain information about the characteristic properties of the resonator systems and their variations, we studied the damping features of the volcano-seismic events at Vulcano by Sompi analysis. This technique was applied on the volcano-seismic events recorded at different volcanoes and highlighted time variations of the quality factor and frequency of these events, that were interpreted as resulting from changes in fluid composition within the plumbing system (e.g. De Angelis and McNutt 2005; Patanè et al. 2008) or changes in geometry of fluid-filled cracks (e.g. Kumagai et al. 2002). In this method of spectral analysis based on an autoregressive (AR) model, a signal is deconvoluted into a linear combination of coherent oscillations, called wave elements, with decaying amplitudes and additional Gaussian white noise. In this approach we define a complex frequency fc = f – ig where f is the frequency, g is the growth rate or gradient (that quantifies the growth/decay of the wave element amplitude) and i is $\sqrt{-1}$ (Kumazawa et al. 1990). The quality factor Q is then given by –f/2g. Generally, in order to represent a set of complex frequencies, they are plotted on a 2D-plane with f and g axes, called f-g

diagram. Since the Sompi method also provides information on the amplitude of the wave elements (Kumazawa et al. 1990), we can add this parameter in the f-g diagram by using a colour scale for the dots **(see figs. 4.9b and 4.4d)**. Widely scattered wave elements in the plot, showing low amplitude values, are considered noise, while densely populated wave elements on the theoretical frequency lines ("iso-frequency" lines) and characterised by high amplitude are considered dominant spectral components of the signal (Hori et al. 1989). This analysis was applied only to long period events (both MX and HB events) and TR events because the other events did not show tails composed of a superposition of simple decaying sinusoids - the necessary condition to calculate the complex frequency. The complex frequencies of the wave elements for AR orders ranging from 4 to 60 were calculated. The spectral content evolution of the HB events, highlighted by the pseudo-spectrogram in **fig. 4.8a**, is confirmed by the frequency values obtained by Sompi method **(fig. 4.8b)**. The Sompi analysis also indicates that the quality factor of these events changed, as shown for unfiltered signals **(fig. 4.8c)** and signals filtered below 3 Hz **(fig. 4.8d)**. In fact, a decrease of quality factor, well evident especially for the signal component at about 2 Hz (from 28±15 to 11±6, **fig. 4.8d**), took place between the second and the third seismic sequences.

FFT and Sompi analyses were also applied on the stacked waveforms obtained for the HB1, HB1_2 and HB2 families reported in **fig. 4.7b**. The spectra **(fig. 4.9a)** and the f-g diagrams **(fig. 4.9b)** confirmed the aforementioned time variations: progressive shift of the frequency peaks toward higher frequency, gradual amplitude decrease of the signal component at 4 Hz and decrease of the quality factor of the signal component at about 2 Hz. **Figures 4.7b, 4.8** and **4.9** show that Family HB1_2 was characterised by intermediate features between families HB1 and HB2.

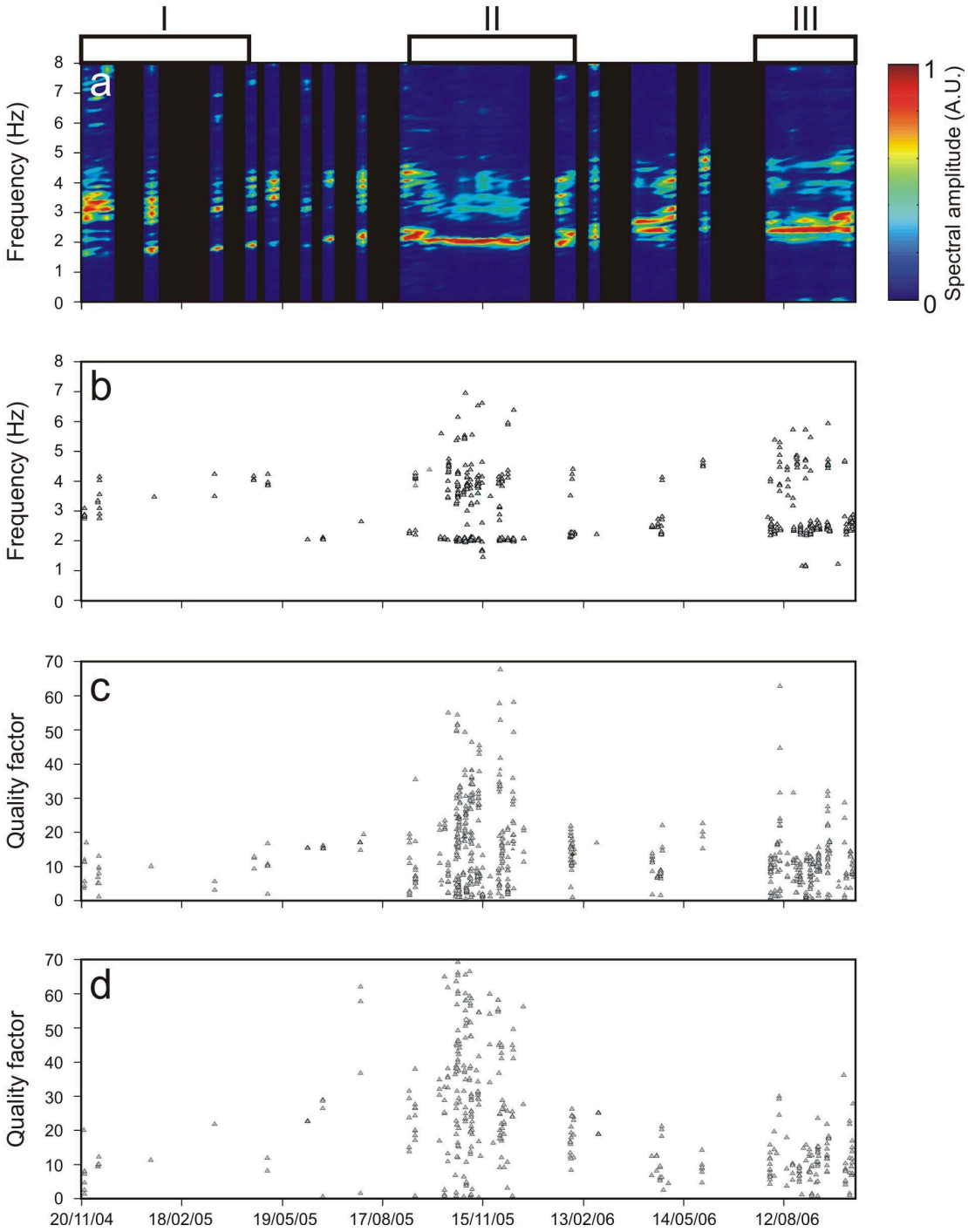

Fig. 4.8 (a) Normalised pseudo-spectrogram of the HB events recorded at the vertical component of IVCR station. Each spectrum was calculated by averaging the spectra of the HB events occurring during 10-day-long interval. The black rectangles, located inside the plot, show time intervals with no HB events. The top empty rectangles and roman numbers indicate the periods characterised by the seismic sequences. **(b)** Peak frequency of the vertical component of the seismic signal of IVCR station, obtained by Sompi method for autoregressive (AR) orders ranging between 4 and 60. **(c-d)** Quality factor of the vertical component of the seismic signal of IVCR station, not-filtered and filtered below 3 Hz, respectively, obtained by Sompi method for AR orders ranging between 4 and 60.

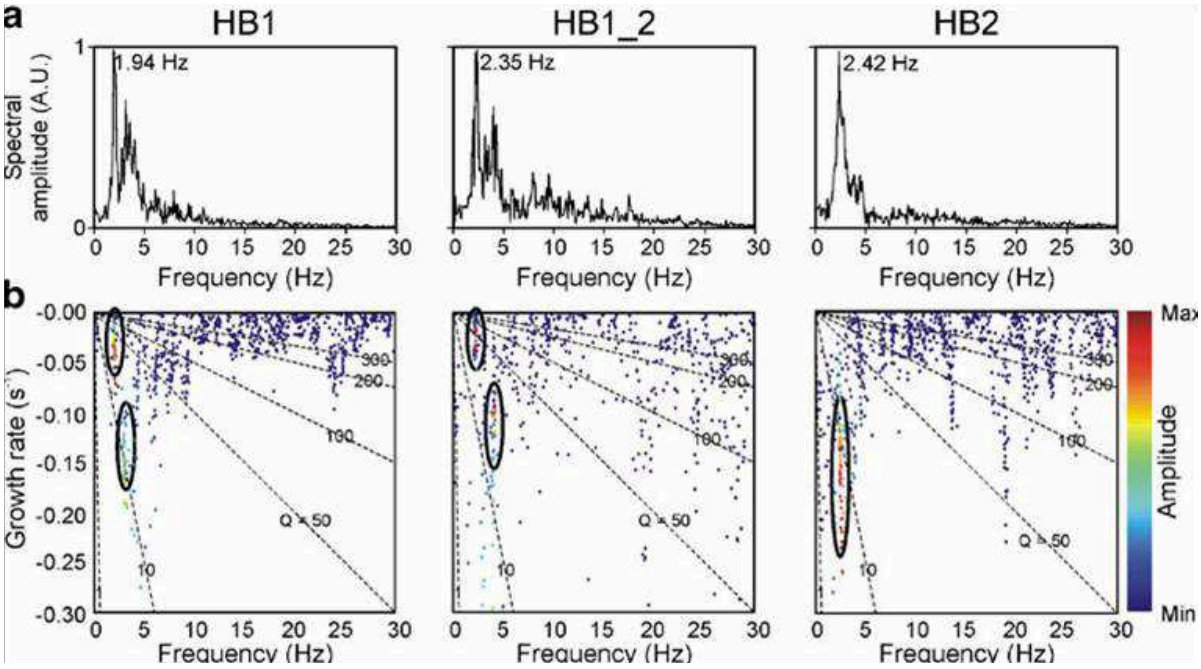

Fig. 4.9 (a) Amplitude spectra of the stacked waveforms of HB1, HB1_2 and HB2 families. The values in the plots indicate the frequency of the highest spectral peak. **(b)** *f-g* diagrams obtained for all the trial AR orders (4-60). Dot colours indicate the amplitude values of the wave elements (see colour scale). The dashed lines represent lines along which the quality factor (Q) is constant. Clusters of points (encircled with solid ellipses) indicate dominant spectral components of the signal, scattered points represent noise.

A slight variation of the spectral content was also noted for the MX events at the end of the first seismic sequence **(fig. 4.10)**: a shift of the spectral content toward higher frequency occurred without any significant changes of the quality factor.

Finally, we focused on TR events that were characterised by frequency peaks at about 6 or 8 Hz and much higher quality factor values than the other analysed events (150-200 on average), as evidenced by the slower amplitude decay **(fig. 4.4d)**.

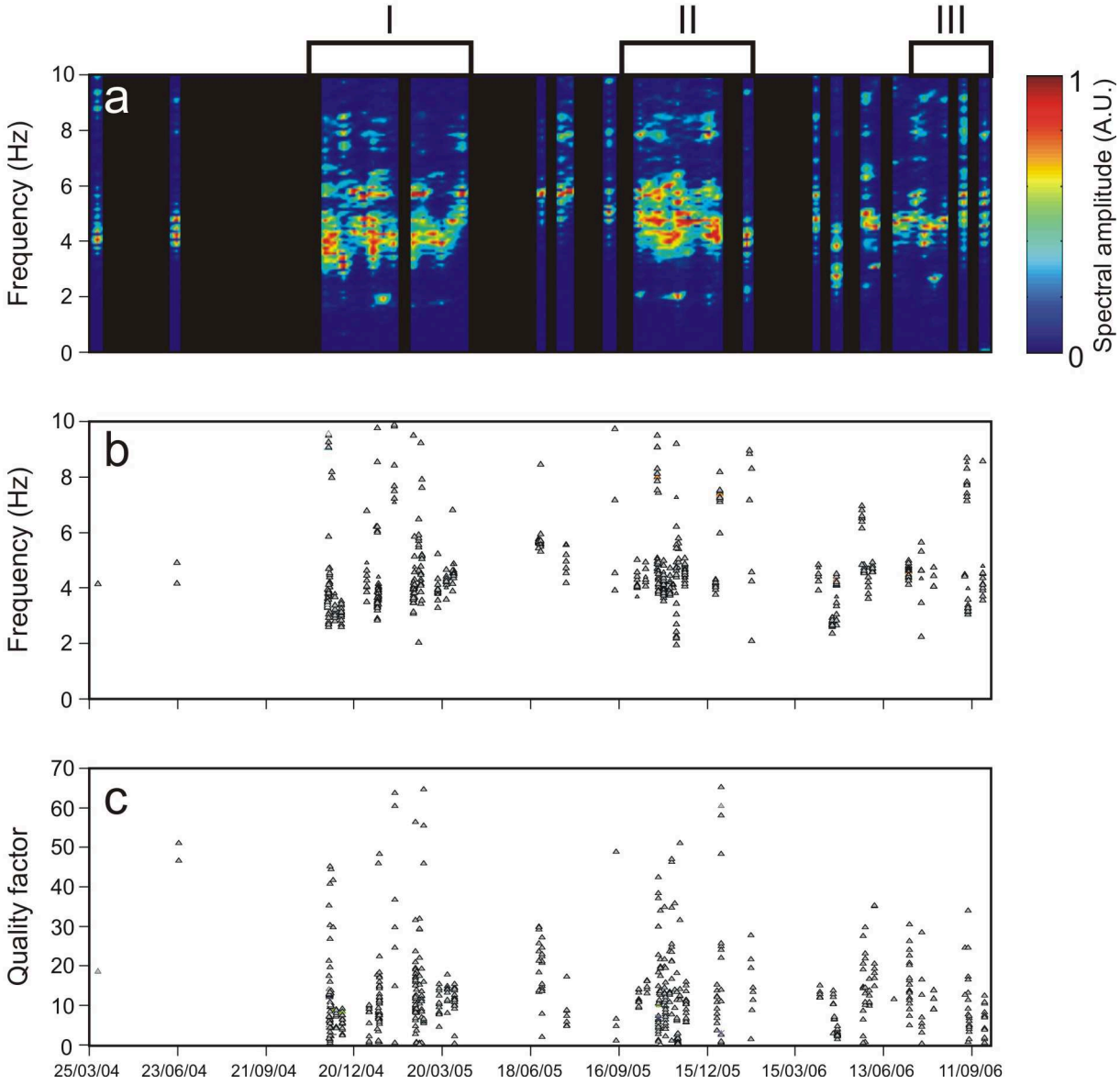

Fig. 4.10 (a) Normalised pseudo-spectrogram of the MX events recorded at the vertical component of IVCR station. Each spectrum was calculated by averaging the spectra of the MX events occurring during 10-day-long interval. The black rectangles, located inside the plot, show time intervals with no MX events. The top empty rectangles and roman numbers indicate the periods characterised by the seismic sequences. **(b-c)** Peak frequency and quality factor of the vertical component of the seismic signal of IVCR station, obtained by Sompi method for AR orders ranging between 4 and 60.

4.5 Location

In order to locate the studied volcano-seismic events we used the HYPOELLIPSE program (Lahr 1989) using the velocity model from Falsaperla et al. (1985). We selected about 60 locations of events belonging to different classes on the basis of: high signal to noise ratio, error lower than 1 km and azimuth gap lower than 190°.

The space distribution of these events is shown in **fig. 4.11**. We noted that the seismic sources are mainly clustered below La Fossa crater, in the depth range 0.3-1.7 km b.s.l. Most of the events are clustered at depths 0.5-1.1 km b.s.l. Moreover, different space distribution can be distinguished for different groups of events. In particular, HB events are located south-east of La Fossa and aligned about NE-SW, as also confirmed by high precision locations (Gambino et al. 2009). Their focal depth is constrained in the narrow range 0.6-0.8 km b.s.l. HF and MX events are located on the western-central sector of the crater. Conversely, MC events are generally located south of La Fossa, with the exception of TR events that are clustered in a small volume to the north-west.

The mean horizontal and vertical errors are about 500 m. Even after taking into account these error values, it should be noted that locations remain constrained inside La Fossa area.

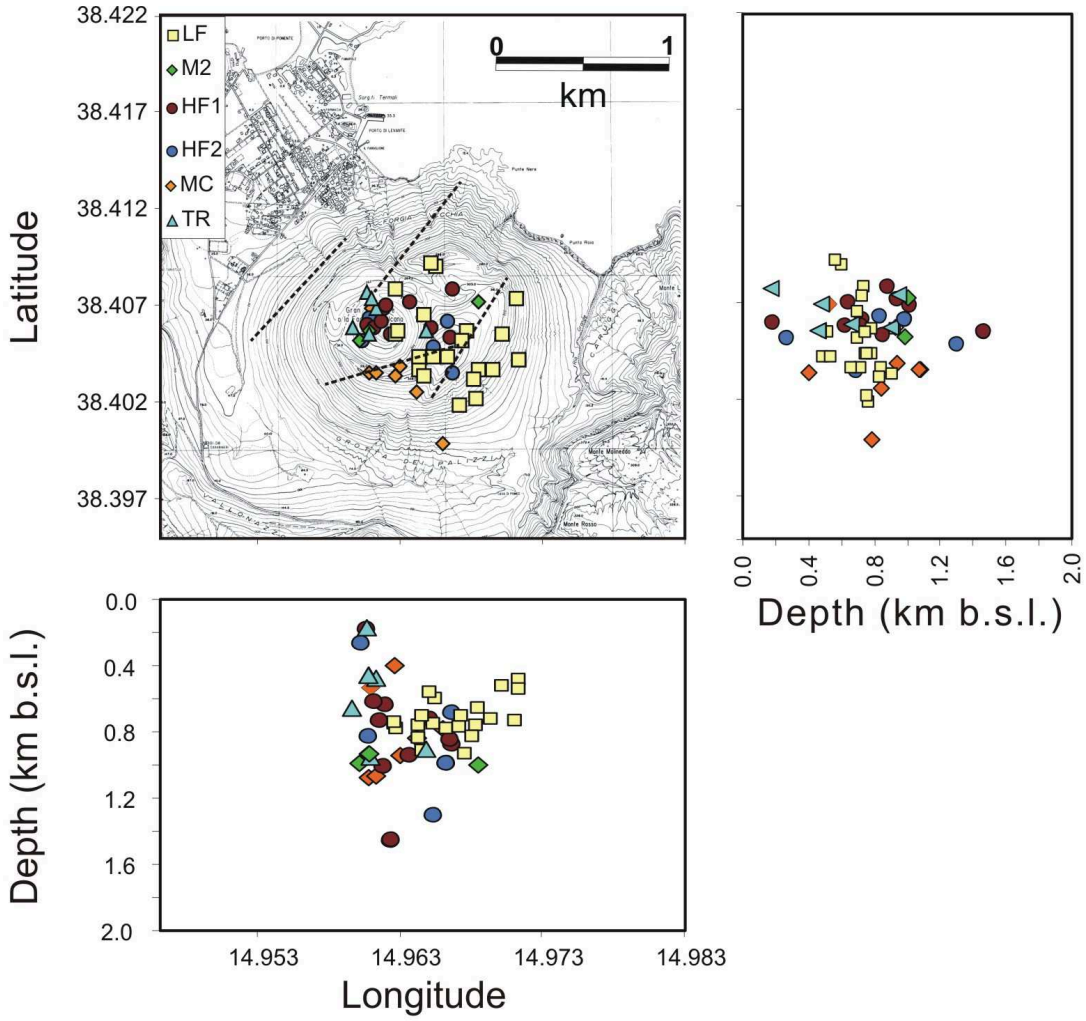

Fig. 4.11 Hypocentral locations of some HB (LF), MX (M2), HF, MC and TR events (see legend in the upper left corner of the map). The dashed black lines in the map indicate shallow fractures and normal faults (Mazzuoli et al., 1995).

4.6 Discussion and conclusions

Reconstructions of the eruptive histories of many volcanoes have shown that inactive periods of hundreds of years between eruptions are not uncommon. This is particularly true for highly explosive volcanoes (Scarpa and Gasparini 1996). Therefore, Vulcano, whose last eruption occurred in 1888-1890, is to be considered potentially active and dangerous for the local population. Moreover, the volcanic risk in this area increases greatly in summer, when the number of inhabitants swells from a few hundreds to several thousands.

During January 2004 - December 2009, six seismic sequences occurred at La Fossa, Vulcano, at the same time as anomalous increases of fumarolic CO_2 flux and temperature, as well as variations of other geochemical parameters were observed (Diliberto et al. 2007) **(fig. 4.2)**. Such geochemical and geothermal anomalies are interpreted as an increase of the deep magmatic component constituting a portion of the hydrothermal fluids (Granieri et al. 2006). The six anomalies, the corresponding seismic sequences and the short time intervals separating them, suggest the importance of the analysed period in the recent history of Vulcano. In light of this, we made a detailed investigation into the volcano-seismic events recorded during 2004-2009. On the basis of the spectral content and waveforms, these events were grouped into three classes **(Table 4.1)**: long period events, comprising HB and MX events; high frequency (HF) events and monochromatic (MC) events. It is also worth noting that other events belonging to monochromatic class were recorded. These events, that show a very long duration (30-50 seconds), are called tornillos, similarly to the volcano-seismic events with the same peculiar long duration recorded in other volcanoes. In particular, long period and monochromatic events are characterised by i) narrow spectrum with sharp dominant spectral peaks, ranging between 2 and 8 Hz, and ii) high degree of waveform similarity, suggesting stationary, non-destructive processes. These features, together with the prevailing theories on the source of long period events and tornillos (e.g. Chouet 1996; Aoyama and Takeo 2001; Kumagai et al. 2002; Molina et al.

2008), suggest the resonance of hydrothermal fluid-filled cracks or conduits, or simply fluid flow inside them, as the source mechanism for long period and monochromatic events of Vulcano. The analysed long period events are characterised by the presence of successive seismic phases with different frequency content **(fig. 4.3)**. This suggests that the triggering mechanism linked to the first phase is different from the resonance process causing the second one (Battaglia et al. 2003; Caplan-Auerbach and Petersen 2005). For the HB events, the first phase may be related to the fluid pressure exceeding the mechanical resistance of obstruction inside the hydrothermal fluid-filled cracks or conduits; in fact, hydrothermal activity at Vulcano gives rise to processes of self-sealing and clogging of the fumarolic system (Montalto 1994b). Then, the second phase is caused by the consequent resonance of the plumbing system (Montalto 1994b). On the basis of the source mechanisms of these two phases the HB events share the same source mechanisms as hybrid events described by Lahr et al. (1994). The decrease in amplitude of the first phase of the HB events at ~ 4 Hz, observed during the studied period, suggests a gradual decrease of effectiveness of the self-sealing and clogging processes. On the other hand, the MX events, that lack a second seismic phase with lower frequency and amplitude comparable to the first phase, may be due to unblocking process resulting in weaker resonance. The significantly longer duration of TR events than long period and the other MC events, also confirmed by the very high quality factor values **(fig. 4.4d)**, may be due to different fluid composition or to different aspect ratio of the resonating crack, generating these seismic events. In particular, the higher quality factor of the TR events could be attributed to the lower gas fraction causing oscillations with longer duration, as shown by Kumagai and Chouet (2000), or to a crack having smaller aspect ratio (Kumagai and Chouet 2001). However, the study of TR events at Vulcano deserves detailed analyses on a larger dataset, which will be the object of future work.

Focusing on high frequency events, their main features are i) the wide frequency content, generally ranging from 5 to 25 Hz, similar to VT earthquakes, and ii) the low degree of waveform similarity, suggesting destructive source

mechanisms. This, together with the interpretation of the source mechanisms of VT earthquakes (e.g. Lahr et al., 1994), would suggest that fracturing processes of the rocks surrounding the hydrothermal system could be the source for the high frequency events (as also proposed by Montalto 1994a).

In view of these source processes, the time-relationship between geochemical and geothermal anomalies and seismic sequences can be inferred. The increasing magmatic component of the hydrothermal fluids during the anomalies can cause both the increase of the pore pressure within the volcanic system and the increase of the fluid flux rising up. Then, increased pore pressure gives rise to increasing fracturing processes, while increased fluid flux favours the resonance and vibration processes in cracks and conduits **(fig. 4.12a)**. This model justifies the occurrence of the seismic sequences at the same time as the geochemical and geothermal anomalies.

Most of the volcano-seismic events affect a small volume (about 0.5 km3) located below La Fossa crater at depths ranging between 0.5-1.1 km b.s.l. **(fig. 4.11)**. Furthermore, the space distribution of the HB event locations **(fig. 4.11)**, aligned roughly NE-SW, as also confirmed by high precision locations (Gambino et al. 2009), is consistent with shallow fractures and normal faults, located in the inner sectors of the island, where intense fumarolic activity is concentrated (Mazzuoli et al. 1995).

The possible time variation of the features of the seismic events was investigated, and only HB events exhibited marked changes. In particular, they showed gradual shift toward higher frequencies and lower quality factors **(figs. 4.8, 4.9)**. Time variations of the spectral features of volcano-seismic events have been observed in several volcanoes around the world, such as Mt. Etna (Patanè et al. 2008; Cannata et al. 2009), Galeras (Torres et al. 1996), Kusatsu-Shirane (Kumagai and Nakano 2005), Mt. Spurr (De Angelis and McNutt 2005) and Tungurahua (Molina et al. 2004). Such changes are generally interpreted to result from variations in the geometry of the resonating crack, which is the most appropriate geometry for mass transport condition beneath a volcano (e.g. Chouet 1986, 1988), and/or the features of the fluid filling the cracks. In

particular, in the case of HB events at Vulcano, on the basis of the shallowness of the source, the fluid can be reasonably considered hydrothermal. Such assumptions are also supported by the obtained quality factor values, mostly ranging between 10 and 30, consistent with resonance of crack filled with hydrothermal fluids, as shown by Kumagai and Chouet (2000). Therefore, making the assumption that the attenuation due to intrinsic losses is negligible, the frequency increase and quality factor decrease may be due to the increase of the gas volume fraction in the fluid likely linked to a process of heating and drying of the hydrothermal system **(fig. 4.12b)** (Nakano and Kumagai 2005; De Angelis and McNutt 2005).

Such processes of increase of gas volume fraction can be due to either a "deep" cause, related to changes in the flux of hot volcanic gases leaking from the magma beneath the volcano edifice, or a "shallow and external" cause, linked to meteorological phenomena such as very rainy periods. As an example of the first hypothesis, Molina et al. (2008) inferred a release of particle-laden gas from an intruding magma batch beneath the Cotopaxi volcano to explain the gradual decrease of frequency peak of LP events accompanied by an increase of quality factor. On the other hand, LP event variations, similar to the HB ones, were observed at Kusatsu-Shirane by Nakano and Kumagai (2005) and systematically took place each year from 1989 to 1992 during July-November. For this reason the authors proposed the existence of seasonal influences on LP events, related to the rainfall. In the case of Vulcano, the HB spectral features did not change seasonally during the 6-year study period. Moreover, the variations in their number did not take place in the same season each year, but in winter during the first and second anomalies and summer during the third one. These indications seem to suggest that external meteoric influences were not responsible for such HB variations. Therefore, it is likely that these changes observed at Vulcano took place in response to increasing heat and fluid flow beneath the volcano. It is also worth noting that the observed HB waveform changes were gradual, and thus also such deep heat and fluid flows were probably slow. However, longer time series, comprising many years, are needed

to completely exclude any external meteoric influences on the volcano-seismic signals at Vulcano.

During the period characterised by these HB changes, many different geothermal and geochemical anomalies occurred. Although the relationship of the anomalies to unrest processes, that could lead to eruptions, is still being debated (Barberi et al. 1991; Italiano and Nuccio 1992; Bukumirovic et al. 1997; Granieri et al. 2006), there is general agreement that such anomalies imply increases of hot gas-rich fluids rising towards the surface. The aforementioned interpretation of HB variations would thus seem reasonable.

Whatever the case, it is worth noting that the observed waveform changes indicate important variations in the characteristics of the fluids, and hence suggest an unsteady and dynamic hydrothermal system. This is also supported by the differences observed between the anomalies in terms of occurrence rate and type of seismic events recorded.

In conclusion, the study of the volcano-seismic signals is of particular importance for diagnosing the state of fluids within the resonator systems and their time variations, which then can prove very helpful for monitoring purposes.

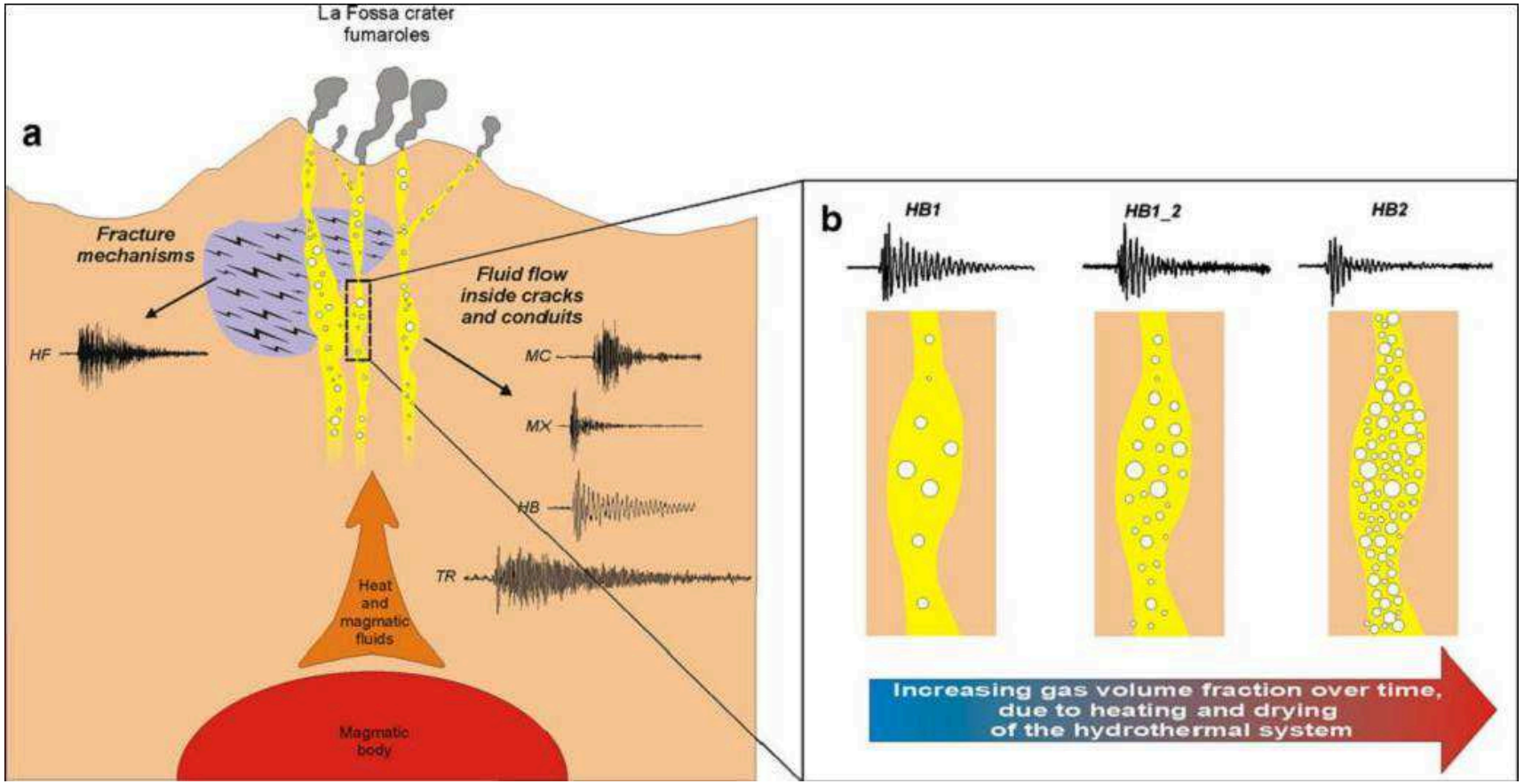

Fig. 4.12. Cartoon showing **(a)** a schematic section of the volcanic system with the source processes of the volcano-seismic events at Vulcano and **(b)** the time evolution of the HB events with the related interpretation.

Chapter 5

Tornillos at Vulcano: clues to the dynamics of the hydrothermal system

5.1 Introduction

Tornillo, the Spanish word for screw, refers to a class of seismic events recorded in volcanic areas, that can last up to several minutes. They are characterized by decaying sinusoidal waveforms, screw-like envelope profiles and one, or at most a few, narrow spectral peaks. In Japan several names have been used to refer to these particular signals: LC (long-coda) events; BS (banded-spectrum) events; SF (single-frequency) events; and T-type (similarity with a T-square) events (Gomez and Torres, 1997). Some authors include them in the classification Long Period (LP) events, based both on spectral content and proposed source process (e.g., Kumagai et al., 2002; Molina et al., 2008). Tornillos (hereafter referred to as TRs) have been observed at many volcanoes

such as Galeras (Gomez and Torres, 1997; Seidl and Hellweg, 2003), Puracé (Arcila, 1996; Gomez and Torres, 1997), Tongariro (Hagerty and Benites, 2003), Tatun Volcano Group (Lin et al., 2005), Asama (Shimozuru and Kagiyama, 1989), Cotopaxi (Molina et al., 2008), Papandayan (Triastuty et al., 2006), Kuchinoerabujima (Triastuty et al., 2009) and Katmai National Park (De Angelis, 2006). TRs are recorded during various stages of volcanic activity. They can precede ash eruptions, as at Galeras in 1992-1993 and Asama in 1983 (Gomez et al., 1999). In other cases they occur after eruptions (Tokachi volcano, Japan, 1989), during seismic swarms (Meakan volcano, Japan, 1982) or simply during quiescence (Puracè volcano, Colombia, 1994-1995; Tarumai volcano, Japan, 1970-1971, 1975) (Gomez et al., 1999). Many different models have been proposed for the physical source of TRs: fluid-filled cracks (Gil-Cruz and Chouet, 1997; Kumagai and Chouet, 1999; Hagerty and Benites, 2003), lumped-parameter models (Julian, 1994), self-excited eddy shedding and turbulent slug flow oscillations (Hellweg, 2000). Moreover, according to Seidl and Hellweg (2003), TRs can be interpreted as the free vibration response of a fluid-filled cavity to a pressure pulse (linear model) or as the initial transient leading into a tremor sequence generated by a non-linear, self-excited oscillator (non-linear model).

As in most active volcanoes around the world, also Vulcano **(fig. 5.1)** is characterised by an ample variety of seismic signals. The different types of these earthquakes were classified, mainly on the basis of waveforms and spectral contents in **chapter 4**.

The aim of this work is to study the TRs which occurred at Vulcano in 2007-2008, in order to identify their main features and investigate the possible physical processes which produce them. Moreover, we will analyse the changes in the TRs' characteristics over time, which may provide information about the evolution of the hydrothermal system. In doing so, we will advantageously exploit the comparison of the seismic signals with the concurrent geochemical anomalies.

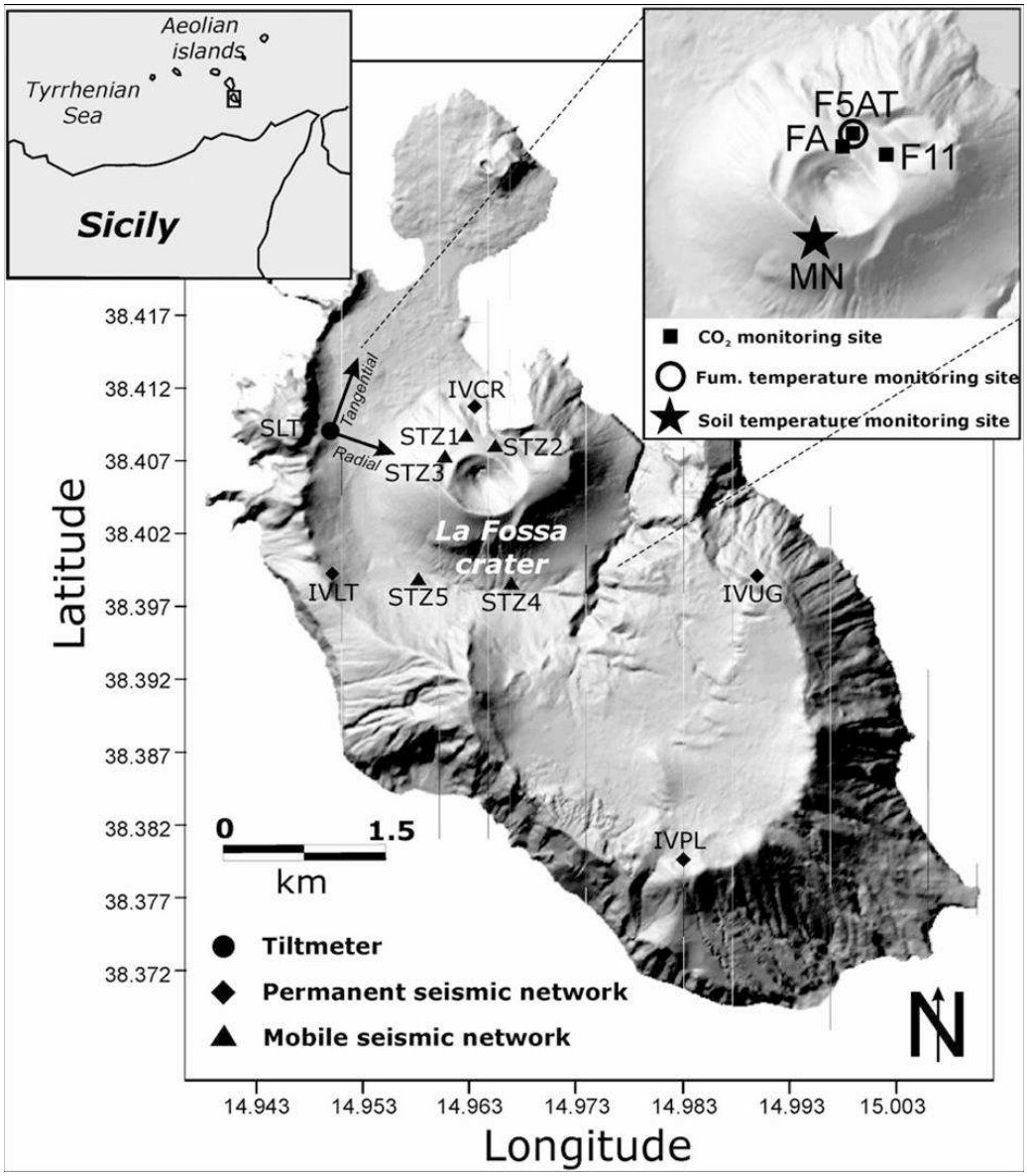

Fig. 5.1 Sketch map of Vulcano island showing the location of the seismic stations, belonging to the permanent and mobile networks, and tiltmeter used in this work (see the key in the lower left corner). In the upper right corner an inset with the location of the monitoring sites of CO_2, fumarole temperature and soil temperature is reported.

5.2 Data analysis

During 2007-2008, seismicity at Vulcano was monitored by a permanent network and mobile seismic stations **(fig. 5.1)**. Before 2007, the permanent network (operated by the Catania Section of Istituto Nazionale di Geofisica e Vulcanologia, INGV), consisted of four analog, 3-component stations (IVCR, IVUG, IVPL and IVLT). Each station was equipped with short period geophones (Geotech S13, 1 s corner period) and acquired at sampling rate of 100 Hz. Successively, the sensors were replaced with digital 3-component broadband Nanometrics Trillium, with flat response in the 40–0.01 s period range. The mobile network was operated jointly by the University of Catania and INGV Catania, and included five digital, 24-bit seismic stations (STZ1, STZ2, STZ3, STZ4, STZ5), equipped with 3-component Lennartz LE-3D (20 s corner period). These stations were deployed on the northern and southern rims of La Fossa **(fig. 5.1)**. Data from the mobile network were acquired at a sampling rate of 125 Hz.

During 2007-2008, about 4000 volcano-seismic events were recorded at Vulcano. According to the classification proposed by Alparone et al. (2010), most events belonged to the High frequency and Monochromatic classes. Moreover, also a large number of TRs occurred. In this paper we focus on 584 TR events (four examples are shown in **fig. 5.2**). The TRs observed at Vulcano exhibit quasi-sinusoidal waveforms characterized by a long duration (30-50 s) due to a very slowly decaying coda **(fig. 5.2)**. These events are characterised by one, or at most a few, narrow spectral peaks, at not necessarily integer harmonic frequencies. Moreover, we noted that some of these events exhibit amplitude modulation effects. The TRs occurrence rate was not steady, but varied significantly over time. The two main increases occurred during July-November 2007 and August-December 2008 when the number of TRs increased from a few events per 10 day windows to over 30 **(fig. 5.3a)**. In the first increase some fluctuations in the number of events took place with two main peaks at the beginning of July and October. Conversely, the second increase was more

"regular" and was characterised by a gradual increase culminating with a peak between the end of September and mid-October, followed by a fairly gradual decrease. Moreover, it is worth noting that while many TR events were observed in 2007-2008, only 15 TRs were recorded during the previous three years, 2004 - 2006 (Alparone et al., 2010). The variation of the TR number over time was compared with the daily number of VT earthquakes, tiltmeter recordings, CO_2 concentration of crater fumarolic emissions, fumarole and soil temperatures **(fig. 5.3)**. A very few VT earthquakes with epicentres within an 10-km-radius area centred on the Vulcano island occurred during 2007-2008 **(fig. 5.3b)**. Moreover, the seismic energy released by these VT earthquakes was very small and the maximum magnitude was equal to 2.7. Finally, no clear relation between TR activity and VT earthquakes can be seen. Tilt recordings at SLT station **(fig. 5.1)** showed only slow long-term variations with no rapid (from hours to days) changes **(fig. 5.3c)** that could suggest important and fast deformation phenomena of the volcanic system (see Gambino et al., 2007 for more details). The monitoring sites of CO_2 and fumarole and soil temperatures are run by I.N.G.V. Sezione di Palermo. The molar percentage of CO_2 in some fumaroles of La Fossa crater **(inset in fig. 5.1)**, increased twice at the same time as TR number increased. The first increase, taking place during the second half of 2007, was more evident than the second one, occurring during the second half of 2008 **(fig. 5.3d)**. Fumarole and soil temperatures during 2007-2008 were measured by monitoring stations located near La Fossa crater **(fig. 5.1)**. The fumarole and soil temperatures were measured by thermocouples (resolution ±0.1 °C) equipped with stainless-steel probes resistant to corrosive acidic gases and datalogger communicating via radio to the data acquisition center. Fumarole temperature mainly changed from 300 up to 450 °C **(fig. 5.3e)**. The seasonal influence cannot account for the main temperature variations, daily variations are small and negligible (<2°C, not shown), while rainfall only caused intense but very short-term disturbs in the time series (see sudden and brief decreases in **fig. 5.3e** and rainfall time series in **fig. 5.3g**). Zones characterised by diffuse

heat flux of hydrothermal origin (Steam Heated Soil; monitoring station MN in **fig. 5.1**) showed surface temperatures ranging from background external values to boiling **(fig. 5.3f)**. In the steam heated soil, steam condenses below the soil surface and this exothermic process warms up the soil more than the conductive and convective heat transfer. Similarly to concentration of CO_2, both fumarole and soil temperatures increased roughly at the same time as TR activity increased **(fig. 5.3e,f)**. However, in 2008 soil temperature increased in March, some months before the 2008 TR increase. To study the features of TRs, we performed: i) spectral analysis using the Fast Fourier Transform (FFT) and Sompi method (Kumazawa et al., 1990); ii) cross correlation analysis among the spectra; iii) polarization analysis; iv) hypocentral location.

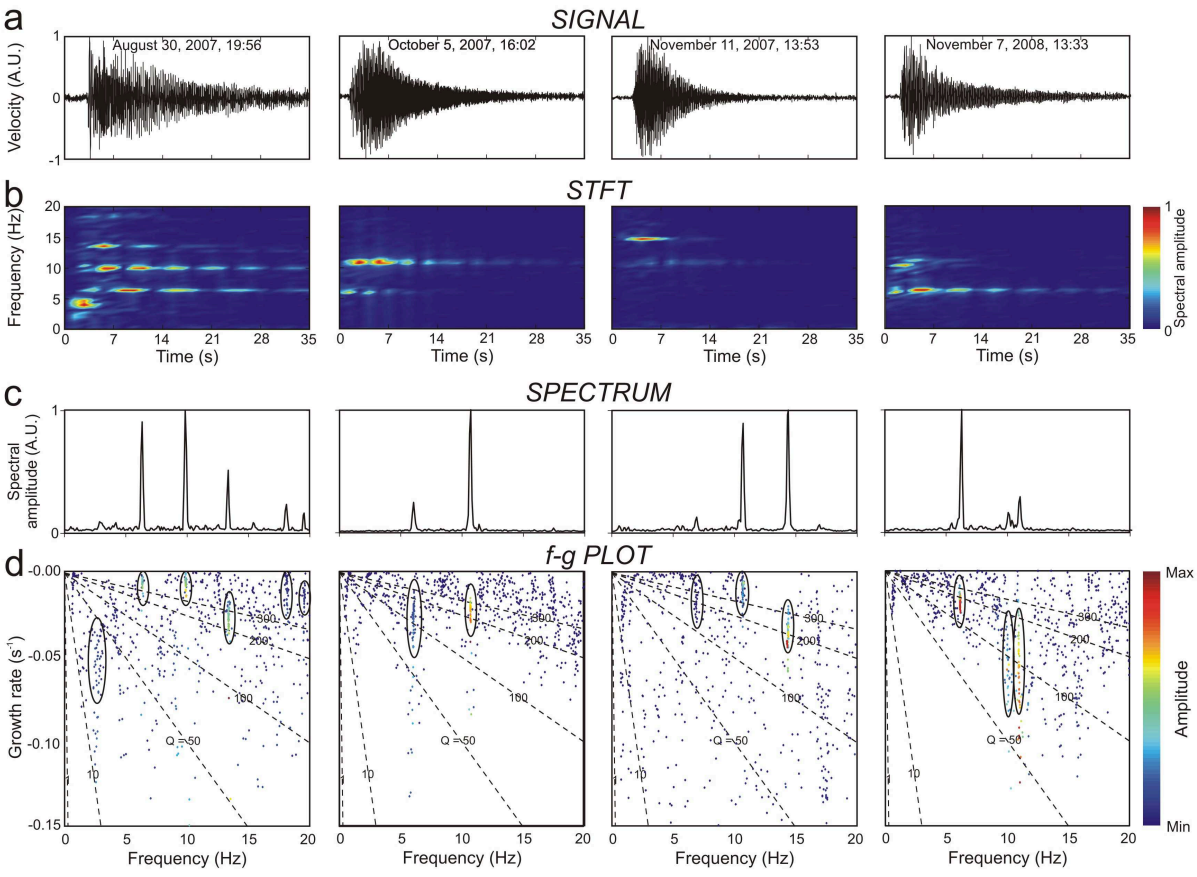

Fig. 5.2 (a) Waveforms, (b) Short Time Fourier Transform (STFT), (c) spectra and (d) f-g plots of four examples of TRs recorded IVCR station. The STFT was obtained by splitting the seismic signal in 2.56-second-long windows with 50% overlap. The spectra and f-g plots were calculated by using 20-second-long windows. The f-g plots were obtained for all the trial autoregressive (AR) orders 4-60. The colour of the dots in (d) indicate the amplitude values of the wave elements (see colour scale). Clusters of dots in (d) (encircled with solid ellipses) indicate dominant spectral components of the signal, scattered dots represent noise.

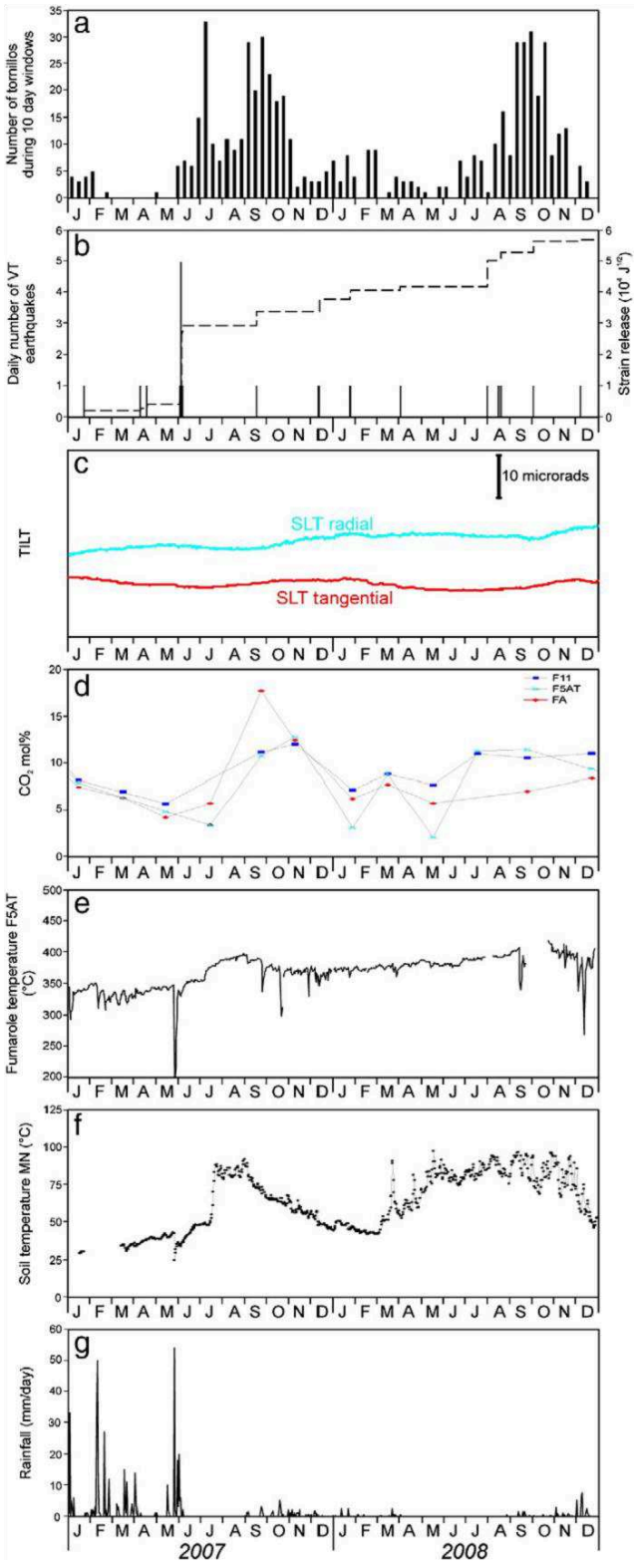

Fig. 5.3 (a) Number of TRs calculated during 10-day-long windows. (b) Daily number of VT earthquakes (histogram) and corresponding strain release cumulative curve (dashed black line). (c) Tilt measurements in the radial and tangential components at SLT station. (d) CO_2 molar percentage in the fumaroles indicated in the upper right corner. (e) Temperature of fluids emitted from F5AT fumarole. (f) Soil temperature at MN station recorded at depth of 0.3 m. (g) Daily amount of rainfall. The locations of the tiltmeter and the monitoring sites of CO_2 and fumarole and soil temperatures are reported in **fig. 5.1**.

5.2.1 Spectral analysis

The spectral characteristics of the LP, VLP events and tornillos recorded in volcanic areas are generally assumed to be related to the geometry of the plumbing system and the features of the fluids it contains (e.g., Chouet, 1996; Almendros et al., 2002; Kumagai et al., 2005). Thus, information about the frequency content of these events and its evolution over time is important for studying and monitoring the dynamics of a volcanic system.

To study the variation of the TRs spectral features over time at Vulcano island, we performed two different frequency domain analyses: FFT and Sompi analysis (Kumazawa et al., 1990, and references therein). Using the former we calculated one spectrum for each event from a 20-second-long window recorded by the vertical component of station IVCR. The window started at the onset of the event. We normalised the spectra of all the events occurring during one day, and averaged them to obtain a daily average spectrum. These daily spectra were visualised as pseudo-spectrograms **(fig. 5.4b)**. The spectra averaging process is justified by the fact that the TR spectral features generally remain steady for a several days at a time, as suggested by the **figure 5.4c**, showing the frequency of the spectral peak with the highest amplitude extracted from the spectra of all the TRs. The FFT analysis shows that most of the TRs are characterised by two sharp spectral peaks at frequencies of about 6 and 10 Hz **(fig. 5.2 and 5.4b,c)**. A few events also exhibited dominant spectral peaks at other frequencies such as 4, 8, 13 and 16 Hz **(figs. 5.2 and 5.4c)**. The frequencies of the two main peaks varied during the two year interval. For example, in August-September 2007 the peak at 10 Hz gradually drifted toward lower frequencies **(see "I" in fig. 5.4b)**, then increased again **(see "II" in fig. 5.4b)**. Later, in March and August 2008 the frequency of this peak decreased suddenly **(see "III" and "IV" in fig. 5.4b).** Moreover, this final change in the spectral content involved both dominant frequency peaks and occurred at the end of August 2008, at the same time as the onset of an increasing trend in the number of the TRs **(fig. 5.4a)**. It is worth noting that the decreases in the TR frequency peak observed in August-

September 2007 and August 2008 took place roughly at the same time as increases in molar fraction of CO_2 and fumarole and soil temperatures **(fig. 5.3d,e,f)**. To obtain information about the decay of the TRs, we applied Sompi analysis (e.g., Kumazawa et al., 1990). In this method of spectral analysis, a signal is deconvolved into a linear combination of coherent oscillations with decaying amplitudes (called wave elements) and additional noise. In this approach we define a complex frequency fc = f – ig which describes each wave element, where f is the frequency, g is the growth rate and i is $\sqrt{-1}$. The quality factor Q is then given as –f/2g. An amplitude value is also calculated for each wave element. Generally, in order to represent a set of complex frequencies, they are plotted on a 2D-plane with f and g axes, called f-g diagram. Wave elements scattering widely in the plot are considered to be noise, while wave elements densely populated on the theoretical frequency lines are considered to be the dominant spectral components of the signal (Hori et al., 1989). The amplitude information (for details about the computation see Hori et al., 1989; Kumazawa et al., 1990) can be added by using a colour scale for the dots **(fig. 5.2d)**. Such amplitude information can be useful to further discriminate noise and dominant spectral components of the signal. Indeed the former and the latter are generally characterised by small and large amplitudes, respectively (Hori et al., 1989). A 10-second-long window from the recording of the IVCR station was analysed for each TR event. The signal was filtered in two frequency bands, 5-8 and 8-12 Hz and the Sompi method was applied to each band. The frequency values obtained confirm the results of the FFT analysis. Moreover, we noted that most of the quality factor values ranged between 20 and 400 in both frequency bands **(fig. 5.4d,e)**. The time distribution of Q values, calculated for the two frequency bands 5-8 and 8-12 Hz, showed no significant pattern **(fig. 5.4d,e)**. A decrease of the dispersion of the Q values for the band 5-8 Hz can be noted in August 2008 **(fig. 5.4d)**, at the same time as the frequency decreases from 6.4 to 5.9 Hz and the occurrence rate of events increases **(fig. 5.4a,b,c)**. As aforementioned, 15 TRs were recorded during the previous three years, 2004 –

2006. These events were mostly monochromatic with a single frequency peak in the band 5.5-8.5 Hz and quality factor values ranging from 50 to 300. It is worth noting that all the TRs occurred during the period November 2004 – June 2005 with the exception of one event taking place on 31 December 2006. This TR, characterised by two spectral peaks with frequencies of 6.5 and 10.1 Hz, was very similar to the events analysed in this work.

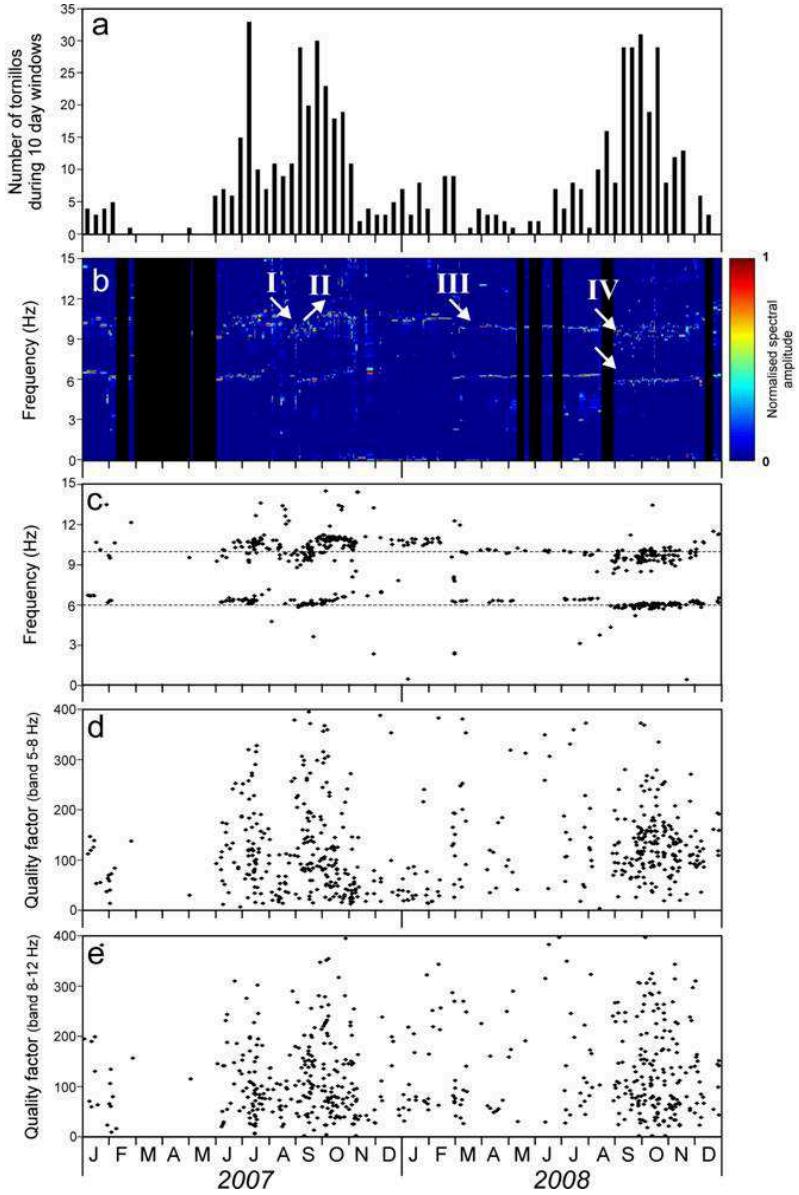

Fig. 5.4 Characteristics of TRs observed at Vulcano. (a) Number of events calculated during 10-day-long windows. (b) Normalised pseudo-spectrogram obtained by the daily average spectra of the TRs at IVCR (see text for details). (c) Frequency of the spectral peak with the highest amplitude at IVCR. (d-e) Quality factor of the seismic signal of IVCR station, filtered in the range 5-8 and 8-12 Hz, respectively, obtained by Sompi method for AR order equal to 2. The black areas in (b) indicate periods with no tornillo recordings. The white arrows and the roman numbers in (b) indicate the main changes in the frequency content. The two dashed horizontal lines in (c) indicate frequency values of 6 and 10 Hz.

5.2.2 Classification

The evolution of the spectral content of the TRs over time was also investigated to group the TRs into families with similar spectral content and better identify time spans characterised by different frequency content of TRs. This method entails the following steps: i) for each event a 20-second-long window starting at the onset of the event was selected from the recording of the vertical component of station IVCR; ii) the spectra of these windows were obtained by averaging spectra calculated on 10-second-long windows with 50% overlap; iii) a cross correlation matrix was obtained by comparing the spectra using cross correlation; iv) a master spectrum was selected as the spectrum which had the largest number of cross correlation coefficients above a fixed threshold; v) an average spectrum for the family was found by stacking all spectra that were well-correlated with the master spectrum (cross correlation coefficient > fixed threshold); vi) this stacked spectrum was then cross-correlated with the original dataset, and all the spectra with a cross correlation coefficient greater than the threshold were grouped into a family; vii) the steps iv)-vi) were repeated until the entire matrix was classified into distinct groups. In this procedure, overlap between clusters was not allowed. In fact, once a spectrum was assigned to a given group, it was removed from the correlation matrix. The threshold of the cross correlation value was fixed equal to 0.7. This method is similar to that proposed by Green and Neuberg (2006) and used to compare volcano-seismic or infrasonic events (e.g., Patanè et al., 2008; Cannata et al., 2009a,b), but it is applied in the frequency domain. Indeed, we are mostly interested in investigating the time evolution of the spectral content of the TRs, that, as aforementioned, may be related to variations of the plumbing system geometry and the features of the fluids it contains (e.g., Chouet, 1996; Almendros et al., 2002; Kumagai et al., 2005).

In all, for the fixed cross correlation threshold of 0.7 eight families with more than 20 members were found, containing more than 50% of all the events **(fig. 5.5)**. This implies the repetitive excitation of stationary sources in a

nondestructive process. The families show spectra with different features: monochromatic spectrum with a frequency peak at about 6 or 10 Hz, and events with both these peaks. Moreover, as already noted by the spectral analysis **(see section 5.2.1)**, the stacked spectra show a time evolution of the spectral features. Indeed, during 2007 and in particular during the first TR number increase (July-November 2007), most events were characterised by the dominant peak at about 10 Hz, as suggested by the time distribution and stacked spectra of the families 4, 6, 7 and 8. Conversely, the stacked spectra of the families 1 and 2, whose events mainly occurred during the second half of 2008, showed the dominant peak at about 6 Hz.

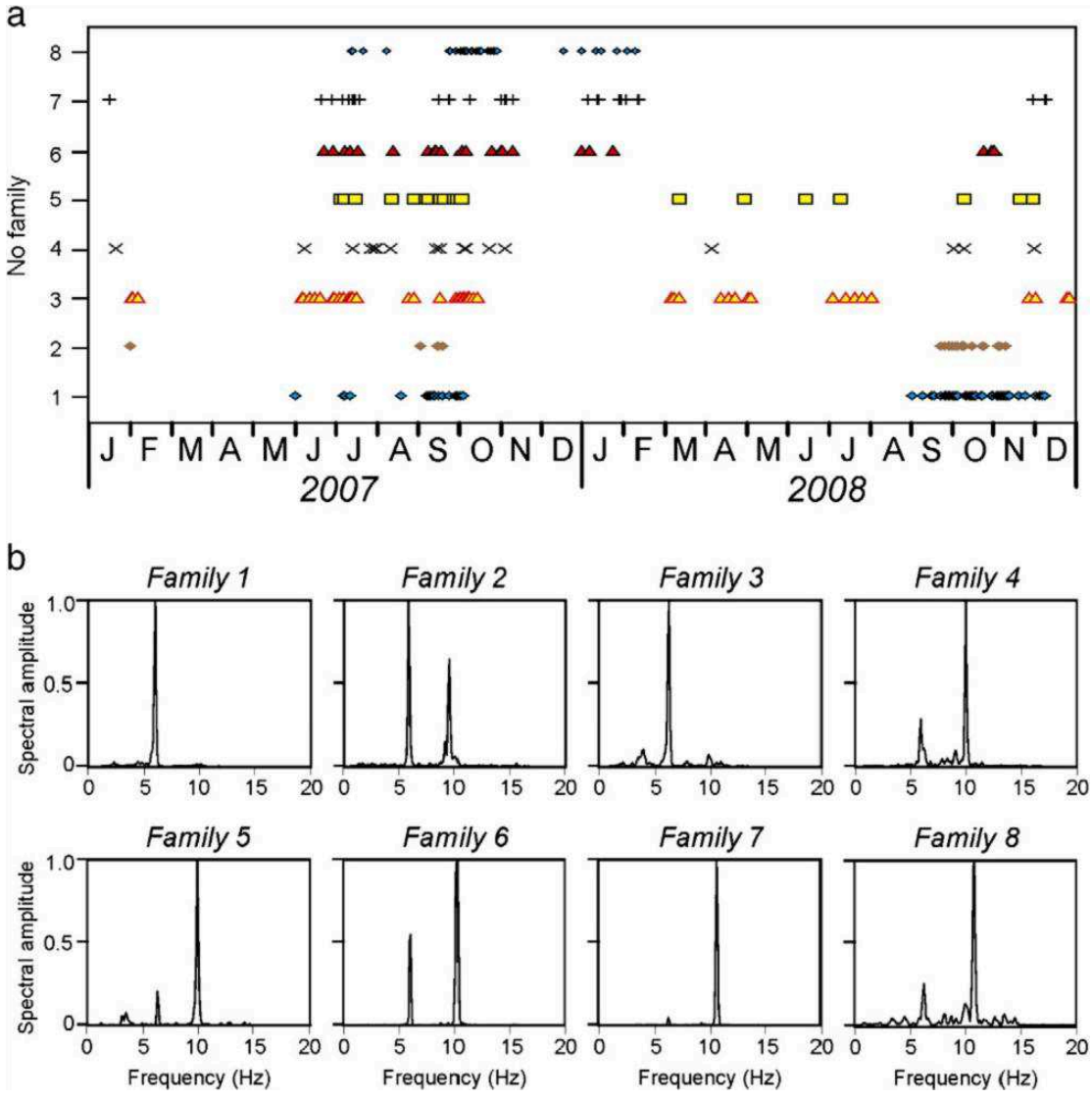

Fig. 5.5 (a) Time distribution of the TRs belonging to the families obtained classifying their spectra by cross correlation function. (b) Average spectra of the families of TRs.

5.2.3 Polarization analysis

In earthquake seismology polarization analysis is able to provide important information about the wave types composing the wavefield and the seismic source location and mechanism (e.g., Alessandrini et al., 1994). However, in volcano seismology polarization analysis cannot necessarily be used for these objectives because of the heterogeneities and rough topography of volcanoes (e.g., Neuberg and Pointer, 2000). On the other hand, as demonstrated by Hellweg (2003) analysing TRs at Galeras, this kind of analysis can be useful to detect even very small variations in location and/or source mechanism. This is especially true for TRs at Vulcano because of their very high number during the studied 2-year-long period.

For each event, a 15-second-long window starting at the onset was selected and filtered in two frequency bands 5-8 and 8-12 Hz. Polarization was determined from non-overlapping, 0.5-second-long windows using eigenvalue decomposition of the covariance matrix of the three components of ground motion (Jurkevics, 1988). Then, we investigated not only the variation of the polarization parameters (azimuth, inclination and rectilinearity) from the onset to the tail of each event, but also noted polarization changes from event to event. In **fig. 5.6b-g** such variations are graphed for the frequency bands 5-8 and 8-12 Hz by using plots with the event number in temporal order in x-axis, the time elapsed during the aforementioned 15-second-long windows in y-axis, and finally the polarization parameters reported with the colour scale. The variations of the polarization parameters from the onset to the tail of each event and the ones from event to event are shown as vertical and horizontal colour changes, respectively. In **fig. 5.6a** the pseudo-spectrogram, composed of the spectra of the 584 TRs recorded at the vertical component of IVCR, calculated by 20-second-long windows, is also reported to compare the wavefield time variations with the spectral changes. The polarization in the band 8-12 Hz was much more complicated than in the band 5-8 Hz and no clear patterns are present. By contrast, the band 5-8 Hz does exhibit some patterns.

Inclination and the rectilinearity coefficient were generally greater than 60° and 0.6, respectively, and remained quite stable during each event. In contrast, azimuth showed greater variation during each individual event. On the basis of the azimuthal variation from the onset to the tail of each event, we subdivided the TRs into three segments. The initial segment, comprising the onsets of the TRs, roughly 1-second-long, was characterised by azimuths between 120°-150° for the whole 2-year period. The second segment, again lasting about 1 second, showed values of about 350°, from the beginning of 2007 through August 2008 with the exception of the month of September 2007. In the remaining periods the azimuth in this segment ranged between 30° and 60°. Finally, the third segment, comprising almost the entire tail of the events, exhibited azimuth values depending strictly on the period. Therefore, periods of steady polarization values, reflecting the repetitive source mechanisms and location, alternated with important variations, highlighting changes over time of TRs mechanisms and/or locations. These changes took place at the same time as the spectral changes **(fig. 5.6a-d)**. Moreover, as previously mentioned, changes can also be noted within the individual events.

Based on the polarization analysis, the wavefield in the frequency band 5-8 Hz of four representative TRs was investigated in detail **(figs. 5.7; 5.8)**. Polarization parameters and particle motion were obtained from 0.5-second-long windows. For each of these four events the particle motion was plotted for three windows coinciding with the three segments of TRs described above.

This detailed analysis confirms that wavefield changes are observed not only within individual TRs but also among different ones during the two years described here.

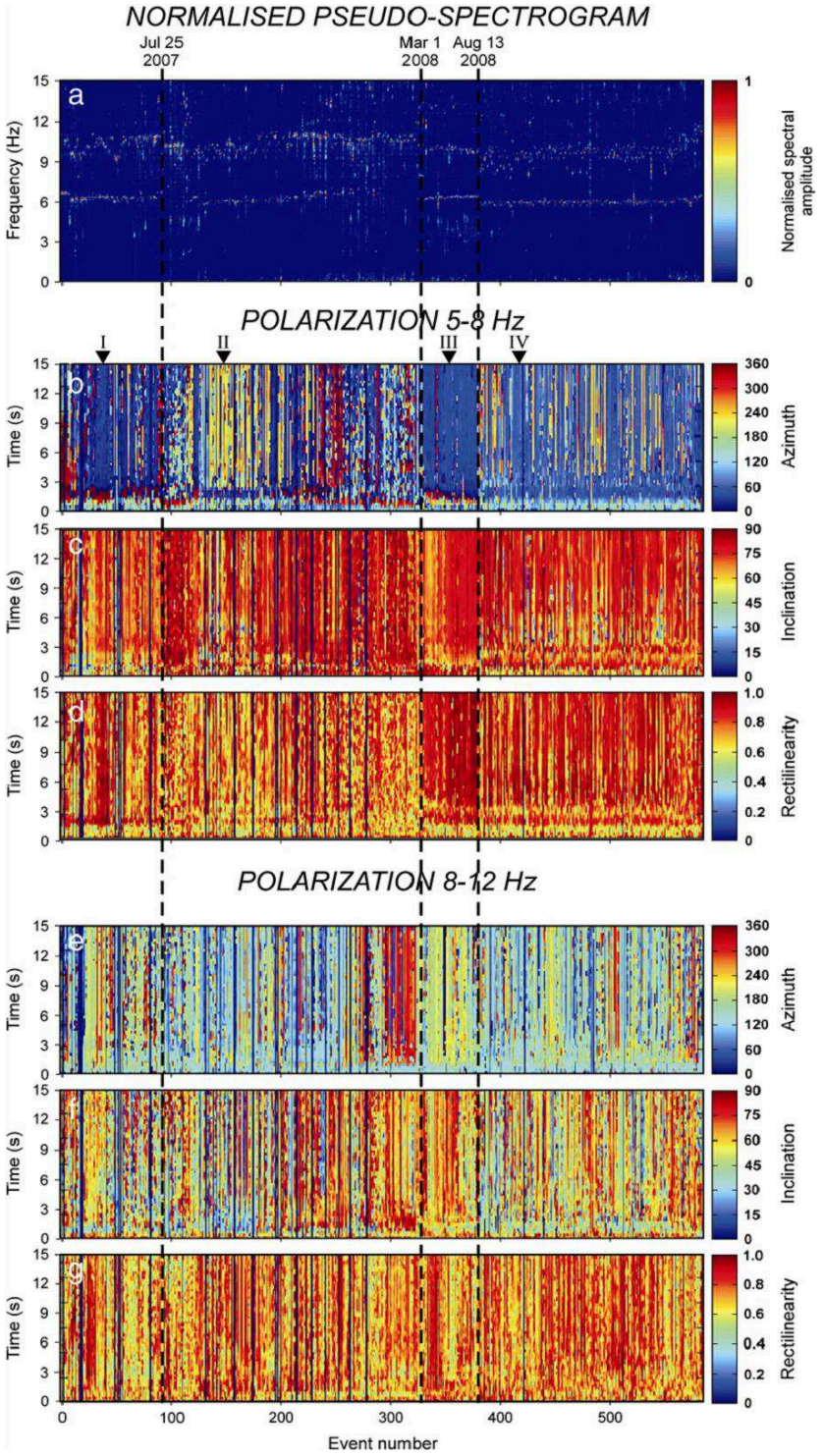

Fig. 5.6 (a) Normalised pseudo-spectrogram, composed of all the spectra of the 584 TRs recorded at IVCR.(b-g) Time variation of the polarization parameters of the TRs recorded by IVCR station and filtered in two frequency bands 5-8 and 8-12 Hz. The event number in temporal order is reported in x-axis, the time elapsed from the onset to the tail of the event in y-axis and the polarization parameters are depicted with the colour scale. The polarization variations during a single event and from event to event are reported along the vertical and horizontal direction, respectively. The black triangles and the Roman numbers at top of (b) indicate the events whose polarization parameters and particle motion are plotted in **figs. 5.7; 5.8**. The dashed black lines and the dates reported at top of (a) indicate the time of the main spectral and polarization changes.

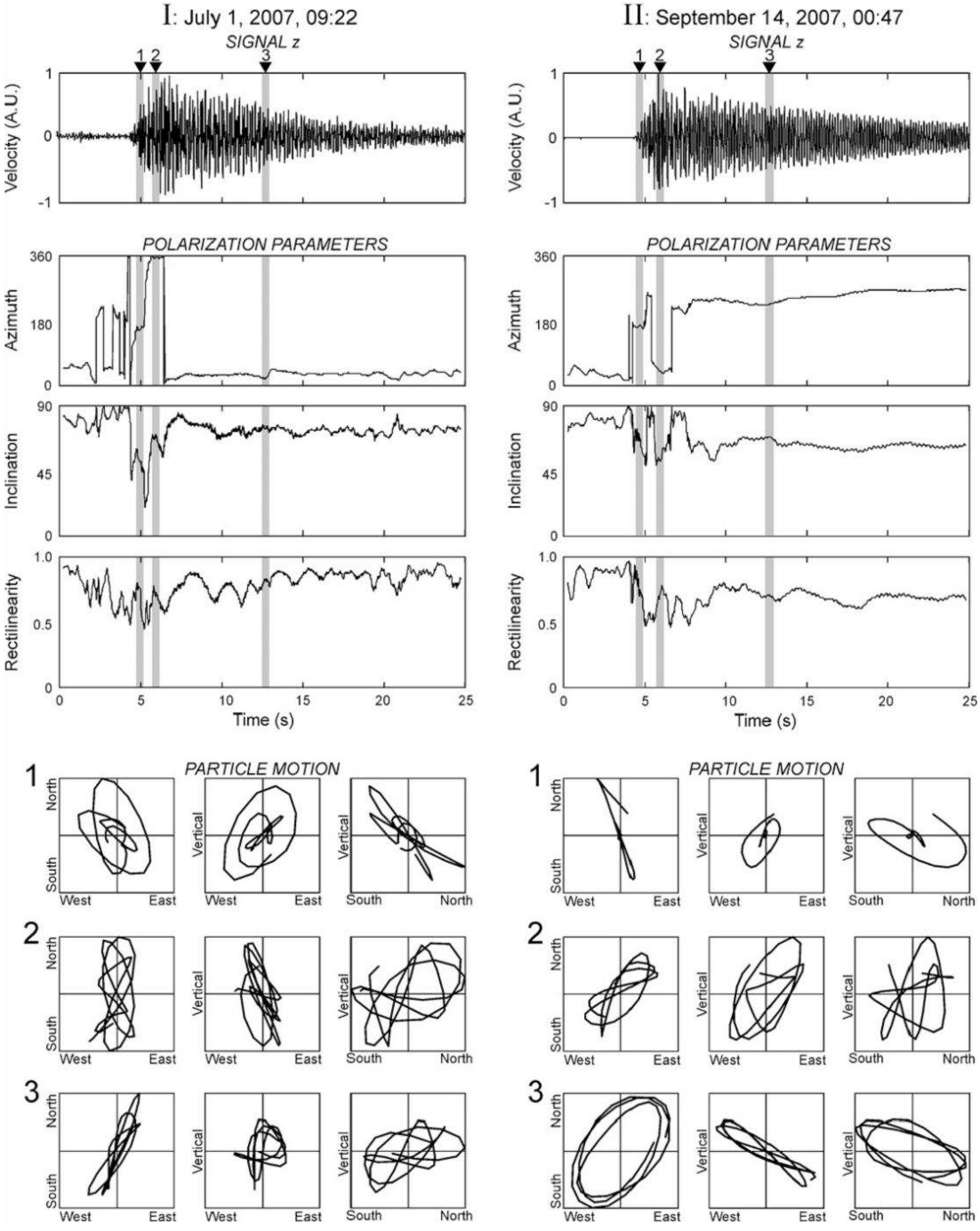

Fig. 5.7 Polarization parameters and particle motion plots of examples of two TRs, filtered in the frequency band 5-8 Hz (see **fig. 5.6** and corresponding caption).

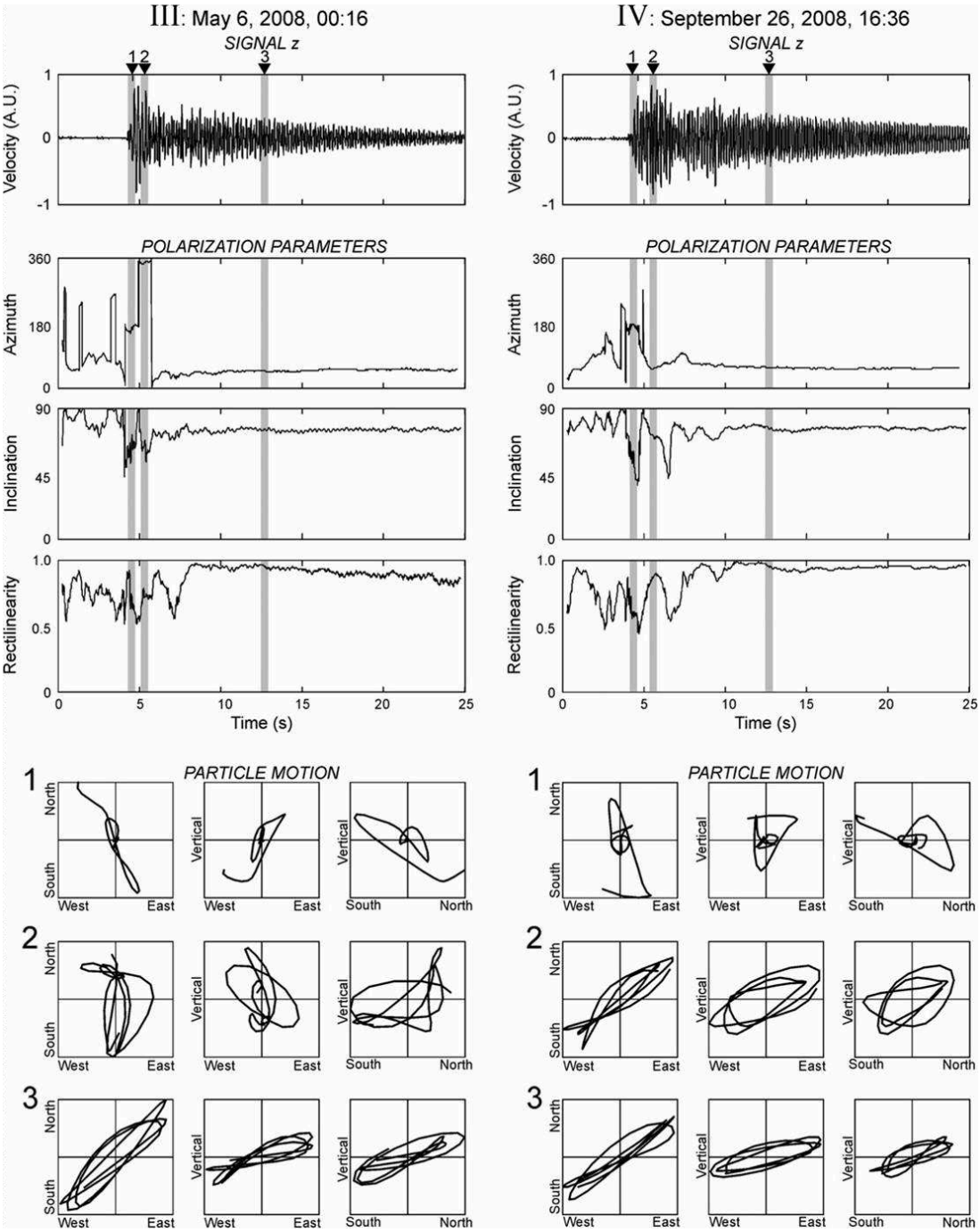

Fig. 5.8 Polarization parameters and particle motion plots of examples of two TRs, filtered in the frequency band 5-8 Hz (see **fig. 5.6** and corresponding caption).

5.2.4 Source location

Using the program HYPOELLIPSE (Lahr, 1989) and the velocity model from Falsaperla et al. (1985), we located about 30 TRs, which were selected for their high signal to noise ratio and clear first arrival, and for having an azimuthal gap less than 190°.

The spatial distribution of these events is shown in **fig. 5.9**. We note that the seismic sources were mainly clustered beneath La Fossa crater at very shallow depths, which ranged from 0.1 to 1 km b.s.l. The fact that TRs are recorded clearly only at the stations nearest to La Fossa crater also indicates that their source is shallow. These source locations are consistent with the locations of the volcano-seismic events recorded during 2004-2006 and reported in **chapter 4**.

The mean horizontal and vertical uncertainties of 0.4 km do not allow to reliably recognize significant time changes (if any) of the TR source locations.

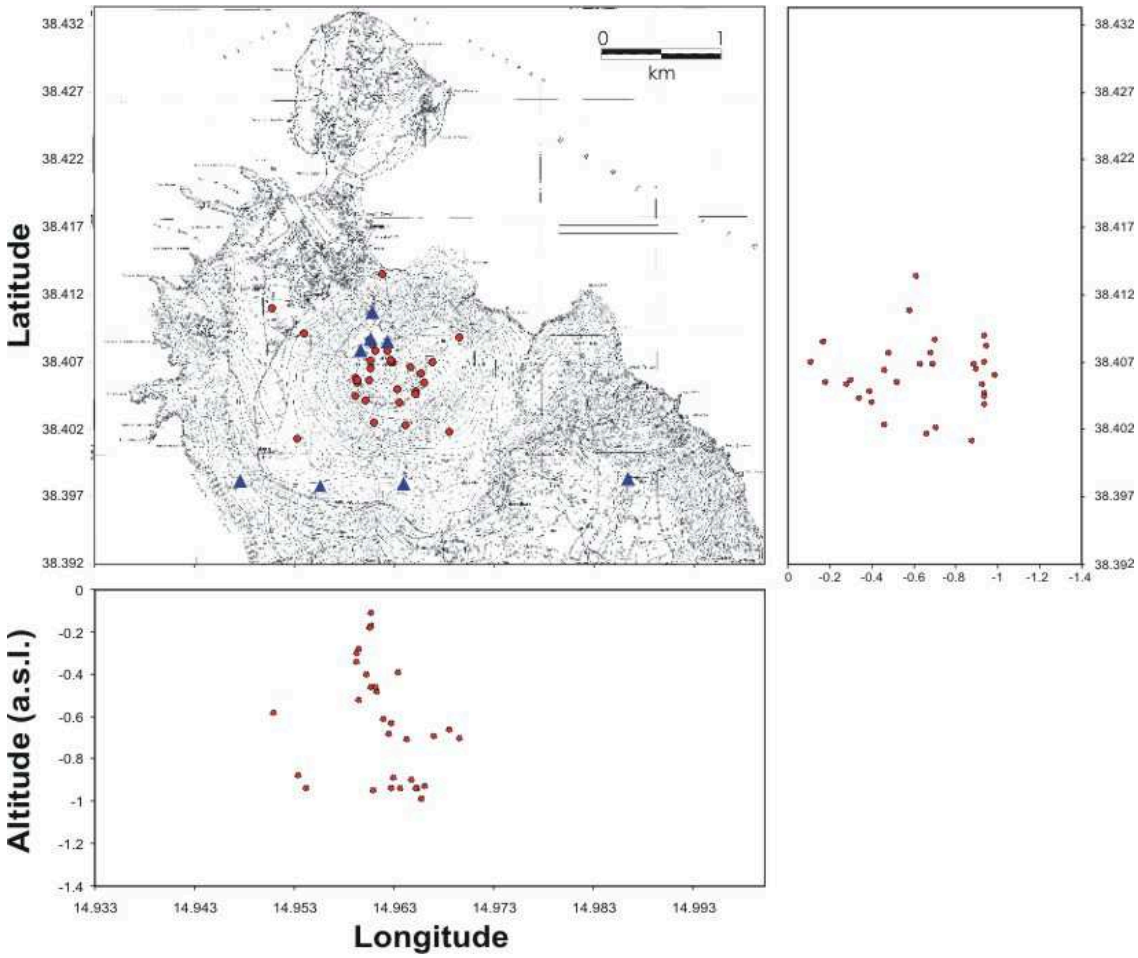

Fig. 5.9 Space distribution in map and sections of the locations of about 30 TRs (red dots). Blue triangles in map indicate the seismic stations.

5.2.5 Amplitude modulation

Several TRs at Vulcano exhibited amplitude modulation, as previously observed at other volcanoes (e.g., Galeras, Gomez and Torres, 1997). We focused on this phenomenon by analysing two TRs, recorded on October 5, 2007, and February 29, 2008 **(fig. 5.10a-d)**. The dominant spectral peaks for these two events were at 6.4 and 7.8 Hz, respectively **(fig. 5.10e-h)**. The former TR was mainly monochromatic **(fig. 5.10e,g)**, while the latter was also characterised by many other minor spectral peaks at 2.3, 6.2, 12.4, 13, 13.7 Hz **(fig. 5.10f,h)**.

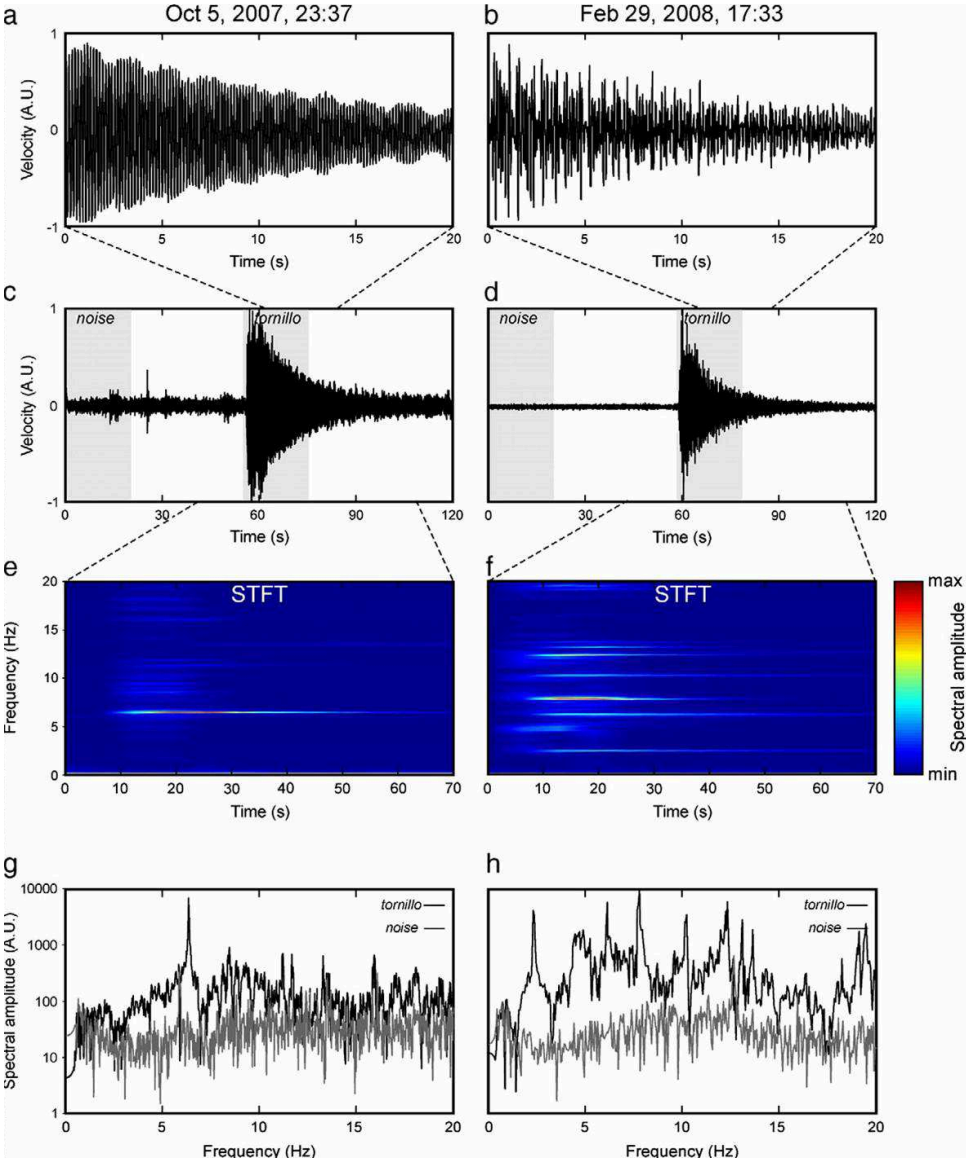

Fig. 5.10 TRs recorded on October 5, 2007, (a,c) and February 29, 2008, (b,d) at the vertical component of IVCR station. (e,f) Short Time Fourier Transform (STFT) of 70-second-long seismic windows containing TR waveforms calculated by using 10-second-long sliding windows with 50% overlap. (g,h) Spectra of the signal windows comprised in the grey areas in (c,d) (see legend in the right upper corner).

Both RMS envelopes calculated at the three components and polarization parameters clearly exhibited periodic oscillations (**fig. 5.11b,c,** respectively). In order to quantitatively investigate these periodicities, spectra of the RMS and rectilinearity coefficient time series were calculated using FFT **(fig. 5.11d)**. They exhibited spectral peaks at various frequencies. It is worth noting that the same modulation frequencies are present in both the polarization and RMS time series. In particular, the spectrum of the former TR has a single peak at 0.5 Hz, while the latter has several peaks, the dominant one at 1.6 Hz.

The observed amplitude modulation has at least two possible explanations: i) slow waves along the interface of the crack and ii) beating. According to the former hypothesis, a slow wave, travelling along a fluid-filled conduit (or crack), reaches the ends and is partially reflected back and partially transmitted into surrounding rocks (Jousset et al., 2003; Sturton, 2003). This process gives rise to subevents causing amplitude modulations (Sturton and Neuberg, 2006). Another explanation for amplitude modulation is beating, namely the alternating constructive and destructive interference as two (or more) waves having slightly different frequencies interact with one each other. In this case the frequency of amplitude modulation equals the difference between the initial two frequencies. In our case, the second explanation seems to be the most likely. In fact, the modulation frequency of the event occurring on February 29, 2008 (1.6 Hz; **fig. 5.10b,d,f,h**) is equal to the difference between the spectral components at 6.2 and 7.8 Hz. Although the event of October 5, 2007, is mainly monochromatic, the same process can also be invoked for it. Indeed, the background noise, recorded before the onset of the TR, showed a sharp spectral peak at 5.9 Hz **(fig. 5.10a,c,e,g)**. The noise waves, interacting with the TR ones peaking at 6.4 Hz, gave rise to the amplitude modulation at 0.5 Hz **(fig. 5.11)**. It is also worth noting that the modulation is especially visible during the tail of TR, when the event amplitude is lower. Assuming that the amplitude of noise remains steady during the whole TR duration, such feature could be related to the lower amplitude difference between noise and TR. Indeed, the amplitude modulation due to beating is more effective when the two frequency components have

similar amplitude. Thus, this observation is a further indication of beating between noise and TR waves as the cause of the observed amplitude modulation in the TR.

In order to further investigate the amplitude modulation caused by beating and its effects on the polarization parameters, we calculated synthetic TRs by using the following equation (Seidl and Hellweg, 2003):

$$x(t) = \frac{1}{\omega_0'} e^{(-q_0 t)} \sin(\omega_0' t) \tag{5.1}$$

where ω_0' is the angular frequency, q_0 is the ratio between the angular frequency and the quality factor multiplied by 2. We performed two different tests generating synthetic signals mimicking the two previously analysed TRs recorded on October 5, 2007, and February 29, 2008. In the first test we calculated a synthetic TR event with frequency of 6.4 Hz, and summed it with a monochromatic noise with frequency of 5.9 Hz **(fig. 5.12a,b,c)**. As shown by the spectra in **fig. 5.12f**, the amplitude ratio between synthetic TR and noise is equal to the one calculated for the recorded TR and noise **(fig. 5.10g)**. The three components of TR and noise were generated so as to be characterised by different wavefield features. As observed in the event recorded on October 5, 2007 **(fig. 5.11a,b)**, the amplitude modulation is evident especially in the tail of the event, that is, when noise and TR show similar amplitudes **(fig. 5.12c,d)**. Likewise, the polarization parameters exhibit evident cyclic variations in the TR tail with the same modulation frequency as the RMS envelope **(fig. 5.12e)**. This behaviour is very clear in the rectilinearity time series. A similar modulation pattern of polarization parameters was observed in the recorded TR event **(fig. 5.11c)**. In the second test, we created a TR by summing two synthetic TRs with the same polarization features and frequency peak of 6.2 and 7.8 Hz **(fig. 5.13a,b,c)**. Also in this case, the amplitude ratio of these two synthetic TRs is equal to the one obtained for the two highest peaks of the recorded TR **(fig.**

5.10h). Unlike the first test, the modulation of amplitude is also well evident at the onset of the event **(fig. 5.13c,d)**, as observed in the TR recorded on February 29, 2008 **(fig. 5.11a,b)**. Moreover, also in this case, the polarization parameters show periodic changes with the same modulation frequency as the RMS envelope **(fig. 5.13e)**.

In summary, the synthetic tests showed that the beating phenomena can be responsible for the modulated amplitudes of both the analysed TRs recorded on October 5, 2007 and on February 29, 2008. Furthermore, it was also clearly shown that the periodic variations of the polarization parameters, sharing the same modulation frequency as the amplitude of the waveforms, were simply due to the interference of two or more sinusoids (either decaying or steady) either with or without different wavefields.

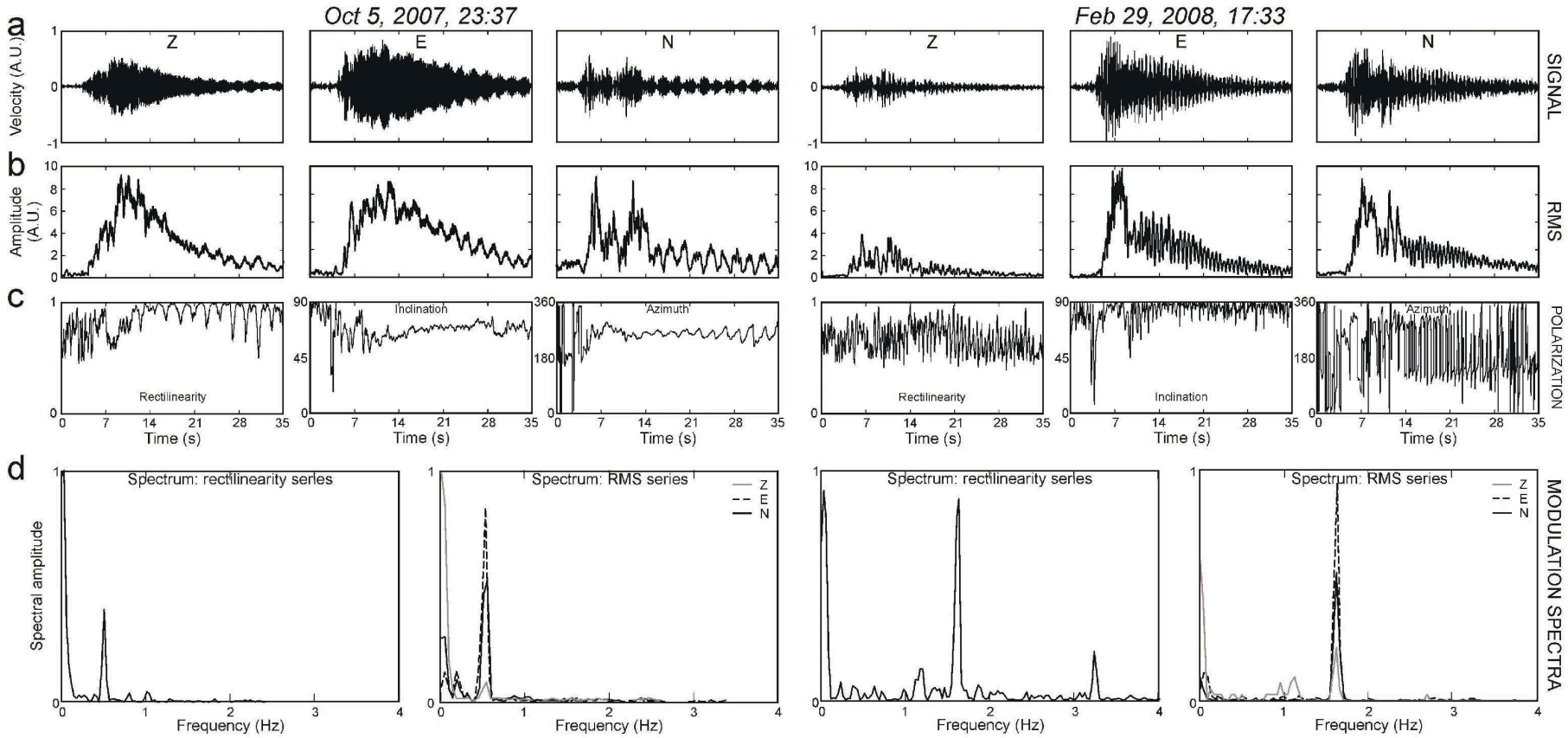

Fig. 5.11 (a) TRs recorded at the three components of IVCR station on October 5, 2007, and February 29, 2008. (b) RMS envelopes and (c) polarization parameters of the TRs shown in (a). (d) Spectra of the RMS envelopes and rectilinearity series shown in (b) and (c), respectively. The RMS envelopes were calculated by using 0.25-second-long moving window, sliding by one sample (0.01 s). The polarization parameters were computed by Jurkevics method (Jurkevics, 1988) on 0.25-second-long moving windows sliding by 0.01 s.

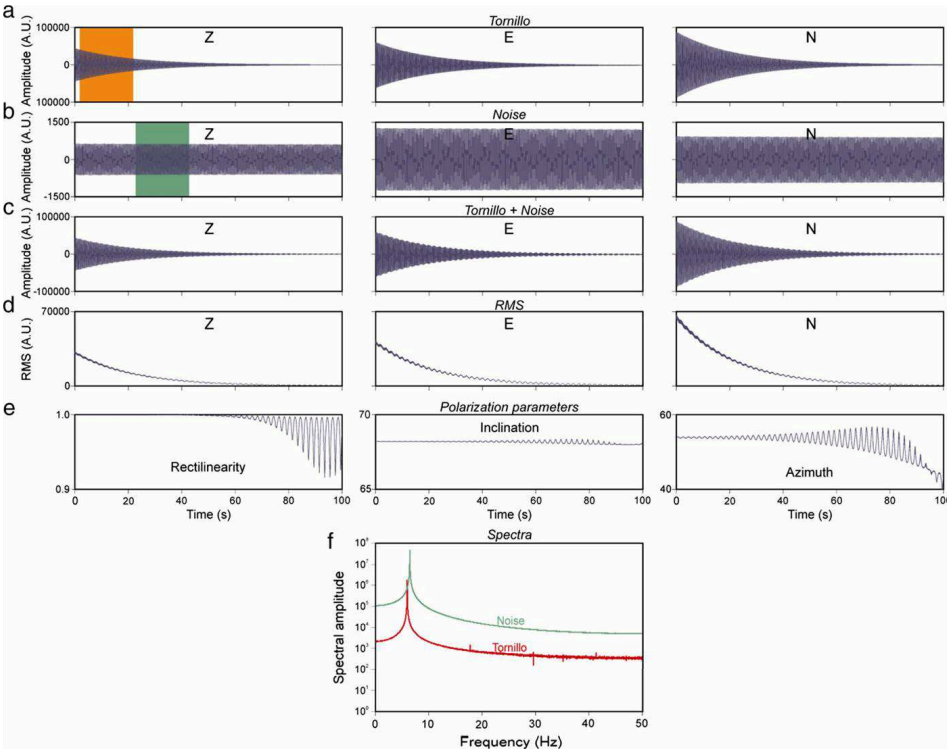

Fig. 5.12 (a) Synthetic tornillo, (b) synthetic monochromatic noise, (c) stacked tornillo and noise, (d) RMS envelopes, (e) polarization parameters and (f) spectra of the windows of signal comprised in the orange (tornillo) and green (noise) areas in (a) and (b), respectively (see **section 5.2.5** for details).

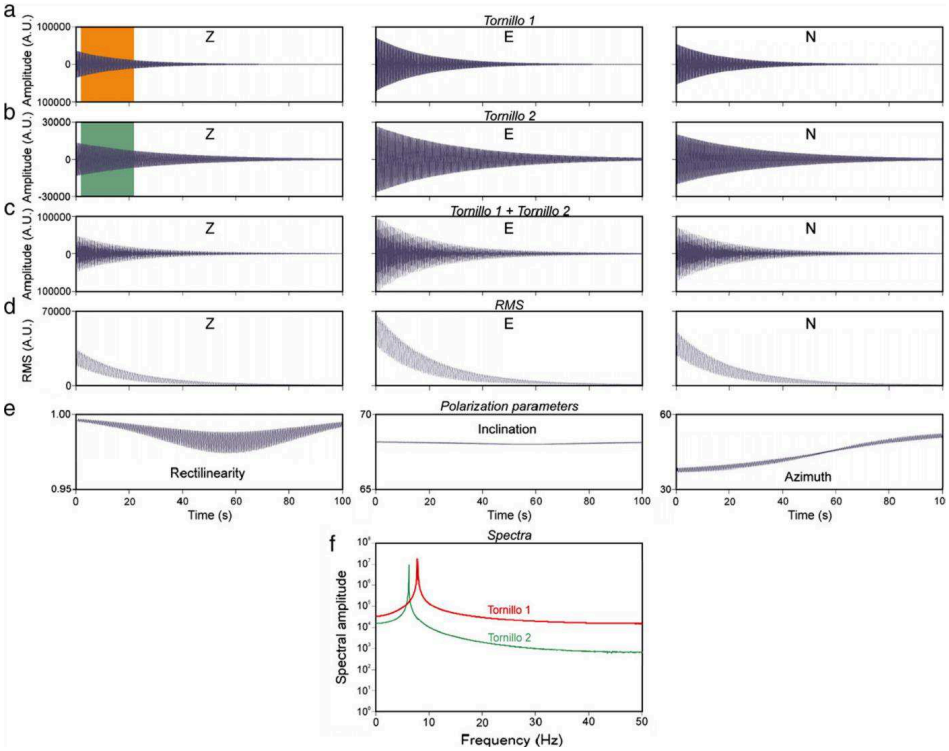

Fig. 5.13 (a,b) Synthetic tornillos, (c) stacked tornillos, (d) RMS envelopes, (e) polarization parameters and (f) spectra of the windows of signal comprised in the orange (tornillo 1) and green (tornillo 2) areas in (a) and (b), respectively (see **section 5.2.5** for details).

5.3 Discussion

Geochemical data clearly demonstrate the existence of active hydrothermal fluid circulation beneath La Fossa crater of Vulcano, at depth of 500 up to 2000 m b.s.l. (Chiodini et al., 1993; Nuccio et al., 1999; Di Liberto et al., 2002). Vapor-dominated zones develop centrally below the crater, where mixed magmatic and hydrothermal fluids rise and feed the fumarolic emissions. When moving from the central column toward the periphery, liquid phase becomes stable and probably coexists with vapour at depth (Nuccio et al., 1999). Volcano-seismic events, related to the hydrothermal activity, are recorded at very shallow depth below La Fossa crater (0.2-1.1 km b.s.l.). A particular kind of volcano-seismic events at Vulcano, characterised by very long duration (30-50 seconds) and sharp spectral peaks, are the tornillos (TRs). In 2007-2008, there was a strong increase in the number of TRs, and, in particular, their number increased twice during this time, in July-November 2007 and August-December 2008 **(fig. 5.3a)**. The very few VT earthquakes with low magnitude, occurring during this period, together with the lack of sharp and important changes in the tilt recordings suggest that such increases of the TR number are not due to magma intrusions within the shallow hydrothermal system **(fig. 5.3b,c)**. At the same time as TR number increased, increases in temperature and CO_2 content of crater fumaroles, as well as soil temperatures, were observed **(fig. 5.3d,e,f)**. The TR sources are mainly clustered below La Fossa crater, at very shallow depth, between 0.1 and 1 km b.s.l. **(fig. 5.9)**. At these depths rock has been weakened by processes associated with hydrothermal circulation, as suggested by aeromagnetic data (Blanco-Montenegro et al., 2006) and electrical resistivity profiles (Revil et al., 2008).

Different source models have been proposed for TRs by various authors. The simplest physical explanation is free eigenvibrations of a fluid volume within a crack or a conduit (e.g., Molina et al., 2008). The resonating fluid-filled crack model is able to explain the presence of more than one spectral components at not equally spaced frequencies as the ones observed in the TR taking place on

February 29, 2008 **(fig. 5.10b,d,f,h)**. There are also nonlinear models in which TRs are initial transients leading into a tremor sequence generated by a nonlinear, self-excited oscillator (Seidl and Hellweg, 2003). In any case, it is clear that fluids play an important role in generating TRs. In view of this, a relationship can be inferred between the increases in the number of TR and the contemporaneous increases in the molar fraction of CO_2 and fumarole and soil temperatures **(fig. 5.3d,e,f)**. Indeed, geochemical anomalies are interpreted as due to an increased involvement of magma-derived fluids in the feeding system of fumaroles (Nuccio et al., 1999), which commonly accompanies notable increases of the fumarolic fluid output (Bukumirovic et al., 1997; Granieri et al., 2006). Ultimately, it means that the hydrothermal fluid circulation below the crater increases during the anomalies, especially in the vapour-dominated zone. The circulating fluids, in turn, penetrate cracks and conduits producing more TRs. Similar interpretations were given by Triastuty et al. (2009) to explain the simultaneous increase of both number of monochromatic events and fumarolic temperature in 2006 at Kuchinoerabujima volcano: the intrusion of hydrothermal fluids into cracks may trigger monochromatic seismicity and fumarolic temperature increase.

If the TR source is assumed to be represented by free eigenvibrations of a fluid volume within a crack or a conduit (e.g., Molina et al., 2008), characteristic properties of the resonator system can be determined from the complex frequencies (frequency f and quality factor Q) of the decaying harmonic oscillations. It has been recognized that the complex frequencies of long period events and TRs recorded at many volcanoes vary in time (e.g., Gomez and Torres, 1997; Kumagai and Chouet, 1999; Nakano and Kumagai, 2005; Patanè et al., 2008; Alparone et al., 2010). Their variations are of particular importance for diagnosing the state of fluids within the resonator. Following Kumagai and Chouet (2000), the high Q values observed at Vulcano (up to 400; **fig. 5.4d,e**) may only be observed if the material in the crack is a mixture of ash and gas or a misty gas composed of water droplet-steam mixture with gas-volume fraction larger than 90%. In order to obtain such long-lasting oscillations, a large

velocity contrast between fluids and the surrounding rock is required. The shallow depth of the TR sources (< 1 km) does not allow to exclude either two fluid kinds and also suggests that the fluids in the resonator should be related to the hydrothermal system. Two changes in the spectral features of the TRs, occurring in August-September 2007 and August 2008, consisted in decreases of the frequency peaks **(fig. 5.4b,c)**. Similar frequency peak changes were also observed at Galeras before eruptions, and were interpreted as the result of an increase in the gas fraction in the source region (Torres et al., 1996; Gomez and Torres, 1997). This is because, when the gas content within a crack increases, the speed of sound and therefore also the resonant frequencies decrease. At the same time the impedance contrast between the region of fluids and the surrounding rock increases, increasing the apparent Q value (Hagerty and Benites, 2003). However, the Q values calculated for TRs at Vulcano do not allow recognising any significant patterns, probably because of uncertainty and instability that derive from fitting exponentially decaying oscillations in the Sompi analysis. Such a problem was also encountered in other works (e.g., Molina et al., 2004). Taking into account the two proposed kinds of fluid contained in the resonating crack and justifying the very high Q values, in the case of misty gas the observed changes might be interpreted as an increase of the liquid phase fraction (e.g., Kumagai and Chouet, 2000; Kumagai et al., 2002; Nakano and Kumagai, 2005). On the other hand, in the case of a mixture of ash and gas, a relative increase of ash particles may be responsible for decreases of the frequency peak values (e.g., Kumagai and Chouet, 2000; Molina et al., 2004). The presence of ash can be caused by either fragmentation of magma in the conduit or interactions magma-water or rock-water, that are generally accompanied by explosive activity. Since there is no evidence of such phenomena at Vulcano during the studied period, the first proposed fluid mixture (water droplet-steam mixture) seems to be the most reasonable. It is also worth noting that the two aforementioned decreases of frequency peaks, occurring in August-September 2007 and August 2008, took place at the same time as increases of temperature and CO_2 content in fumaroles, as well soil

temperatures **(fig. 5.3d,e,f)**. Therefore, beyond changes in the relative contribution of the components of the aforementioned mixtures, also these geochemical and temperature variations can modify the acoustic properties of the resonating crack. For instance, increasing temperature and pressure of the misty gas can cause a decrease of the resonance frequency and an increase of the quality factor (Kumagai and Chouet, 2000). The changes in the spectra, also highlighted by the variability of the stacked spectra obtained by the cross correlation analysis **(fig. 5.5b)**, indicate important variations in the characteristics of the hydrothermal fluids, and hence suggest an unsteady and dynamic hydrothermal system. This is also supported by the increase in the number of events taking place at the same time as the spectral variations **(fig. 5.4)**. Changes in the frequencies of the dominant peaks of TRs or LP events, accompanied by changes in their occurrence rate, similar to those taking place at Vulcano, have also been observed at other volcanoes, such as Tongariro in 2001 (Hagerty and Benites, 2003), Tungurahua in 2001 (Molina et al., 2004) and Galeras in 1993 (Gomez and Torres, 1997). At Tongariro no changes in the volcanic activity occurred after such variations in number and spectral features of TRs or LP events, whereas ash emission eruptions took place in the two other cases.

The spectral variations are accompanied by wavefield changes **(figs. 5.6; 5.7; 5.8)**. As also shown for other volcanoes (e.g., Galeras, Hellweg, 2003; Tongariro, Hagerty and Benites, 2003), the wavefield associated with the TRs is complex, and its constituent wave types are difficult to determine. In fact, several phenomena affect the polarization of seismic waves, particularly at high frequencies, such as the reflection at the free surface, topography, anisotropy along the path and scattering in the medium (Hellweg, 2003). In addition to the wavefield variations noted among the different TRs, the particle motion also changes during the course of an individual event. As suggested by Hellweg (2003), if the source of the seismic waves moves, the polarization observed at the receiver will change as a function of time. In fact, small changes in the location of the source may produce large variations in the polarization

parameters if high frequencies and their concomitantly short wavelength are taken into account. Therefore, both the observed wavefield variations (within a single event and among all the events) may be related to small changes in the source location. In view of the possible migration of the vapour-dominated hydrothermal zones as resulting from the geochemical studies (see above), such changes in the source location among all the events would seem reasonable. For instance, Giudicepietro et al. (2009) attributed the changes in the polarization parameters of VLP events observed during the 2007 eruption at Stromboli as an effect of slight changes in the depth of the VLP sources. On the other hand, another possible cause of the wavefield variations among the events could be the change in the source mechanism, that would impact the relative amount of radial and transverse waves: e.g., given a crack as the source, transition from longitudinal to transversal modes of resonance could modify the wavefield, as would a change in the orientation of the crack. A similar interpretation was also given by Lokmer et al. (2008) to explain changes in time of the polarization parameters of LP events at Mt. Etna before and after the 2004-2005 eruption. Finally, also a variation of the medium in between the source and the seismic station could give rise to wavefield modifications. Also this explanation is reasonable since two of the main variations, taking place in July 2007 and August 2008, occurred at the same time as temperature and geochemical anomalies were observed. Such anomalies likely produced slight medium variations such as opening of fractures and changes of permeability, that can affect the seismic waves propagation.

Finally, some TRs exhibited amplitude modulation **(fig. 5.11)**, similar to that observed at other volcanoes (Gomez and Torres, 1997). Based on the spectral analysis performed on the seismic signals, as well as on RMS and polarization time series, this feature can be due to beats: two or more slightly different frequencies interact with each other to give rise to alternating destructive and constructive interference. The two neighbouring frequency components can be present either both in the TR signals or in the TR signal and in the background noise.

5.4 Concluding remarks

Tornillos were recorded in large number at Vulcano during 2007-2008, while there were very few in the previous years **(chapter 4)**.

The following points summarise their main features and changes over time:

- The number of tornillos increased and their spectral features changed at the same time as temperature and geochemical anomalies, suggesting that their occurrence is closely related to the increased fluid circulation in a dynamic hydrothermal system.

- Spectral analyses reveal that tornillos were characterised by one or more frequency peaks and by very high values of quality factor (up to 400). On the basis of such features and assuming a crack-like resonating source, the fluid filling the resonator could be a mixture of water droplets and gas. Moreover, the variations in the spectra suggest changes in the characteristics of the fluids filling the resonating cracks, and hence are suggestive of an unsteady and dynamic hydrothermal system.

- Wavefield changes were observed at the same time as spectral variations, not only within individual tornillos but also among different ones. Both such changes can be related to small variations in the location of the source. Other possible causes of the wavefield variations among the tornillos can be variations in their source mechanism and/or in the medium in between the source and the seismic station.

- The amplitude modulations, observed in some tornillos, are due to beating phenomena.

Chapter 6

Multiparametric approach in investigating Volcano-Hydrothermal systems: the case study of Vulcano

6.1 Introduction

The most promising approach to detect and investigate the volcanic unrest phases and forecast the eruptions is the joint monitoring of geophysical signals and other parameters such as geochemical and temperature data (Scarpa and Gasparini, 1996; Tilling, 2008). Several studies over the last few years involved the analysis of combined geophysical and/or geochemical data sets aimed at the characterization of quite different volcanoes, such as Erta 'Ale (Harris et al., 2005), Nisyros (Caliro et al., 2005; Gottsmann et al., 2007), Etna (Aiuppa et al., 2010) and Dallol (Carniel et al., 2010). In all these cases the multidisciplinary approach was helpful to investigate the complex dynamics of the volcanic systems. For instance, according to Gottsmann et al. (2007) the combined geodetic, gravimetric, seismic and electromagnetic records at Nisyros indicated that aqueous fluid migration can contribute significantly to periodic unrest, explaining the lack of eruptions in many cases of unrest. At Dallol joint thermal,

seismic and acoustic records indicate the presence of two regimes characterized by a different energy distribution alternating with timescales of tens of minutes (Carniel et al., 2010).

The results of a multi-parametric study performed at Vulcano, the southernmost of the Aeolian Islands, are here shown. The main structural system of the studied area is known as the Aeolian-Tindari-Letojanni fault (**fig. 6.1**; e.g. Ventura et al., 1999). It trends roughly NNW-SSE and is composed of right lateral strike-slip faults, still active on Vulcano (Mattia et al., 2008). Vulcano has been active in the last few centuries, erupting calc-alkaline and shoshonitic products (Barberi et al., 1974) and showing an explosive nature with frequent transitions from phreato-magmatic to magmatic activity (Mercalli and Silvestri, 1890; Barberi et al., 1988). A magmatic body was identified at depth of about 2-3 km below La Fossa crater by geophysical and geochemical studies (**fig. 6.1**; Ferrucci et al., 1991; Clocchiatti et al., 1994). La Fossa is a calcalkaline volcanic cone, with an altitude of about 400 m a.s.l. and a basal diameter of about 1 km. Its current slope is due to the construction phases that began about 5000 years ago within a roughly circular caldera (Keller, 1980; De Astis et al., 2006). Since the last eruption (1888-1890), the main conduit has been obstructed, exhibiting only fumarolic emanations. Geochemical and geophysical data clearly demonstrate the existence of an active hydrothermal system beneath La Fossa crater, at a depth of between 500 and 1000 m b.s.l. (Chiodini et al., 1992). Nowadays, fumarolic fluids at Vulcano are discharged mainly from La Fossa crater (field) reaching temperatures of over 400 °C. These have been interpreted as a mixture of two components which vary their relative proportions in time: i) a magmatic component, released from a magma body at depth; ii) a hydrothermal component, of shallower origin being formed by the evaporation of fluids of marine origin, which enter the fracture zone hosting the ascent of deep hot fluids (Chiodini et al., 1995; Paonita et al. 2002; Granieri et al, 2006). In particular, the magmatic component is richer in CO_2, N_2 and He with respect to H_2O (Paonita et al. 2002).

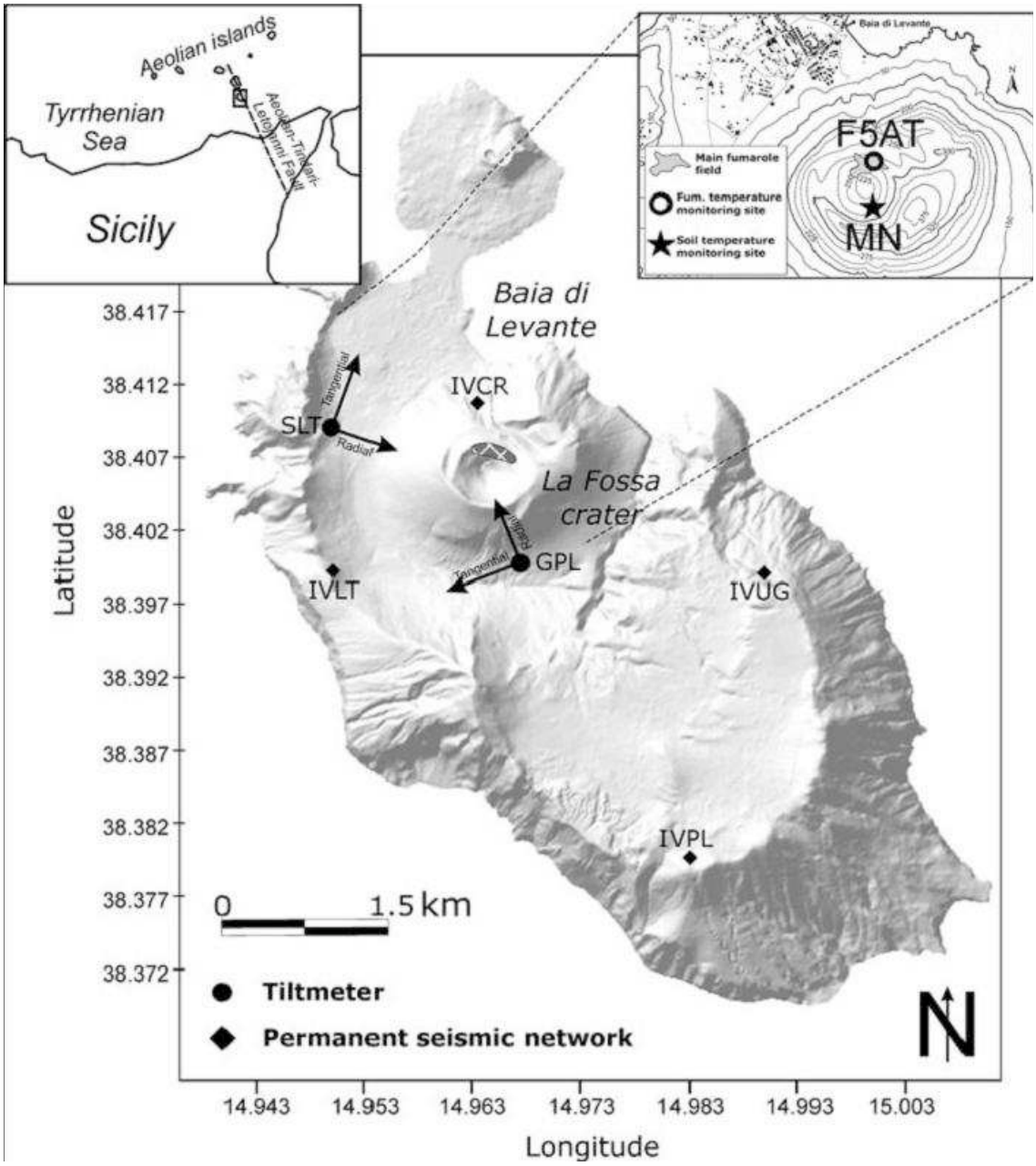

Fig. 6.1 Digital elevation model of Vulcano island showing the location of the seismic stations belonging to the permanent seismic network (diamonds), the tiltmeters (black dots) and the temperature sensors at fumaroles and soil (circle and star, respectively, in the upper right inset). The cross-hatched area indicates the main fumarolic field in the La Fossa area.

As in most active volcanoes around the world, also Vulcano is characterised by several kinds of seismic signals. All these signals at Vulcano are "transients", i.e., are limited in time, and thus we call them seismic events. The different types of these seismic events are briefly classified, mainly on the basis of waveforms and spectra **(chapter 4)**. The first group of events comprises the volcano-tectonic (VT) earthquakes, characterised by clear P and S phases (Aubert and Alparone, 2000), they are originated by shear failure caused by stress buildup and resulting in slip on a fault plane. The other seismic events, called volcano-seismic events, were associated to the shallow dynamics of the hydrothermal system at Vulcano (focal depth generally < 1 km b.s.l.) and grouped into three classes: long period (LP), high frequency (HF) and monochromatic (MC) events **(chapter 4)**.

Significant increases in the temperatures of the fumaroles and changes in the chemical composition of their emissions (mainly an increase in the CO_2 flux and concentration) are considered anomalies. They occur at the same time as increases in the number of volcano-seismic events (Granieri et al., 2006; Inguaggiato et al., 2008; Alparone et al., 2010). During the last century, several temperature and geochemical anomalies occurred at La Fossa that were not followed by eruptions: 1916–1924, 1977-1993, 1996 (Italiano et al., 1998; Capasso et al., 1999; Carapezza and Granieri, 2004). The most recent anomalies, consisting in temperature, chemical composition and seismicity changes, were observed in 2004, 2005, 2006 (Alparone et al., 2010) 2007, 2008 and 2009. There is a broad agreement among researchers that the anomalies are related to increased inputs of magmatic fluids into the fumarolic system, but their relationship to unrest processes that could lead to eruptions has frequently been debated (e.g. Barberi et al., 1991; Bukumirovic et al., 1997; Granieri et al., 2006). In any case, changes in composition and temperature of gases released at fumaroles, as well as volcano-seismic activity, can provide insights both into the dynamics of magmatic and hydrothermal systems (Barberi et al., 1991), and into the way in which the two systems interact (Chiodini et al., 1992, 1995; Capasso et al., 1997).

Ground deformation recorded at Vulcano since the late 70's were not associated with magma dynamics: the observed variations were interpreted as resulting from either regional tectonics (e.g. Aeolian-Tindari-Letojanni fault; Mattia et al., 2008) or changes in the shallow geothermal reservoir (Gambino and Guglielmino, 2008).

This work attempts a comparative analysis of geophysical and temperature data, which are representative for a recent period of activity (from 2004 to 2007). We couple the geophysical approach, monitoring local and regional seismic activity and soil deformation, with surface temperature data, related to steam flow.

6.2 Seismic data

During 2004-2007, seismicity at Vulcano was monitored by the permanent seismic network **(fig. 6.1)**. Before 2007, this network (operated by the Catania Section of Istituto Nazionale di Geofisica e Vulcanologia, INGV) consisted of four analog, 3-component stations (IVCR, IVUG, IVPL and IVLT). Each station was equipped with short period geophones (Geotech S13, 1 s corner period) and acquired at a sampling rate of 100 Hz. Successively, the sensors were replaced with digital 3-component broadband Nanometrics Trillium, with a flat response in the 40–0.01 s period range.

From 2004 to 2007, about 6550 volcano-seismic events were recorded **(fig. 6.2a)**. The number of the events was estimated by using the signal recorded by IVCR, the closest station to the sources of the events (Alparone et al., 2010). Some examples of events are reported in **fig. 6.3**. Their sources were located below La Fossa crater area at a depth 0.5-1.1 km b.s.l. (see grey area in **fig. 6.4**; Alparone et al., 2010; Milluzzo et al., 2010). As mentioned in **section 6.1**, some increases in the event number took place during the studied period: i) November 2004 - March 2005; ii) October 2005 - February 2006; iii) August - October 2006; iv) July - December 2007. In particular, taking into account the time distribution of the volcano-seismic events, 13% of them occurred during the first anomaly period, 28% in the second, 9% in the third and 26% in the last one. Thus, the events that occurred during these anomalies represent about the 76% of the total. The maximum daily number of events was 57, reached during the second anomaly. We selected a subset of about 2000 volcano-seismic events from the original 6550 events by using a static amplitude threshold. The events belonging to this subset were classified into LP, HF, MC and TR classes; monthly number and percentage with respect to the total number of events are reported in **fig. 6.5a,b**. It is clear that there is not a uniform time distribution of the different kinds of events during the studied period. For instance, the LP events completely lack during the first months of 2004, but the third seismic sequence, that is not as clear as the others owing to the total low event number

(fig. 6.2a), is characterised by an increase in the number of only LP events. Further, TR events, that at Vulcano are mainly characterised by one-two dominant spectral peaks near 6 and 10 Hz and source location just below La Fossa crater at depths 0.1-1 km b.s.l., more than the other volcano-seismic events showed a certain time variability: 15 tornillos occurred from 2004 to 2006, while up to ~300 occurred during 2007 (Milluzzo et al., 2010). We also calculated the maximum peak-to-peak amplitude of the events; the increases in the event number were accompanied by amplitude increases **(fig. 6.5c)**. This was very evident during the last anomaly, which was characterised by a sharp amplitude increase of most events.

Moreover, also the daily number of VT earthquakes, occurring during the studied period in an area centred on Vulcano island with a radius of 10 km, and the corresponding cumulative seismic strain release were taken into account **(fig. 6.2b)**. These VT earthquakes, totalling 52, differ from the volcano-seismic events mainly because of clear P and S phases. They were located at depth 0.3-20 km b.s.l. using the HYPOELLIPSE program (Lahr, 1989) taking into account the velocity model by Jeffreys and Bullen (1967) **(fig. 6.4)**. The mean horizontal and vertical errors are about 1.4 and 1 km, respectively. The magnitude of these VT earthquakes ranged from 1.4 to 3.4. Both VT earthquakes isolated in time and small swarms occurred.

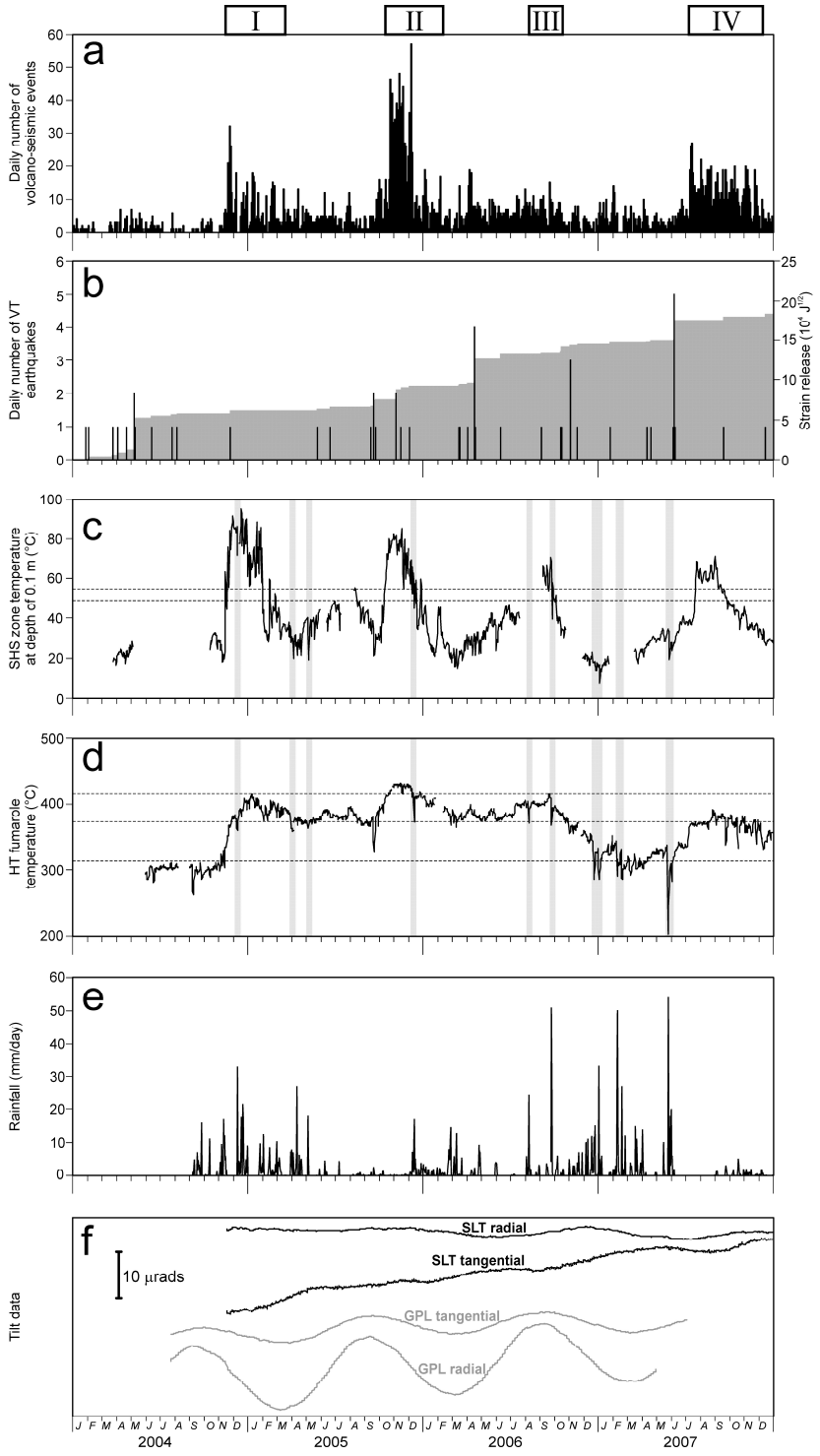

Fig. 6.2 (a) Daily number of volcano-seismic events. (b) Daily number of VT earthquakes (histogram) and cumulative seismic strain release (grey area). (c) Soil temperature at MN station **(see fig. 6.1)**. Dashed lines are the limits between seasonal modulation and enhanced steam release **(see fig. 6.6a)**. (d) Fumaroles temperature at F5AT station **(see fig. 6.1)**. Dashed lines are the limits between different subgroups of data **(see fig. 6.6b)**. (e) Daily amount of rainfall. (f) Tilt measurements in the radial and tangential components at SLT (black lines) and GPL (grey lines) stations **(see fig. 6.1)**. The grey areas in (c) and (d) indicate periods characterised by strong rainfall. The rectangles and the roman numerals at top of (a) indicate the anomalous periods characterised by increases in both volcano-seismic event number and temperatures.

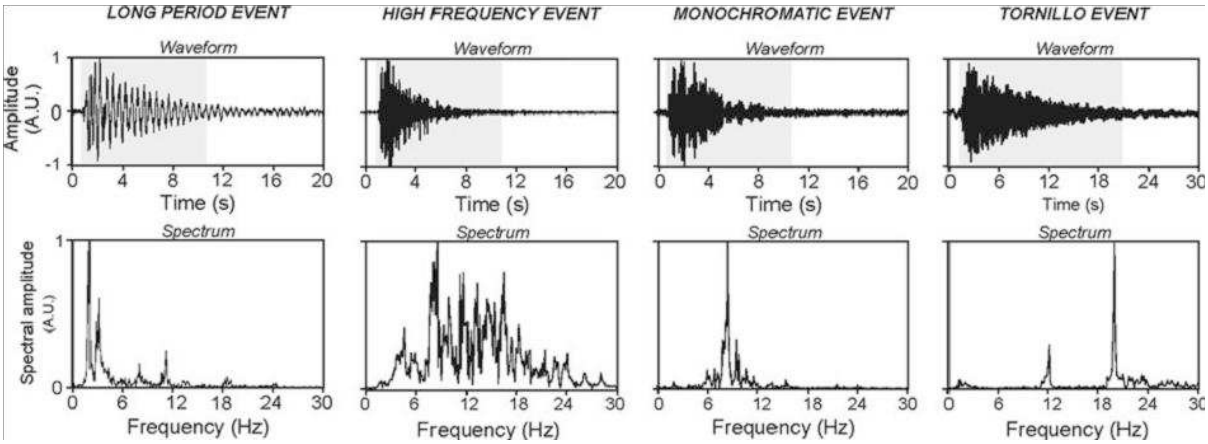

Fig. 6.3 Examples of waveforms and spectra of volcano-seismic events recorded at Vulcano. The grey areas in the upper plots show the windows used to calculate the spectra.

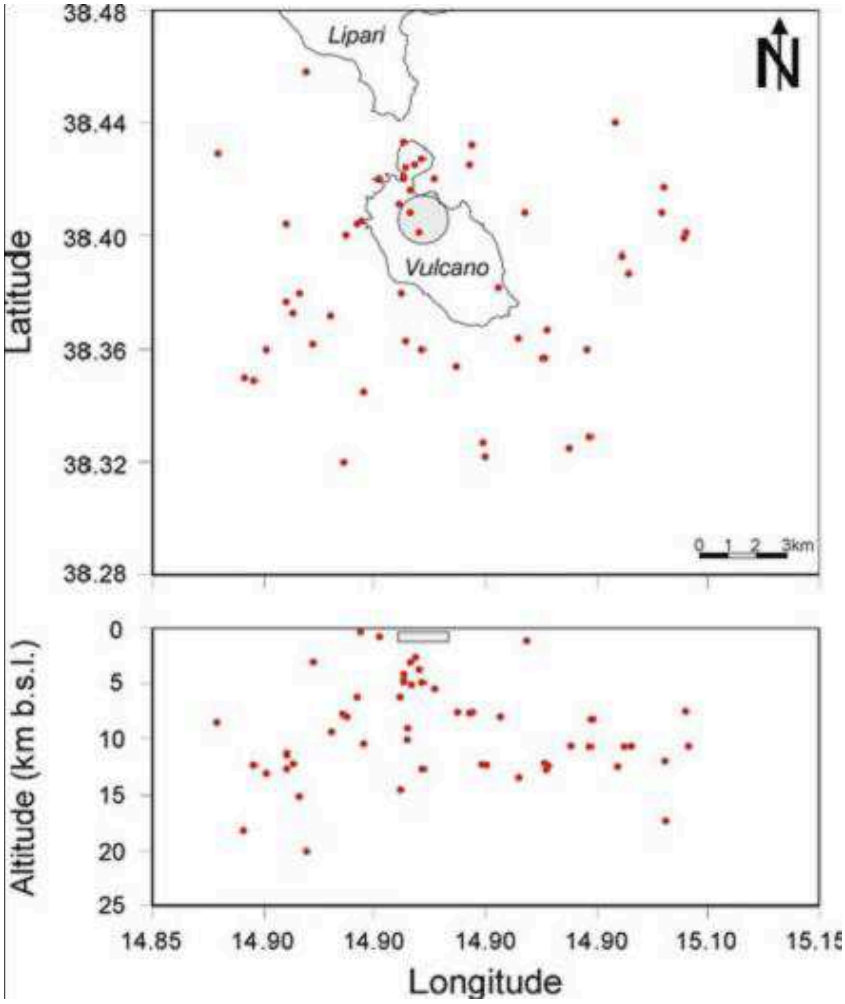

Fig. 6.4 Space distribution in map and section of the locations of the VT earthquakes (red dots) and volcano-seismic events (grey area).

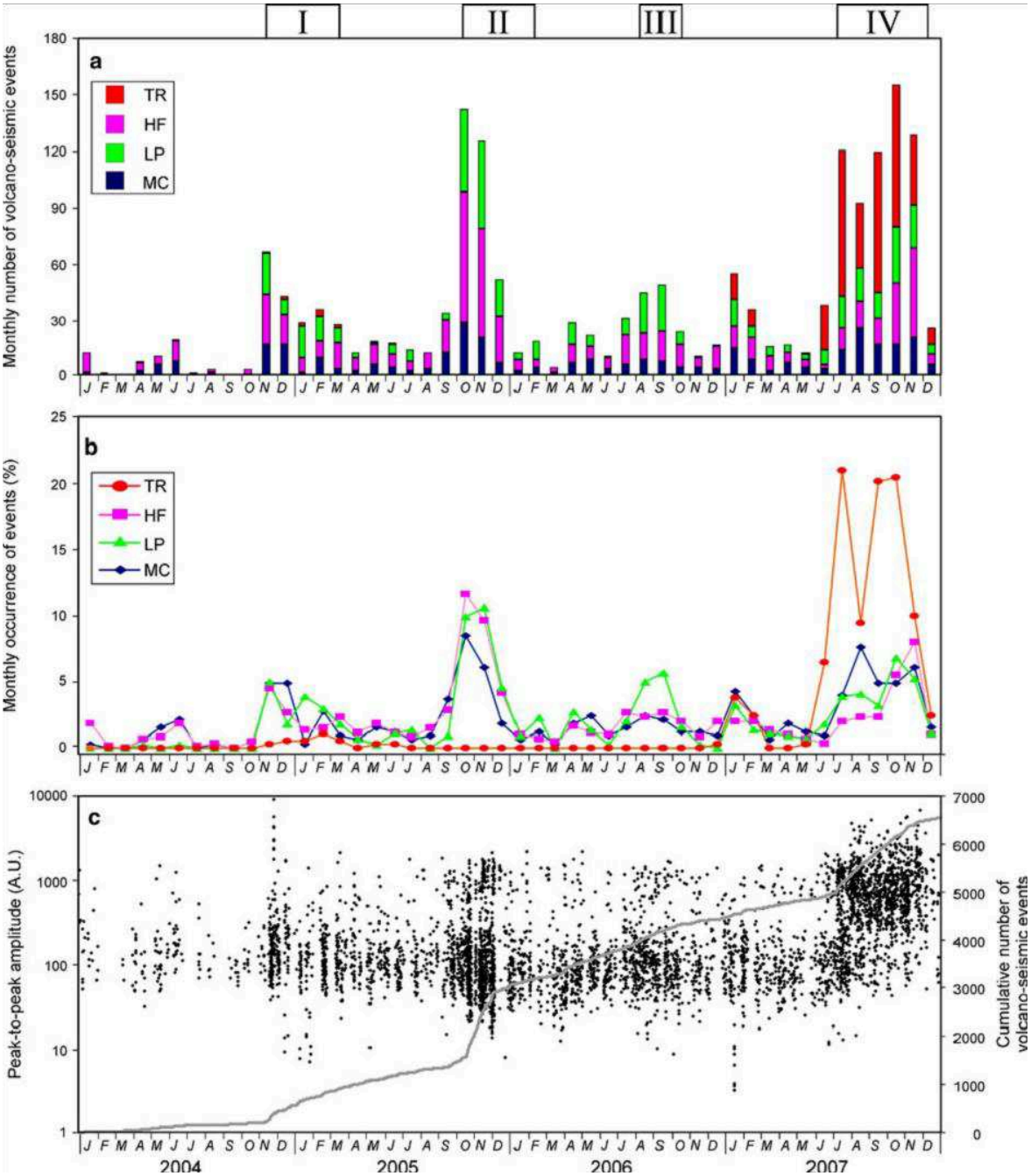

Fig. 6.5 (a) Monthly number of volcano-seismic events belonging to TR, HF, LP and MC classes. (b) Monthly distribution of TR, HF, LP and MC events in percentage with respect to the total number of events belonging to the same class. (c) Peak-to-peak amplitude (black dots) and cumulative number (grey line) of all the volcano-seismic events recorded at Vulcano during 2004-2007. The top rectangles and the roman numerals indicate the anomalous periods characterised by increases in both volcano-seismic event number and temperatures.

6.3 Temperature data

From a thermal point of view the surface of La Fossa cone can be distinguished as follows: some vent free areas characterised by diffuse heat flux of hydrothermal origin (Steam Heated Soil, hereafter referred to as SHS zones); some localized regions of high temperature (HT) vents located in the northern side (cross-hatched area in **fig. 6.1**), mainly on the rim and the inner slope; areas of low temperature vents; and some other areas (like the Background Zones by Harris et al., 2009), where the surface heat flux depends essentially on exhogenic factors like sun radiation, air temperature and rainfall. Here, we focused on the data acquired in the HT and SHS zones in order to highlight temperature variations related mainly to the fluid contribution from the magmatic and hydrothermal systems, with only minor influences due to external variations.

Two time series of temperatures will be analysed, chosen as representative of high temperature fumaroles and of areas characterised by diffuse heat flux. In particular, mean daily values of F5AT fumaroles and of MN soil temperatures (0.1 m deep) are discussed and compared; we did not further modify or filter thermal data to avoid affecting somehow the results of analyses. Some gaps in the data are due to temporal failure of the system caused by chemical corrosion of sensors. However, the monitoring system of fumarole temperatures has supplied data since 1984, allowing us to observe time variations of surface temperature and to follow the recent evolution of heat release from the active cone.

During 2004-2007, SHS zones showed surface temperatures (0.1 m deep in the soil) ranging between background and boiling point, as recorded by MN station **(fig. 6.1, 6.2c)**. In these areas also the vertical profile of soil temperature (0.1-0.9 m) has been continuously monitored to evaluate the surface heat flow (Diliberto et al., 2007; Aubert et al., 2008). SHS zones receive heat from steam released by the hydrothermal system underneath, but unlike the fumarole vents, the steam condenses below the surface. Then the surface heat flow results from

the combination of conductive and convective components. The conductive component may then be evaluated by the temperature gradient measured along the direction of the heat flux, and supplies the main component of the balance of heat flow from the ground, out of the fumaroles. However, occasionally, the convective component of heat transfer becomes dominant up to the ground surface, in these cases stations allowed us to follow the episodes of increased heat flow also beyond the main fumarolic field. Moreover, such stations helped distinguish the temperature variations coming from below from the temperature variations due to external factors (sun radiation, rain, wind) on the basis of observed delay among the different depths.

The cumulative frequency diagram also called probability diagram (**fig. 6.6**; Lepeltier, 1969), applied to SHS zone temperature, shows that data are grouped in two populations of normal distributed values, overlapping in the range 50÷54 °C (dashed lines in **figs. 6.2c and 6.6a**). The lower class represents the local variability for seasonal variation; 76% of recorded data fall in this class. The upper class of values ranges from 54 to 95 °C, and represents the soil temperature during transition from diffuse to convective heat transport, when increased steam fluxes are released toward the ground level. More than 22% of recorded data fall in this upper class. The anomalies of heat flux recorded in the steam heated soil begin with very fast increases in soil temperature **(fig. 6.2c)** sometimes reaching the boiling point of pore water. In all the anomalous periods the convective heat transfer became the dominant component of the heat flux, as confirmed by the lowering of temperature gradient to zero. From 11 November 2004 to 5 March 2005 (first anomalous period), soil temperature increased sharply and reached the boiling temperature, while in the other periods soil temperature showed similar rates (up to 5°C/h) but reached lower maximum values.

During the studied period 2004-2007, HT vents showed a wide range of temperatures, as shown by the station F5AT exhibiting temperatures from 180 up to 440 °C (**fig. 6.2d** shows the daily average of recorded values). In these years, the exhaling surface expanded but all the monitored points showed the

same behaviour. The seasonal influence cannot account for the main temperature variations, daily variations were negligibly small (<2°C). At Vulcano, fumarole temperatures show that most data range from 305 to 410 °C (78%), and lie on two straight-line segments on the cumulative frequency diagram **(fig. 6.6b)**, suggesting two different groups of normally distributed data with values ranging about 305-366 °C (23%) and 366-410 °C (55%). On the time series of daily measurements of temperature **(fig. 6.2d)**, some trending variations and other stationary periods can be observed. Moreover, the limit values from the cumulative frequency diagram suggest that values from 305 to 366 °C represent transition periods when the outlet temperature varied, approaching new stationary states, while output temperatures ranging from 366 to 410 °C represent stationary periods of relative high temperature (see dashed lines in **figs. 6.2d and 6.6b**). These time periods are February - September 2005; March - July 2006; July - November 2007. Conversely, outlet temperatures lower than 305 °C represent stationary periods of lower thermal state of the system (before October 2004 and in the spring of 2007). Finally, the values higher than 410 °C represent less than 5% of this data set and were recorded in autumn 2005, when the daily average of fumarole temperature peaked 428 °C (30 November 2005).

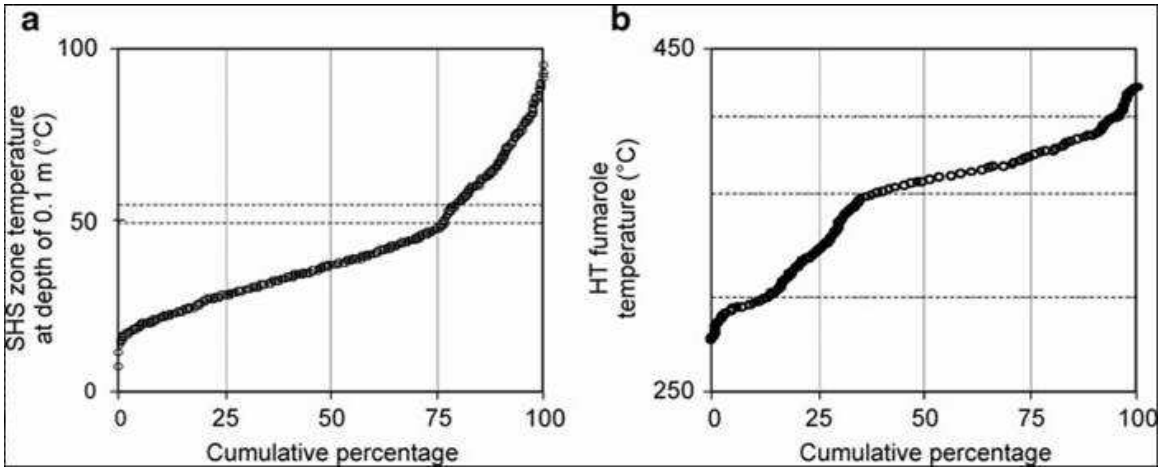

Fig. 6.6 (a) Cumulative frequency diagram of SHS zone temperature measured from 2004 to 2007. Dashed lines are the limits between seasonal modulation and enhanced steam release. (b) Cumulative frequency diagram of HT fumarole temperature measured from 2004 to 2007. Dashed lines are the limits between different subgroups of data.

Periodic campaigns of soil temperature measurements in the summit area of the crater in different periods (Bonfanti et al., 2004) showed that a large part of the active cone has been affected by enhanced dynamics of fluids, causing significant increases in the soil temperatures as well as in the diffuse degassing (Granieri et al., 2006), at the same time as temperature at monitoring stations and CO_2 content in the fumaroles increased. The invoked process is that the greater flow of emerging fluids, out of the fumarole conduits, leaves most condensable phases under the ground level, allowing the heat produced by the condensation process to diffuse towards the ground surface.

6.4 Tilt data

During 2004-2007, the permanent tilt network comprised of five borehole stations equipped with bi-axial instruments, four of which were installed at 8-10 m depth beneath the ground level (Gambino et al., 2007). The instruments are AGI models, with a precision of 0.1 μrad, that use a high precision electrolytic bubble sensor to measure angular movement. All the bi-axial sensors are installed inside a sand covered hole oriented towards the crater; then a positive signal indicates uplift of the crater area (radial component). The second axis is oriented 90° counter-clockwise (tangential component). The first stations were installed in the 1980s at about 2-3 m depth. These tiltmeters showed several kinds of daily and seasonal noise (Bonaccorso et al., 1999). In late '90s, the network was expanded by the addition of 8-10 meter deep sensors producing an improvement in the signal-to-noise ratio compared to a near-surface installation. Since noise amplitude decreases with depth, daily variation was removed and seasonal change reduced.

In **figure 6.2f** we report the signals of the two stations GPL and SLT located south and north-west of La Fossa cone, respectively **(see fig. 6.1)**. Tilt signals showed no rapid (from hours to days) changes, while the slow long-term variations are probably linked to the regional dynamics (Bonforte and Guglielmino, 2008).

6.5 Comparison among daily number of volcano-seismic events, fumarole temperatures and rainfall

Both the daily number of volcano-seismic events and temperature at HT fumaroles and SHS zones did not remain steady during the studied interval (2004-2007). As previously mentioned, four periods, characterised by increases in both volcano-seismic event number and temperatures, can be recognised, namely: i) November 2004 - March 2005; ii) October 2005 - February 2006; iii) August - October 2006; iv) July - December 2007 **(fig. 6.2)**. In this section we neglect the period iii) because the increase in the volcano-seismic event number is not as clear as in the other periods. Therefore, we focus on the comparison between the trends of the daily number of volcano-seismic events and HT fumarole temperature during the periods i), ii) and iv) (**figs. 6.7a,b,c,** respectively).

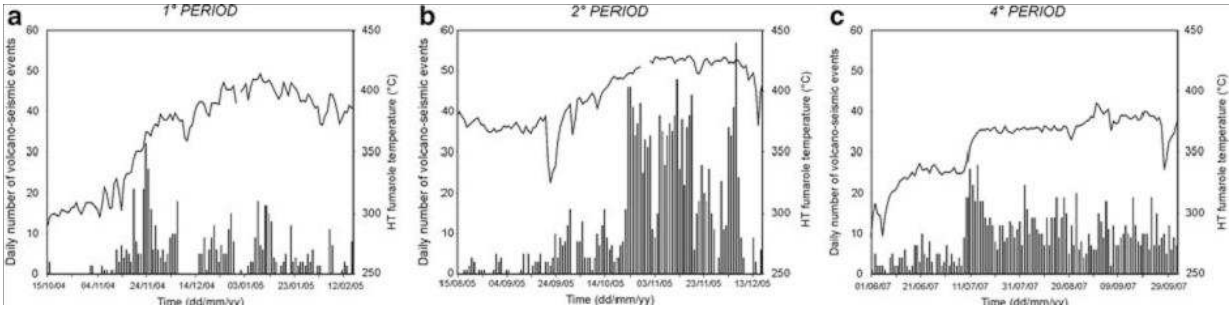

Fig. 6.7 Daily number of volcano-seismic events (histograms) and fumaroles temperature at F5AT station (black lines) during periods (i), (ii) and (iv) **(see section 6.5)**.

In the first two periods the increases in volcano-seismic event number and especially in temperatures were fairly gradual, thus because of the "emergent onsets" it is not clear whether the variations took place at the same time in both the time series or if there was a certain delay between them. Moreover, in these cases it is also very difficult to define an exact onset time of the anomalies and hence, concerning the volcano monitoring, the prompt detection of the start of this kind of anomaly is almost impossible. Conversely, period iv) shows "impulsive onsets" in both the time series (a couple of days to reach very high values from background levels) highlighting contemporaneous increases.

Because of the sampling of the temperature data we were not able to measure short time delays (if any) between the two considered time series. In this case the onset time can be clearly fixed not only with hindsight but in near real-time. Period iv) was also characterised by very high values of peak-to-peak amplitude of the volcano-seismic events **(fig. 6.5c)**. All these four periods were also characterised by increases in molar percentage of CO_2 in some fumaroles of La Fossa crater (Alparone et al., 2010; Milluzzo et al., 2010).

Both seismicity and temperatures time series were also compared with the rainfall. There is no clear evident link between occurrences of VT earthquakes and volcano-seismic events, and meteoric phenomena **(fig. 6.2a,b,e)**. On the contrary, at Merapi (Indonesia) Richter et al. (2004) reported some evidences that rainfall may influence seismicity rates. Concerning SHS zone temperatures, rainfall has small effects depending on the amount of precipitation and on the convective component of the heat transport vs. the whole heat transfer toward soil surface **(fig. 6.2c)**. The disturbances on HT fumarole temperatures are generally short (less than a few days) but more evident than SHS zone temperatures (see sudden and brief decreases in **fig. 6.2d**). The meteorological influences in the fumaroles emissions have already been analysed at Merapi (Richter et al., 2004), but though the outlet temperatures are similar to that of Vulcano Island, the effect of rainfall is not comparable for many reasons. Merapi fumaroles, as well as Vulcano ones, showed temperature ranging between 320 and 400 °C, but Richter et al. reported 1400 mm of rainfall during only 6 months at Merapi while at Vulcano 1450 mm was the total amount of rainfall over 4 years. Moreover, the sources of vapour released by the 2 systems are very different: for Vulcano fumaroles, the vapour sources are an extended hydrothermal system and deeper fluids of magmatic origin, unlike the Merapi fumaroles that are close to an active lava dome. Furthermore, the time series discussed for Vulcano have been registered during a period of low fumarolic activity, while for Merapi volcano the activity during the studied period changed from quietly effusive dome growth to partial lava dome collapse.

6.6 Discussion

Vulcano is an active volcano, whose last eruption took place during 1888-1890. Moreover, it is characterised by an active hydrothermal system with fumarole emanations (e.g. Chiodini et al., 1992), volcano-seismic events located below La Fossa (e.g. Montalto, 1994; Alparone et al., 2010), and temperature and geochemical anomalies (e.g. Carapezza and Granieri, 2004; Granieri et al., 2006). Data for eruptions at many worldwide active volcanoes clearly indicate that they are almost always preceded and accompanied by volcanic unrest, as manifested by physical and/or chemical changes in the state of the volcano and/or its associated hydrothermal system (Tilling, 2008). The volcanic unrest phases, that do not necessarily culminate in an eruption, are detected and studied by the joint monitoring of geophysical signals and geochemical parameters (Scarpa and Gasparini, 1996; Tilling, 2008).

After several years (1999-2004) of no significant geophysical and geochemical variations (INGV-PA, 2006; Granieri et al., 2006), during 2004-2007 continuous monitoring networks registered four "anomalous" periods at Vulcano. Such periods were characterised by increases of temperature at both HT fumaroles and SHS areas, accompanied by increases in the number and amplitude of volcano-seismic events **(fig. 6.2 and 6.5c)**. Moreover, during these periods there were intense variations of CO_2 content in fumaroles (Alparone et al., 2010; Milluzzo et al., 2010). Additional geochemical data acquired around the crater area during the first and second anomalous periods (November 2004 - March 2005; October 2005 - February 2006) highlighted increases of diffuse CO_2 flux, interpreted as an increase in the concentration of the magmatic component of the fumarolic fluid (e.g. Granieri et al., 2006; Aubert et al., 2008; Inguaggiato et al., 2008). This evidence, together with the fact that the analysed anomalies took place during different meteorological seasons over years (for instance the first and the last analysed anomalies occurred in autumn-winter and summer-autumn, respectively), leads us not to consider meteorological phenomena (such as rainy periods) as "external" causes of the anomalies . All

these data suggest an ongoing unrest process. Indeed, a high rate of LP seismicity has often been associated with pre-eruptive behaviour at many volcanoes, including Redoubt, Alaska (Chouet et al., 1994), Galeras, Colombia (Gil Cruz and Chouet, 1997) and Colima, Mexico (Varley et al., 2010). Similarly, eruptive activities at many volcanoes have sometimes been preceded by thermal anomalies within or near to craters, such as at Soufrière (St. Vincent) in 1971, where increases in lake temperature and evaporation rate took place (Sheperd and Sigurdsson, 1978), and at Tokachidake, where the 1962 and 1988-1989 eruptions were preceded by increases of geothermal activity (Okada et al., 1990). However, the analysed 4-year period at Vulcano had only a very few VT earthquakes of low magnitude and they not show clear significant changes in both number and magnitude during the anomalies **(fig. 6.2b)**. This evidence, together with the lack of sharp and significant changes in the tilt recordings indicating no major shallow deformations **(fig. 6.2f)**, suggests that the inferred increases in the concentration of the magmatic component of the hydrothermal fluids are not due to magma intrusions within the shallow hydrothermal system, but rather to an increased release of fluids from a deep magma body.

On the basis of the aforementioned considerations, the inferred increasing fluid circulation rising from depth during the four anomalous periods can be considered the common cause of increases in both temperatures and volcano-seismic event number. Indeed, the fluid circulation can promote an increase in the number of volcano-seismic events in different ways:

(i) Fluid circulation locally increases pore pressures due to the buildup of fluids in cracks, thereby reducing the effective stress (hydrofracturing; e.g. Moran et al., 2000; Alparone et al., 2010). If the rocks are close to a critical state of a failure equilibrium, small perturbations of the pore pressure can modify the effective normal stress and trigger seismicity (e.g. Shapiro et al., 2003; Miller et al., 2004). In geothermal systems, temporal increases in pore pressure are important factors in contributing to induced seismic activity (e.g. Nishi et al., 1996).

(ii) Fluid circulation reduces the yield strength of the country rock by the alteration of rock to secondary minerals, including clays, thus reducing the shear stress required to initiate fracturing (geochemical weakening; Nishi et al., 1996; Moran et al., 2000).

(iii) Hot fluid circulation locally increases temperatures in the country rock, giving rise to local gradients of temperature in the rocks and then to thermal forces that could lead to rock fracture (e.g. Moran et al., 2000).

(iv) Fluid circulation favours resonance and vibration processes in cracks and conduits. For instance, the choked flow model (Morrissey and Chouet, 1997; Petersen, 2007) can explain how fluid circulation can trigger resonance and vibration processes. In such a model a shock wave is generated downstream of a constriction within the conduit/crack by the acceleration of fluids to supersonic speeds. The shock waves near the walls can produce recurring step-like pressure transients in the flow, which in turn induce resonance of the fluid-filled crack/conduit (Morrissey and Chouet, 1997; Petersen, 2007).

In the light of the above factors, the volume containing the volcano-seismic sources is inferred to be coincident with the volume affected by the hydrothermal fluid dynamics. Moreover, according to the above described source mechanisms of the volcano-seismic events at Vulcano **(see section 6.1)**, the phenomena (i), (ii) and (iii) can generate high frequency events, whereas the phenomenon (iv) may give rise to monochromatic, long period events and tornillos **(fig. 6.8)**. The fracturing processes (i-iii) are also able to enhance the rock vertical permeability, thus favouring the rise of fluids. On the other hand, circulating fluids can also generate deposition of hydrothermal minerals at depth, that results in clogging of portions or all of the system, causing impediment or diversion of rising gases (Carapezza et al., 1981; Chiodini et al., 1995). Such phenomena can strongly modify the permeability of the rocks through which the hydrothermal fluids move and, as suggested by the studies of Todesco et al. (2010), could be responsible for the different trends observed in the measured geochemical and geophysical time series during the anomalous periods. Indeed, the first and second anomalous periods were characterised by

gradual increases in both fumarole/soil temperatures and volcano-seismic event rate ("emergent onsets" of the anomalies), while the fourth by sharp increases ("impulsive onset"). In this last case the increase of both temperature and volcano-seismic event number took place contemporaneously. This concurs with the results obtained by Richter et al. (2004), who observed changes in fumarole temperature at Merapi just a few minutes after seismic ultra-long-period signals and simultaneously with higher-frequency seismic transients. The different increasing trends in the measured geochemical and geophysical time series during the anomalous periods could be due to a permeability increase of the system favouring the fast upward migration of the hydrothermal fluids and then the quick variations of the recorded time series **(fig. 6.7)**, However, we cannot exclude that the different increasing trends of the geochemical and geophysical time series would be due to a release of gas from a deep magma body. Temporal changes of permeability of the rocks containing the hydrothermal system may be able to affect the monitoring data so strongly to cause the departure of the monitored signals from their baseline (apparent unrest; Todesco et al., 2010). These different time series trends, characterising the anomaly onsets, also imply a variable difficulty in defining an exact onset time of the anomalies and then for monitoring purposes also in promptly recognising a starting anomaly.

Time-relationships between variations in temperature and/or composition of hydrothermal fluids and seismic event occurrences have also been observed in other volcanoes such as Merapi, Indonesia (Richter et al., 2004), Kuchinoerabujima, Japan (Triastuty et al., 2009), Mammoth Mountain, California (Hill and Prejean, 2005) and Nisyros, Greece (Caliro et al., 2005). For instance, Richter et al. (2004) noted a statistically significant correlation between certain types of seismic activities and increases in fumarole temperature, interpreted as sudden releases of pressurised gas, followed by the generation of small cracks. In another paper, to explain the simultaneous increase of both number of monochromatic events and fumarolic temperature in 2006 at Kuchinoerabujima volcano, Triastuty et al. (2009) suggest the intrusion

of hydrothermal fluids into cracks to trigger both monochromatic seismicity and fumarolic temperature increase.

Finally, we also noted a certain variability in the time distribution of the events belonging to the different classes **(fig. 6.5a,b)**. This information, together with the waveform and spectral time variations observed in LP (Alparone et al., 2010) and TR events (Milluzzo et al., 2010) at Vulcano, suggest that the seismic sources of these events change their features in time (e.g. rate of activity, geometry of the resonating crack/conduit, chemical and physical properties of the fluids filling the resonator). In view of this and of the observed variations of temperature and fumarole gases composition, the hydrothermal system at Vulcano can be considered unsteady and dynamic.

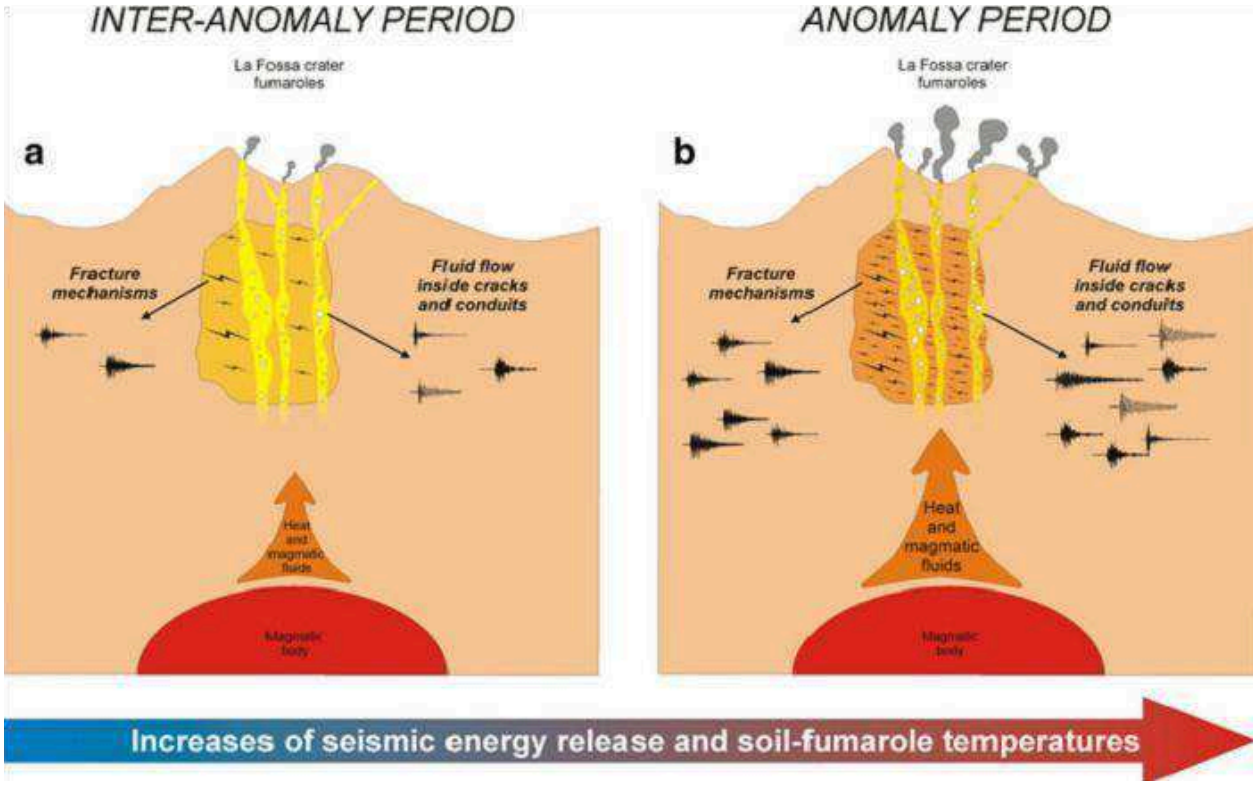

Fig. 6.8 Cartoon showing a schematic section of the volcano-hydrothermal system during inter-anomaly (a) and anomaly (b) periods.

6.7 Concluding remarks

Seismic activity, ground deformation and soil and fumarole temperatures acquired during 2004-2007 at Vulcano were analysed to investigate "anomalous" periods characterised by increases of soil and fumarole temperatures, and increase of volcano-seismic events number. The following points summarise the main conclusions:

- The very few VT earthquakes, taking place during the anomalies, together with the lack of sharp and significant changes in the tilt recordings, suggest that the observed geophysical and geochemical variations are not due to magma intrusions within the shallow hydrothermal system, but rather to an increased release of fluids from a deep magma body.
- The increasing fluid circulation rising from depth during the four anomalous periods is the common cause of increases in both temperatures and volcano-seismic event number.
- The different increasing trends observed in the measured temperature and geophysical series during the anomalies can be due to either time changes in the medium permeability or a changing speed of gas release from a deep magma body.
- On the basis of the variations of the time distribution of the different kinds of volcano-seismic events and the observed changes in temperature and fumarole gases composition, the hydrothermal system at Vulcano can be considered unsteady and dynamic.

The data presented in this paper suggest that the comparison of seismic, ground deformation and temperature data can be useful for better understanding the dynamics of a complex volcano-hydrothermal system, including a better definition of the origin of a volcano unrest, and hence for improving the estimation of the level of the local volcanic hazard.

Chapter 7

Relocation and focal mechanisms of earthquakes in the south-central sector of the Aeolian Archipelago: new structural and volcanological insights

7.1 Introduction

High precision in earthquake locations is one of the most important elements for accurate seismic investigation, allowing reconstructing seismogenic structures, discriminating the fault plane from the auxiliary in the focal mechanism solution and defining the relationship between seismicity and volcanic activity (e.g. Alparone and Gambino, 2003; Scarfì et al., 2005).

The Aeolian Archipelago is located in the Southern Tyrrhenian Sea and represents the manifestation of a submarine volcanic arc originating in the central sectors of the Tyrrhenian Sea during the Pliocene and successively

migrating towards the south-east. Salina, Lipari and Vulcano form a NNW–SSE volcanic chain departing from the central part of the Aeolian arc **(fig. 7.1)**; they are controlled by a complex NNW-SSE lithospheric fault system and by second order N-S and NE-SW oriented structures (De Astis et al., 2003).

With the aim of improving our knowledge on the seismo-tectonic process in the Aeolian Archipelago, we analyzed the crustal seismicity in a rectangular sub-area comprising Vulcano, Lipari, Salina and Filicudi **(fig. 7.1)**.

Network geometry in archipelagos is highly related to island positions and for this reason some areas may be characterized by a poor network azimuthal coverage. This is one of the main reasons we focused our study on this sector for which we have calculated a new velocity model by including information from 1993-2010 recorded earthquakes by a joint inversion hypocentre-velocity (Kissling et al., 1994). Successively, we applied the double-difference relocation technique on the 351 events, recorded in the same period by using the Hypodd algorithm (Waldhauser and Ellsworth, 2000), which can be used to produce more accurate locations than the standard absolute location procedures, particularly when seismogenic regions are dominated by spatial clustering of events. Relocated seismicity has enabled identifying preferential alignments, indicating the geometry of currently active structures; fault plane solutions, calculated for the shocks with magnitude greater than 2.7, helped define the kinematics of these structures.

7.2 Geological and structural setting

The Aeolian Archipelago represents the emerged part of a submarine volcanic arc located within the Tyrrhenian Sea extensional back arc basin (Malinverno and Ryan, 1986). It can be subdivided into three sectors with different structural and tectonic evolution (De Astis et al., 2003). In the western sector, comprising the Alicudi and Filicudi Islands **(fig. 7.1)**, volcanic activity started at about 1.3 Ma (Gillot, 1987) and ended at about 30–40 kyr. At present, seismicity occurs in the crust along the WNW-ESE Sisifo Fault System **(fig. 7.1)** showing strike slip to oblique (strike slip/reverse) focal solutions with a main NNW-SSE compression (Pondrelli et al., 2004; 2006). The eastern sector, which comprises Panarea and Stromboli Islands and where volcanism developed from 0.8 Ma ago and is still active, is affected by a prevailing NE-SW striking fault system. The central sector includes the islands of Salina, Lipari and Vulcano. Here, the volcanism began at 0.4 Myr (Beccaluva et al., 1985) and is still active at Lipari (last eruption in 580 AD) and Vulcano (1888–90 AD); at Salina, the last eruption occurred 13 kyr ago (Keller, 1980); These volcanoes are aligned along a lithosperic NNW-SSE fault system, the Aeolian-Tindari-Letojanni Fault System (hereafter ATLFS) that shows right-lateral to oblique kinematics along which seismicity is roughly aligned (e.g. Neri et al., 2003; 2005; Billi et al., 2006). However, ATLFS is probably more complex than a simple strike–slip fault (Argnani et al., 2007); moreover, Vulcano island is also characterized by NE-SW and N–S trending normal structures **(fig. 7.1)** which accommodate the horizontal movements of the main system (Mazzuoli et al., 1995). Dikes, vents and eruptive fissures are aligned along these two oblique trends (Mazzuoli et al., 1995; Ventura et al., 1999; De Astis et al., 2003).

Seismogenic stress inversion calculated in the Aeolian Archipelago area allowed Neri et al. (2005) to detect a compressional domain around the islands; also GPS data (Hollestein et al., 2003) indicate that, on a large scale, N–S compression is active in the north of Sicily and Argnani et al. (2007), using marine seismic reflection surveys, found that compressional structures

predominate around the Aeolian islands, whereas a NW-SE extension characterizes the south-eastern Tyrrhenian and Calabria (D'Agostino and Selvaggi, 2004; Scarfì et al., 2009)

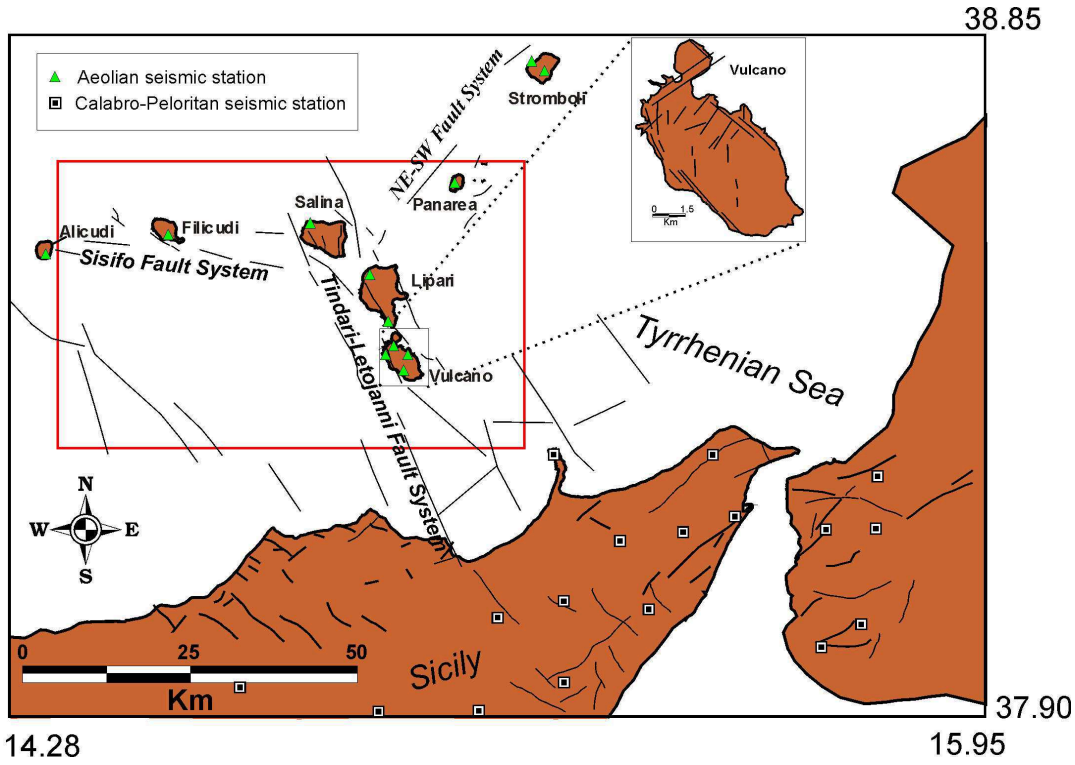

Fig. 7.1 Structural map and seismic network. The investigated area is shown in red.

7.3 Network and data analysis

Since the late 70's, continuous seismic monitoring activity on Aeolian Archipelago has been performed by a permanent seismic network composed of a few analog 3C stations. Starting from the 80's, the network was developed with other stations deployed over the entire Aeolian Archipelago equipped with short-period seismometers, having a natural frequency of 1 Hz. During 2005 and 2007, almost all stations were replaced by new digital 24-bit ones, equipped with broadband (40s) three-component sensors, with a dynamic range of 144 dB. To date, the Aeolian permanent seismic network, managed by INGV-CT (Istituto Nazionale di Geofisica e Vulcanologia – Sezione di Catania), consists of 12 three-component digital seismic stations **(fig. 7.1)**. In order to reduce the azimuthal gap, in this study we have also used the stations deployed in the Calabro-Peloritan area and on the northern flanks of Mt. Etna **(fig. 7.1)**. Furthermore, where possible, we added data from the INGV national permanent seismic network.

The data-set used in this study is composed of 351 earthquakes recorded from Oct. 1993 to Dec. 2010 with magnitude $1.5 \leq Md \leq 4.6$, whose location, performed for surveillance purposes, is obtained using the Hypoellipse code (Lahr, 1989) **(fig. 7.2)**. In the Sept. 1999 – Mar. 2002 period, technical problems have significantly reduced the possibility to locate microseismicity in this area.

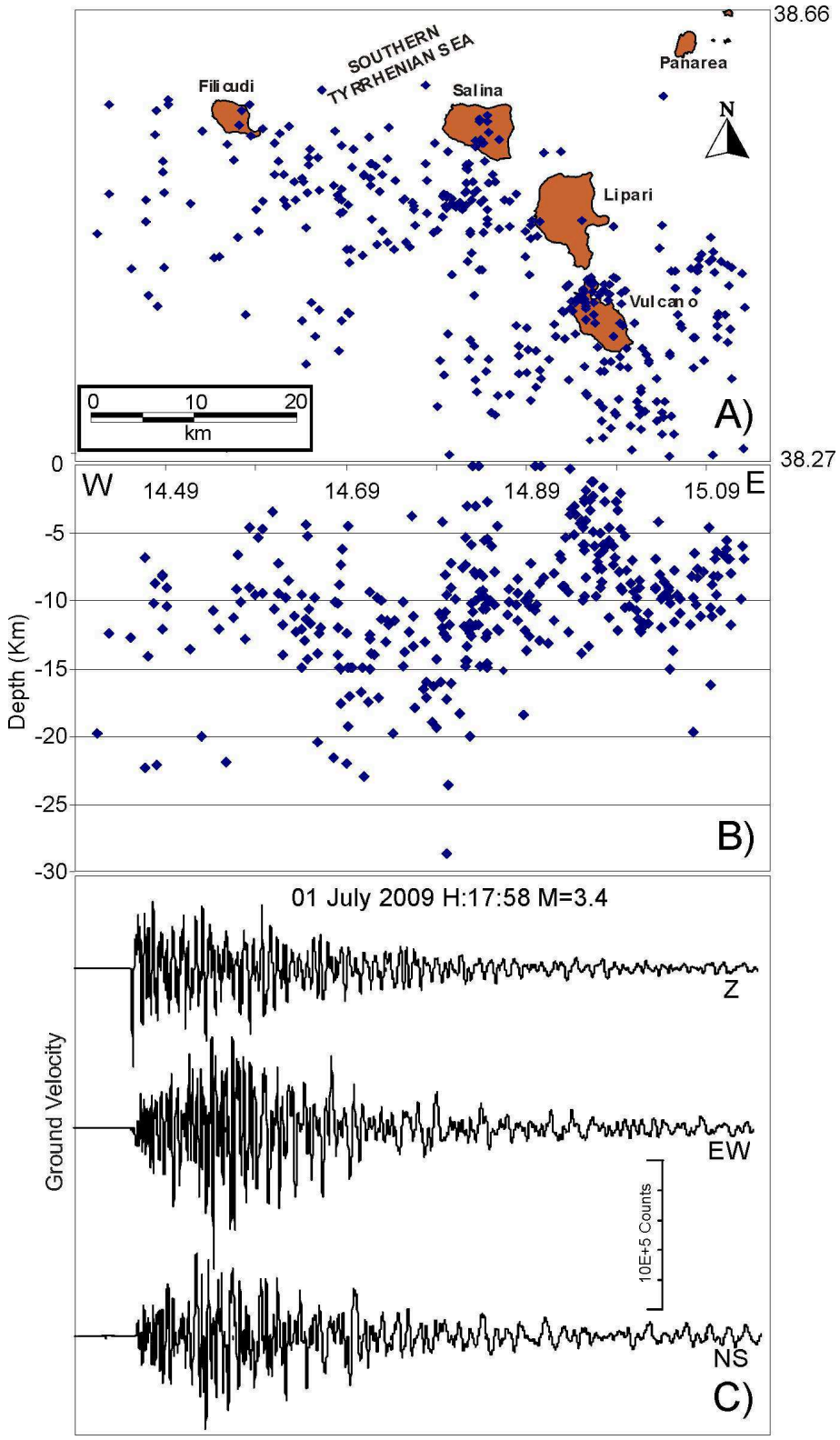

Fig. 7.2 Map (A) and E-W vertical section (B) of the earthquake locations performed for surveillance purposes. An example of three-component waveforms of one earthquake is shown in (C).

7.4 Accurate hypocenter locations

The precision of the catalogue locations is adequate for routine purposes but the determination of hypocentral parameters are not compatible with the reduced size of some seismogenetic structures whose seismotectonic interpretation is required. An important issue in this context is the identification of a suitable velocity model. Neglecting the coupling between hypocentral and velocity parameters during the location process, may well introduce systematic errors in the hypocenter location (Thurber 1993), which depends closely on the assumed a priori velocity structure (Kissling et al. 1994). This is relevant both for standard and high precision location techniques (e.g. Michelini and Lomax, 2004). Precise hypocenter locations and error estimates, therefore, demand the simultaneous solution of both velocity and hypocentral parameters. In the next paragraphs, we focus on the improvements in the precision and reliability of earthquake locations that can be achieved by a procedure in two steps: i) computing a minimum 1D model and ii) applying a relative relocation technique that can be used to produce more accurate locations than the standard absolute location procedures, particularly when seismogenetic regions are dominated by spatial clustering of events.

7.4.1 Inversion for the minimum 1D model

In order to improve the level of accuracy of hypocenter locations, we constructed a new 1-D velocity model including information from recorded earthquakes by a joint inversion hypocenter-velocity (Kissiling et al.,1994). Since a reference 1-D velocity model must approximate a weighted average of the data but must also reflect the gross features of the structure, the computation of such a model starts with the definition of two elements: 1) the selection of a high-quality set of local earthquake data; 2) an initial 1-D velocity model.

For our objectives, we selected only well located events matching minimum requirements with respect to location quality, i.e. events with at least five well

readable P-arrivals, two clear S-arrivals and with a maximum azimuthal gap of 200°. The maximum gap is an important parameter that ensures events are well localizable by the local network. We also chose to consider a few epicenters with a gap larger than 200° because their ray-paths are useful to sample the study volume. On average, 12 pickings were available for each event. We further rejected all events with root mean square (rms) residuals larger than 0.30 s and standard location errors (ERH and ERZ) larger than 3.0 km. In this framework, a major problem is the identification of a good start solution for the hypocenter locations and the assessment of the sensitivity of the inversion process in this respect. It should be noted that the presence of events with unstable locations could introduce biases as the inversion process may decrease the travel-time residuals by shifting around the hypocenter coordinates instead of adjusting the velocity model parameters properly. Hence, before including the earthquakes in the joint inversion of velocity and hypocentral parameters, we tested the location stability by relocating the events several times, each time shifting the trial hypocenters randomly in the space up to ±6 km for the hypocenter spatial coordinates. This provides a way to identify events for which different locations with equivalent travel-time residuals can be found. In fact, if the proposed 1D velocity model and the available travel times for each event provide a robust minimum in the solution space, there should be no significant changes in the hypocentral locations (Husen et al. 1999). We examined the differences between the solutions and removed the events with horizontal or vertical location variations greater than 3 km. After the selection process, our data-set for the velocity model calculation consisted of 144 events, with a total of 1280 P and 395 S-observations.

Eliminating the events of poor quality, we focused on the identification of the starting velocity structure; to this end, we collected all the available a-priori information (velocities and layer thickness) regarding the Aeolian region.

Hence, we considered three 1-D a-priori models. The first is derived from the studies of Ventura et al. (1999), who, interpreting “Deep Seismic Soundings” data, provided velocities and depths of the main crustal discontinuities

(including Moho) for the Salina-Vulcano area. The other two models result by combining respectively the information from Falsaperla et al. (1985) and Castellano et al. (1988), which are limited to 3 km of depth for the restricted area between Vulcano and Lipari, and velocities derived from Jeffrey and Bullen, (1967) for the deeper part of the model.

We then performed a simultaneous inversion of velocity structure and hypocentre locations by using the software VELEST (Kissling, 1995), considering the global misfit (RMS of the travel-time residuals) as measure for the goodness of fit. As the number of readable S-wave onsets was limited, we refrained from inverting S-wave velocities. S-phases were included in the inversion procedure by simply assuming a constant Vp/Vs ratio of 1.75 (see Neri et al., 2002), to better constrain the earthquake location, in particular the focal depth (see e.g., Laigle, 1998).

From the results, we noted that the obtained Minimum 1-D P-wave velocity models reach an equivalent goodness of fit (about 0.1 s) and that initial differences are smoothed on converging to similar velocities and discontinuities, particularly below 5 km of depth, where most of the foci is located; there, the maximum difference encountered between the models is 0.2 km/s.

In the end, we considered our best Minimum 1-D the one derived from Ventura et al. (1999). Its velocity structure is shown in **fig. 7.3**, together with the station corrections. It provided an improvement of about 80 % in the RMS residual, compared to the initial model. The model starts with a velocity of about 3 km/s near the surface, consistent with that estimated for lavas and compacted sediments, and shows two main jumps. The first one at the depth of 2 km (5.2 km/s) is related to the velocity of the upper crust; the second at 23 km of depth (7.7 km/s) is corresponding to the Mohorovicic ('Moho') discontinuity (Ventura et al., 1999); in this case, the small thickness of the slower upper layers can be explained by the thinning of the crust of the Tyrrhenian region with respect that of the neighboring Calabro-Peloritan Arc. The second major discontinuity (7.7 km/s), set to 23 km of depth, according with the data provided by Ventura et al. (1999) and Dezes and Ziegler (2001), corresponds to the Moho.

Station corrections **(fig. 7.3)** are an integral part of the velocity model, since they should to some extent reflect the overall three-dimensionality of the velocity structure and in particular, the highly heterogeneous near-surface structure which is otherwise not represented in a 1-D model (Kissling et al., 1994). Negative corrections are encountered when the true velocities are supposed to be higher, positive corrections occur for lower velocities than predicted by the model. The station delays encountered here, given as relative values with respect to the reference station IVPL in the Vulcano island, are positive in the islands north of Vulcano (between 0.1 and 0.3 s) and very close to 0 in the Mt. Peloritani area. We suppose that this behavior is probably caused by the slower velocity on the island's surface materials with respect to the metamorphic rocks of the Calabro-Peloritan Arc.

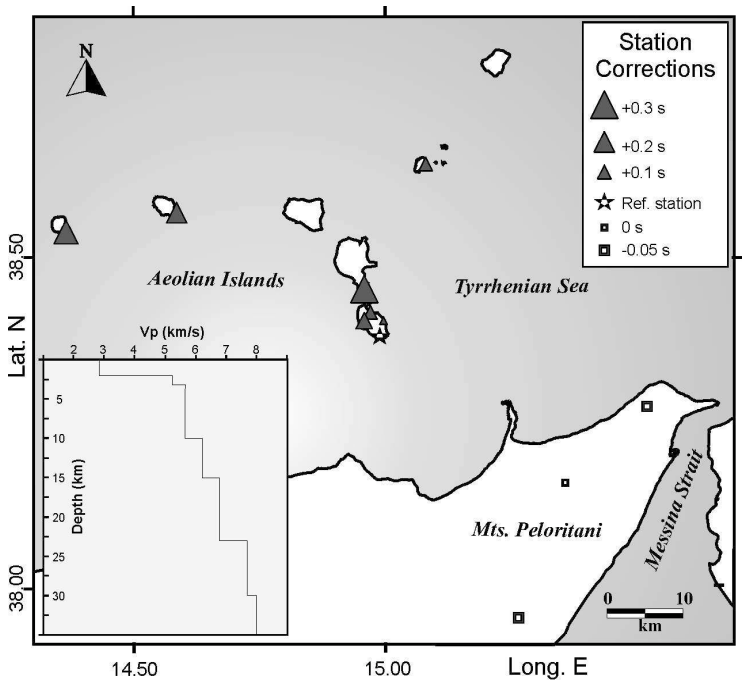

Fig. 7.3 Station corrections computed with the minimum 1-D velocity model shown in the inset. The star indicates the "reference station". See text for more details.

7.4.2 Earthquake relocations and focal mechanisms

We use the new obtained minimum 1-D P-wave velocity model and a Vp/Vs ratio of 1.75 to obtain more precise relocations applying the double-difference earthquake algorithm of Waldhauser and Ellsworth (2000) and the HypoDD routine (Waldhauser, 2001). The algorithm takes advantage of the fact that if the hypocentral separation between two earthquakes is small enough compared to the event–station distance and the scale length of velocity heterogeneity, then the ray paths are similar along almost the entire length (Got et al., 1994). Under this assumption, the differences in the travel times for two earthquakes recorded at the same station can be attributed to differences in their hypocenter spatial separation. In this way, errors due to inaccurately modeled velocity structure are minimized without the use of station corrections. This technique has been used in several studies (e.g. Lippitsch et al., 2005; Gambino et al., 2004; Bonforte et al., 2009) producing sharp images of studied fault structure.

During computation, HypoDD performs a reduction in the data because it groups the events into clusters of well-connected earthquakes and removes those that are considered as outliers.

Although we started with an initial set of 351 events obtained by the first selection, our final data comprises 316 well-connected events. These events are connected through a network of links that consists of 17913 P and 3248 S-wave phase pairs. The average number of links per event pair is 10, while the average offset between strongly linked events if of about 3.2 km.

New locations show mean hypocentral formal errors of 90 meters on the horizontal component and about 105 meters in the vertical direction. The mean rms residual decreases from the initial value of 0.14 s to 0.03 s in the relocated catalogue.

In **figure 7.4**, maps and an oriented sections of the seismicity located using HypoDD are shown and a significantly reduced scatter in locations, with respect to **figure 7.2** is observable. The most recognizable features on the seismicity distribution are related to the presence of three main clusters: the first (*C1* in **fig.**

7.4), NE-SW oriented, 3-8 km deep, slightly NW dipping, positioned in the north part of Vulcano; *C2*, 13-16 km deep, strikes in the NE-SW direction south of Salina; *C3*, with NNW-SSE trend, 8-11 km deep, almost vertical, is located south of Vulcano. Two minor clusters positioned 10 km East of Lipari and just below Salina island are also observable **(fig. 7.4)**.

The cross-sections also show how seismicity of the western sector is distributed in a 7-18 km interval of depth, whereas earthquakes of Lipari-Vulcano eastern area are no deeper than 12-13 km.

Besides the locations, we computed the fault plane solutions (FPSs) for the major and best recorded earthquakes by using the first arrival P-wave polarities and the FPFIT code by Reasenberg and Oppenheimer (1985). We were able to determine 22 FPSs, considering at least 13 first motion P-polarities (typically, events with a magnitude Md ≥ 2.7) **(Table 7.1)**. They are shown in **figure 7.5** together with directions of the P-axes. There is a prevalence of subhorizontal to moderately dipping P-axes, predominantly NNW–SSE directed in the central part and E-W and WNW–ESE directed in the eastern sector.

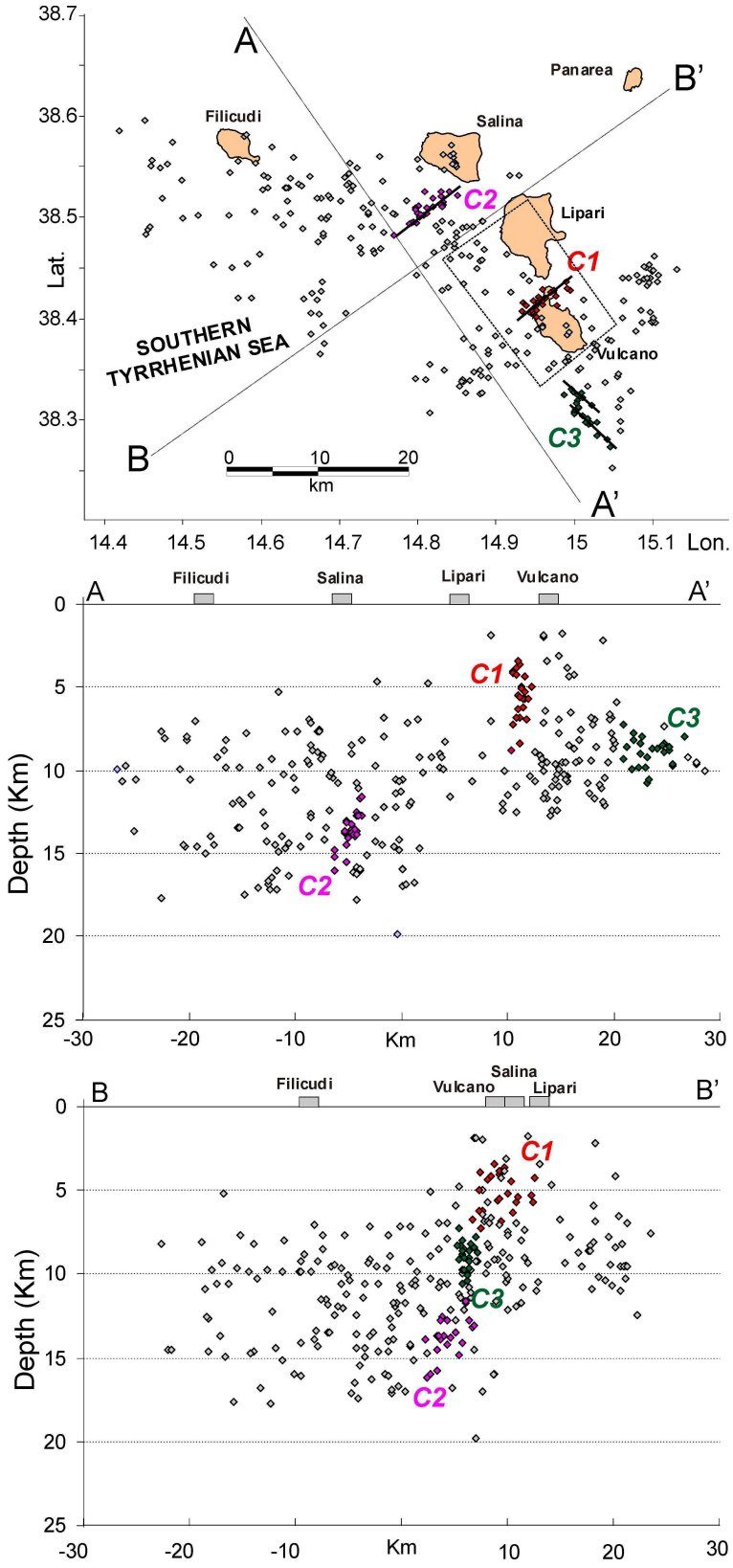

Fig. 7.4 Map and vertical cross sections of the seismicity relocated using HypoDD. Lines indicate the main structural features described in the text. Directions of the vertical cross sections are indicated in the maps by A-A' and B-B' lines.

Table 7.1
Main hypocentral and focal parameters of earthquakes reported in **fig. 7.5**

N	DATE	O.T.	LAT	LON	Z (km)	Md	Strike	Dip	Rake
1	09-mag-06	07:31:10.48	38,527	14,633	13,49	3,4	315	90	-140
2	17-mag-07	05:48:12.59	38,517	14,678	16,5	3,6	15	65	-20
3	21-ago-10	11:00:56.41	38,493	14,793	13,91	3,1	5	60	20
4	23-set-07	07:12:46.32	38,502	14,8	13,74	3,6	20	85	10
5	30-set-07	15:41:20.61	38,509	14,802	13,73	3	120	85	-180
6	14-lug-07	18:13:03.55	38,615	14,771	12,21	3,3	200	85	10
7	16-mag-04	20:44:28.60	38,51	14,834	12,75	2,8	120	80	160
8	05-set-07	21:24:13.56	38,492	14,843	12,17	3,3	65	20	180
9	03-ott-04	21:05:23.22	38,359	14,824	14,4	3,4	225	80	-70
10	17-apr-06	20:16:14.52	38,34	14,891	11,75	3,2	35	75	50
11	16-ago-10	12:54:47.03	38,347	14,881	11,72	4,5	195	70	-30
12	02-mag-08	01:26:04.76	38,441	14,935	9,11	2,9	125	85	160
13	08-lug-94	05:36:15.60	38,317	14,988	7,17	3,2	310	90	-130
14	07-lug-94	14:03:58.80	38,304	14,987	8,66	4	65	85	20
15	23-mag-09	14:56:32.69	38,304	15,001	10,53	2,7	305	85	-160
16	01-lug-09	17:58:54.24	38,294	15,019	8,82	3,4	45	75	30
17	27-lug-08	11:59:57.37	38,394	15,099	8,35	2,7	185	25	80
18	06-giu-07	21:24:44.96	38,36	15,02	12,15	2,7	50	40	100
19	01-ago-08	22:38:10.38	38,395	15,098	8,65	2,7	20	60	90
20	10-giu-02	19:14:00.54	38,435	15,078	10,26	2,9	30	75	70
21	05-apr-02	04:51:25.95	38,446	15,095	8,84	4,2	132	50	50
22	05-apr-02	04:52:21.70	38,451	15,096	11,12	4,6	20	50	120

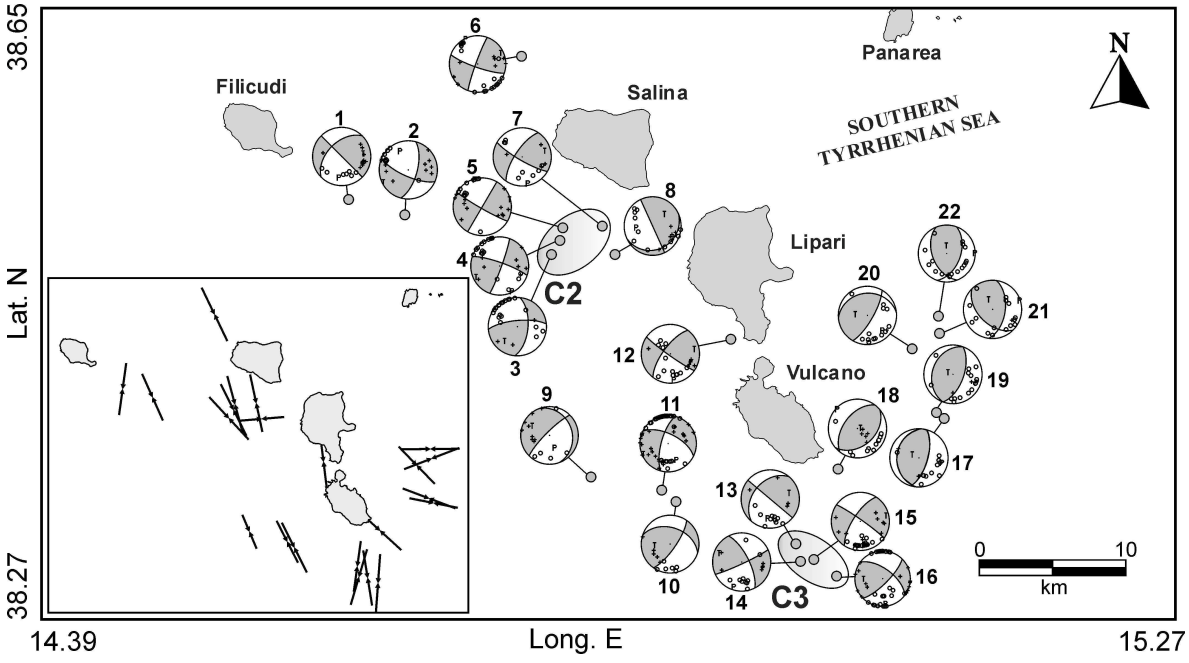

Fig. 7.5 Focal mechanisms of the major seismic events in the investigated area. The FPS numbers refer to **table 7.1**. Gray areas include the events belonging to *C2* and *C3* clusters. Directions of the P-axes are shown in the inset.

7.5 Discussion

In the following paragraph, we will discuss the relationships between the tectonic and volcanic setting which characterize the studied area and the relocated seismicity, in combination with fault plane solutions. In order to discuss the detailed features of hypocentral distribution, we distinguish the focal mechanism and other structural behaviors in two sub-areas:

7.5.1 The Filicudi-Salina area

In this zone the earthquakes show a general focal depth between 7 and 18 km and are rather sparse **(fig. 7.4)**. Focal mechanisms obtained for some events located in this area underline a strike-slip movement, with almost sub-horizontal P-axis on NNW-SSE direction and one nodal plane striking WNW-ESE **(fig. 7.5)**. The seismic pattern is in agreement with the Sisifo Fault System which characterizes the area **(fig. 7.1)**.

Looking in more detail, in the zone of Salina, which may be considered a transitional area between the western central and eastern sectors, we recognize the *C2* cluster **(fig. 7.4)**. These events, 11-16 km deep, show a geometry consistent with a roughly 8-10 km long, NE-SW oriented structure, also compatible with the orientation of one nodal plane of the FPSs computed for three events of the cluster **(fig. 7.5)**. The main releases in this sector have been recorded on March 2004 and September 2007 as seismic swarms **(fig. 7.6)**. Features in NE-SW direction were also revealed by structural observations on Salina island (De Rosa et al., 1989) and by marine geology data in the area between Salina and Lipari (Ventura, 1994 and references therein). Indeed, Salina is located at the intersection of the Lipari-Volcano axis with the arc and the three main active trends characterizing the Aeolian arc (NW-SE, N-S, NE-SW) are all present in this area (Barberi et al., 1994).

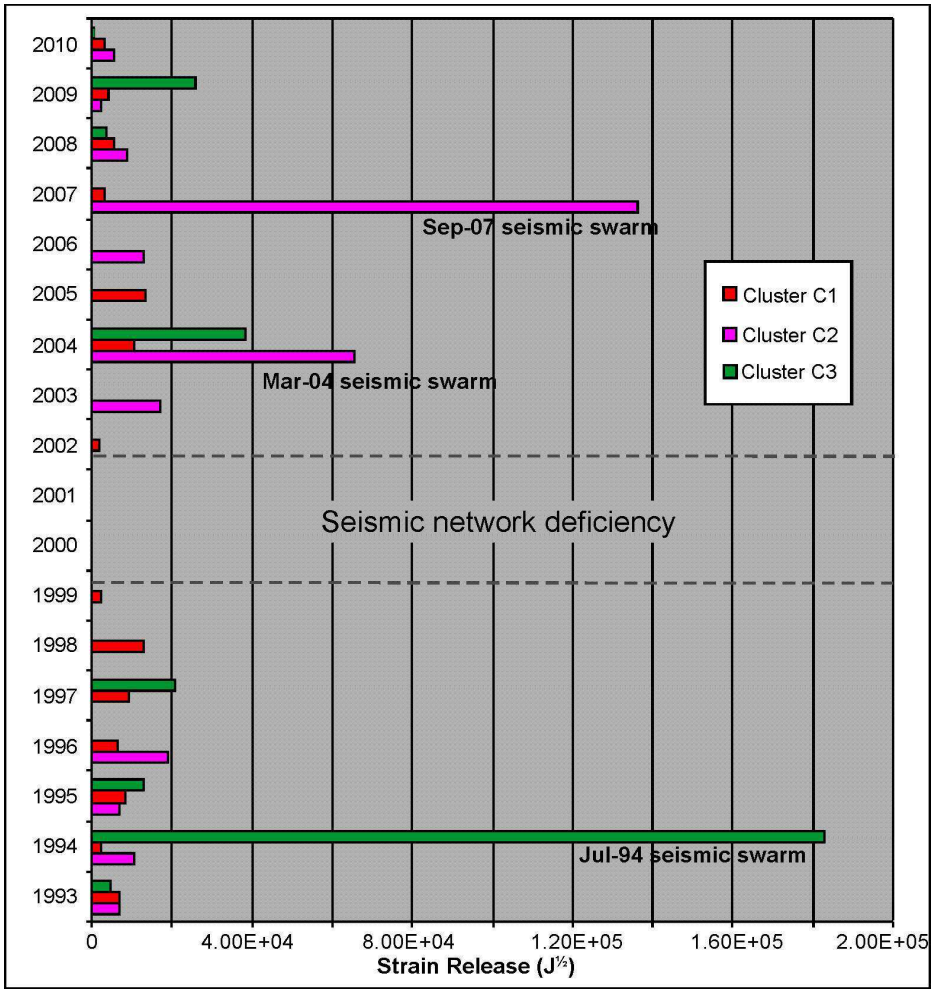

Fig. 7.6 Yearly seismic strain release for *C1*, *C2* and *C3* clusters calculated as √E using the relationship Log E = 9.9 + 1.9 M_d – 0.024 M_d^2 (Richter, 1958) where M_d is the duration magnitude.

7.5.2 The Lipari-Vulcano area

In this area, the ATLFS passing through Lipari and Vulcano plays a key role in controlling the kinematics and volcanism of this sector of Aeolian Archipelago. Earthquake distribution in this area shows that Lipari is almost aseismic while there is a higher concentration of seismic events around Vulcano island.

The relocated seismicity highlights some alignments and grouping of events. The *C3* cluster (**fig. 7.4**) positioned 5-7 km south Vulcano shows two parallel NW-SE trends, 8-11 km deep. Focal mechanisms are characterized by right-

lateral strike-slip with a NW-SE oriented plane **(fig. 7.5)**, suggesting that this seismogenetic area may represent an ATLFS evidence.

The ATLFS is the main lithospheric structure of the Aeolian Archipelago (De Astis et al., 2003), NNW-SSE oriented structure affected by dextral and compressive deformation (e.g. Neri et al., 2005; Bonforte and Guglielmino, 2008).

Recent volcanism in this strain regime could be due, as suggested by Ventura (1994), to the presence of a local pull-apart basin, revealed by N–S to NE–SW faults. The northern sector of Vulcano island is in fact characterized by NE-SW and N–S trending normal structures which accommodate the horizontal movements of the main system (Mazzuoli et al., 1995; De Astis, 2003). Submarine surveys on the eastern flank of Vulcano have shown clear NE-SW morpho-structural lineaments, suggesting that the NE-SW trend is at present the most active system in the northern area of Vulcano and probably controls the volcanic activity (Gabbianelli et al., 1991).

Vulcano, at present is in quiescence state that is periodically interrupted by "crises" characterized by changes in the crater fumarolic activity sometimes preceeded by seismicity with negligible ground deformations (Chiodini et al., 1992; Gambino and Guglielmino 2008 Carapezza et al., 2011). These "crises" likely reflect an increasing degassing of a deep (> 3-3.5 Km) steady-state magma body by fracturing depressurization (Granieri et al., 2006).

NE-SW alignments have been evidenced in the shallow (0.4-1.0 km b.s.l) hydrothermal seismicity at La Fossa (Alparone et al., 2010; Gambino et al., 2009).

In this structural framework, we recognize the events of the cluster *C1*. These events reveal an almost vertical, NE-SW oriented, 3-8 km deep seismogenetic structure passing below Vulcanello which is the very northern part of Vulcano island **(fig. 7.4)**.

The occurrence of shear seismicity in North Vulcano area is fairly low (few events/year with $1.0<M<2.6$), so that it is difficult to obtain reliable focal mechanisms, and is uniformly distributed along the considered period **(fig. 7.6)**.

This kind of seismicity seems to have preceded the ascent of hot fluids to the surface (Chiodini et al., 1992; Montalto, 1996; Aubert and Alparone, 2000; Gambino et al., 2007).

In order to consider the possible relationships with the Vulcano magmatic system, we take into consideration the model proposed by Peccerillo et al., (2006), which integrates petrological, geophysical, and fluid-inclusion models for the internal structure of the volcano, concluding that the present structure of the magma storage system in the crust consists of two major deep accumulation zones located at 17–21 km (at the Moho) and 8–13 km depth, plus a shallow minor one at 3–5 km (1-3 km under La Fossa) **(fig. 7.7)**.

At Vulcano, the magmas formed by evolution processes within the deep chamber are less dense and can ascend to a shallower level and this process may be triggered by fracture opening induced by regional tectonic events (Peccerillo et al., 2006).

Figure 7.7 shows how the 1993-2010 seismicity under Vulcano (red dots) develops in a crust portion comprised between the intermediate and the shallow accumulation zones indicated by Peccerillo et al. (2006). These earthquakes suggest the existence of a seismogenic structure (passing just below Vulcanello), which could be interpreted as a discontinuity linking the two magma accumulation zones, thereby rapresenting a possible preferential pathway along which magma may intrude as well as being responsible for fluid migration toward the surface.

Finally, we wish to point out that in the Vulcano-Lipari offshore region there is a seismogenic volume at about 10 km east of Lipari **(fig. 7.4)**. These earthquakes are grouped in 6-11 km depth range without identifying a preferential alignment and fault plane solutions show prevailing thrust faults along N-S to NE-SW striking planes, indicating a compressional regime with E-W to ESE-WNW directed P-axis **(fig. 7.5)**. This is a visible difference with respect to the N-S compression that characterize the Aeolian Archipelago (Hollestein et al., 2003; Neri et al., 2005).

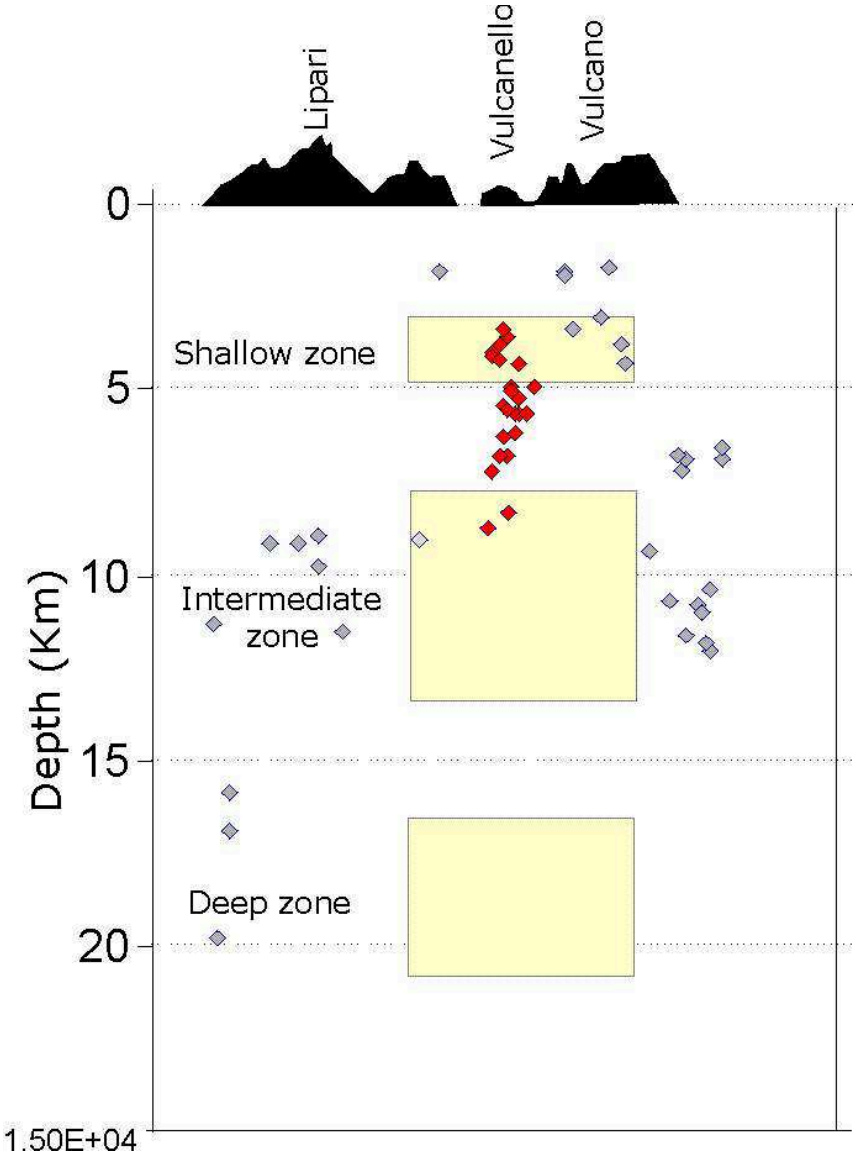

Fig. 7.7 The NNW-SSE section of Lipari-Vulcano area reporting the seismicity falling within the box area of **figure 4**, inside the model proposed by Peccerillo et al. (2006).

7.6 Conclusions

High precision locations in the Aeolian Archipelago area were performed in the present work, by applying the concept of the velocity model-hypocentres joint inversion and earthquakes relocations, along with an analysis of the fault plane solutions. In order to improve our knowledge on the active seismo-tectonics of the Aeolian Archipelago we exploited a dataset encompassing 351 events recorded during a 17 year period.

Overall, our results show that part of the seismicity is clustered along active seismogenic structures that concur with the main regional tectonic trends whose activity furnishes new elements to better understand the dynamics of the area:

- The *C1* cluster (24 events) in the northern part of Vulcano, NE-SW oriented, marks the presence of a structure that seems to play a key role in magma uprising at Vulcano.
- The *C2* cluster (25 events) is positioned just south of Salina, a gathering area of the western, central and eastern structural systems of the Aeolian Archipelago. The seismogenic structure shows a NE-SW direction that suggests how the eastern system (Panarea-Stromboli) is currently the most active in this area.
- The *C3* cluster (24 events), located south-west of Vulcano island, is evidence of the ATLFS, the main active structure in the Aeolian Archipelago. However, *C3* seems to be the only alignment with this trend, in the investigated area and this fact may be a confirmation of the complexity of this structure that cannot be imaged as a simple strike–slip fault (Argnani et al., 2007).

Finally, **figure 7.5** shows P-axis orientation obtained by focal mechanism analyses. While in the central and western part of the investigated area the stress direction is in agreement with the regional one (N-S to NNW-SSE), the earthquakes located 10 km east of Lipari and Vulcano show different mechanisms with E-W oriented P-axis. Those events may be associated to the transitional zone going from the N-S compressive domain which dominates the

Aeolian Islands, to the NW-SE extensional domain characterizing the south-eastern Tyrrhenian, north-eastern Sicily and southern Calabria area (e.g. Scarfì et al., 2009).

Chapter 8

Conclusions

In this thesis have been reported the results of a study on seismo-volcanic events, that characterizes the area of La Fossa of Vulcano (Aeolian Islands), and on the earthquakes recorded in Aeolian island. The seismo-volcanic events, with very local character consequently to the low energy associated, show morphological and spectral characteristics different from those of other events typically tectonic recorded on the same island. The two categories of events have been analyzed at first separately and only in the final phase a relationship between them and the volcanic activity at Vulcano was searched. In this chapter the main results are summarised, along with suggestions for future extensions to this work.

The investigations of seismo-volcanic signals in hydrothermal systems can give useful information to follow the evolution of hydrothermal fluids (e.g. Kumagai and Nakano, 2005). Also the comparison between seismic signal and

geochemical data, shows that combined geophysical and geochemical studies are a powerful tool to investigate the magma dynamics inside the volcano edifice as well as in its deep roots. The comparison of a large number of geophysical and geochemical time series will be carried out in order to seek prospective repetitive pre-eruptive behaviours.

Reconstructions of the eruptive histories of many volcanoes have shown that inactive periods of hundreds of years between eruptions are not uncommon. This is particularly true for highly explosive volcanoes (Scarpa and Gasparini 1996). Therefore, Vulcano, whose last eruption occurred in 1888-1890, is to be considered potentially active and dangerous for the local population. Moreover, the volcanic risk in this area increases greatly in summer, when the number of inhabitants swells from a few hundreds to several thousands.

During January 2004 - December 2009, six seismic sequences occurred at La Fossa, Vulcano, at the same time as anomalous increases of fumarolic CO_2 flux and temperature, as well as variations of other geochemical parameters were observed (Diliberto et al. 2007). Such geochemical and geothermal anomalies are interpreted as an increase of the deep magmatic component constituting a portion of the hydrothermal fluids (Granieri et al. 2006). The six anomalies, the corresponding seismic sequences and the short time intervals separating them, suggest the importance of the analysed period in the recent history of Vulcano.

In light of this, we made a detailed investigation into the seismo-volcanic events recorded during 2004-2009. On the basis of the spectral content and waveforms, these events were grouped into four classes:

- **MC** Monochromatic Events
- **HF** High Frequency Events
- **LP** Long Period Events
- **TR** Tornillos Events

For these classes, in agreement with most of the available literature, two different source mechanisms have been supposed:

I. a process of fracturing of material little competent hydrothermal altered (Chouet, 1988; Neuberg et al., 2000; Stephens et al., 2000), for high frequency events (HF) (Montalto, 1994);

II. a process of resonance conduits or "cracks" filled with magma fluid (Chouet, 1988 and Neuberg et al., 2000), for the monochromatic events, long period and tornillos events (MC, LP, TR) (Blot, 1971 ; Latter, 1971; Del Pezzo et al., 1981; Godano et al., 1991; Bottari et al., 1992; Montalto, 1994).

The resonance of "cracks" or conduits filled with hydrothermal fluids is a very variable and complex mechanism because it is function of many variables, including (Chouet et al., 1994; 1996):

- the geometry of the "crack" or conduits;
- the physical properties of the conduits and the fluid contained in it (temperature, density, stiffness of the duct);
- pressure fluctuations within the "crack" in both time and space;
- the impedance contrast fluid-solid;
- the proportion of volatiles present in the fluids inside conduits and their possible variation;

In view of these source processes, the time-relationship between geochemical and geothermal anomalies and seismic sequences can be inferred. The increasing magmatic component of the hydrothermal fluids during the anomalies can cause both the increase of the pore pressure within the volcanic system and the increase of the fluid flux rising up. Then, increased pore pressure gives rise to increasing fracturing processes, while increased fluid flux favours the resonance and vibration processes in cracks and conduits. This model justifies the occurrence of the seismic sequences at the same time as the geochemical and geothermal anomalies.

The time evolution which interest, in varying degrees, the various classes can be associated with a gradual change of physical properties of the source (Baptie et al., 2002; Kumagai et al., 2002). What might change is both the geometry of the conduits, that the physical and chemical properties of the fluids contained in

them (temperature, pressure, density, ratio of liquid phase and vapour phase). More precisely, changes in source properties affect the waveform of seismic events, instead changes in trigger mechanism may be reflected in variations in amplitude of the recorded events (Stephens et al., 2000).

In the light of this the possible time variation of the features of the seismic events was investigated, and only HB events (subclass of LP events) exhibited marked changes. In particular, they showed gradual shift toward higher frequencies and lower quality factors. Time variations of the spectral features of seismo-volcanic events have been observed in several volcanoes around the world, such as Mt. Etna (Patanè et al. 2008; Cannata et al. 2009), Galeras (Torres et al. 1996), Kusatsu-Shirane (Kumagai and Nakano 2005), Mt. Spurr (De Angelis and McNutt 2005) and Tungurahua (Molina et al. 2004).

In particular, in the case of HB events at Vulcano, on the basis of the shallowness of the source, the fluid can be reasonably considered hydrothermal. Therefore, making the assumption that the attenuation due to intrinsic losses is negligible, the frequency increase and quality factor decrease may be due to the increase of the gas volume fraction in the fluid likely linked to a process of heating and drying of the hydrothermal system (Nakano and Kumagai 2005; De Angelis and McNutt 2005). Whatever the case, it is worth noting that the observed waveform changes indicate important variations in the characteristics of the fluids, and hence suggest an unsteady and dynamic hydrothermal system. This is also supported by the differences observed between the anomalies in terms of occurrence rate and type of seismic events recorded.

Having associated to events belonging to different classes the same source mechanism, can be justified by the possibility that a source could have different behaviour. In the resonance of conduits, for example, could change the trigger mechanism, or two or more resonators may or not may operate simultaneously, thus generating events belonging to different classes but however having common characteristics, because they are generated from the same type of source (Morrissey et al., 1997).

Seismic activity, ground deformation and soil and fumarole temperatures acquired during 2004-2009 at Vulcano were analysed to investigate "anomalous" periods characterised by increases of soil and fumarole temperatures, and increase of seismo-volcanic events number. The following points summarise the main conclusions:

- The increasing fluid circulation rising from depth during the six anomalous periods is the common cause of increases in both temperatures and seismo-volcanic event number.
- The different increasing trends observed in the measured temperature and geophysical series during the anomalies can be due to either time changes in the medium permeability or a changing speed of gas release from a deep magma body.
- On the basis of the variations of the time distribution of the different kinds of seismo-volcanic events and the observed changes in temperature and fumarolic gases composition, the hydrothermal system at Vulcano can be considered unsteady and dynamic.

In conclusion, the study of the seismo-volcanic signals is of particular importance for diagnosing the state of fluids within the resonator systems and their time variations, which then can prove very helpful for monitoring purposes.

After careful analysis of the seismo-volcanic events of the Aeolian Islands area, the attention was paid to the tectonic events, in order to find possible relationships with the volcanic activity in the area. The aim of this part of the thesis was to identify spatial clusters of earthquakes, locate active seismogenic zone and their relationships with the volcanic activity in the Aeolian Islands.

High precision locations were performed in the present thesis, by applying the concept of the velocity model-hypocentres joint inversion and earthquake relocations, along with an analysis of the fault plane solutions. In order to improve our knowledge on the active seismo-tectonics areas we exploited a dataset encompassing 351 events recorded during a 17 year period (1993-2010). Overall, our results show that part of the seismicity is clustered along active

seismogenic structures that concur with the main regional tectonic trends whose activity furnishes new elements to better understand the dynamics of the area.

A cluster of 24 events in the northern part of Vulcano, NE-SW oriented, marks the presence of a structure that seems to play a key role in magma uprising at Vulcano. These earthquakes suggest the existence of a seismogenic structure (passing just below Vulcanello), which could be interpreted as a discontinuity linking the two magma accumulation zones, thereby representing a possible preferential pathway along which magma may intrude as well as being responsible for fluid migration toward the surface.

The results presented in this thesis suggest that the comparison of seismic, ground deformation and temperature data can be useful for better understanding the dynamics of a complex volcano-hydrothermal system, including a better definition of the origin of a volcano unrest, and hence for improving the estimation of the level of the local volcanic hazard.

Acknowledgments

Deepest gratitude is due to Prof. Stefano Gresta, without his help, advices, this thesis would not have been possible. I feel lucky and proud to have had the chance to learn seismology from him. Special thanks to my Tutors of INGV, Dr. Salvo Alparone and Dr. Salvo Gambino, for their useful comments and suggestions which helped me to significantly improve the thesis. I am also very grateful to Dr. Andrea Cannata, his deep humanity and great scientific knowledge make him the best researcher I have ever known. I wish him to get what he really deserves. I also acknowledge the technical staff of INGV, Section of Catania, for the help in installation and maintenance of the seismic networks, and the U.O. Fumarole Vulcano of the INGV-Section of Palermo for making available geochemical data. I'm grateful to Dr. Marco Maugeri for his constructive criticism. I am very grateful to my family, mother and father, and I'll never stop to thank my sister Ausilia, my mere expression of thanks likewise does not suffice. She is a great "fighter", a wonderful example of dignity and strength.

References

- Aiuppa, A., Cannata, A., Cannavò, F., Di Grazia, G., Ferrari, F., Giudice, G., Gurrieri, S., Liuzzo, M., Mattia, M., Montalto, P., Patanè, D., and Puglisi, G. (2010). Patterns in the recent 2007–2008 activity of Mount Etna volcano investigated by integrated geophysical and geochemical observations, Geochem. Geophys. Geosyst. 11, Q09008, doi:10.1029/2010GC003168.
- Alessandrini, B., Cattaneo, M., Demartin, M., Gasperini, M., Lanza, V., (1994). A simple P-wave polarization analysis: its application to earthquake location. Ann. Geophys. 5, 883-897.
- Almendros, J., Chouet, B., Dawson, P., Huber, C., (2002). Mapping the sources of the seismic wave field at Kilauea volcano, Hawaii, using data recorded on multiple seismic antennas. Bull. Seismol. Soc. Am. 92, 2333-2351.
- Alparone, S., Cannata, A., Gambino, S., Gresta, S., Milluzzo, V., Montalto, P., (2010). Time-space variation of the volcano-seismic events at La Fossa (Vulcano, Aeolian Islands, Italy): new insights into seismic sources in a hydrothermal system. Bull. Volcanol., 72, 803-816, doi:10.1007/s00445-010-0367-6.
- Alparone, S., Gambino, S., (2003). High precision locations of multiplets on south-eastern flank of Mt. Etna (Italy): reconstruction of fault plan geometry. Phys. Earth Plan. Int. 135, 281-289.
- Aoyama H., Takeo M. (2001) Wave properties and focal mechanisms of N-type earthquakes at Asama volcano. J Volcanol Geotherm Res 105:163-182
- Arcila, M., (1996). Geophysical monitoring of the Puracé volcano, Colombia. Ann. Geofis. 39, 265-272.
- Argnani, A., Serpelloni, E., Bonazzi, C., (2007). Pattern of deformation around the central Aeolian islands: evidence from multichannel seismic and GPS data. Terra Nova 19, 317-323.

- Aubert, M., Alparone, S., (2000). Hydrothermal convective flux variation related to a seismo-tectonic crisis in the Fossa of Vulcano (Italy). Comptes Rendus de l'Academie des Sciences Series IIA Earth and Planetary Science, 330, 603–610.
- Aubert, M., Alparone, S., (2000). Variation d'origine sismique du flux de chaleur convectif dans La Fossa de Vulcano (Italie). Earth Planet. Sci. 330, 603–610.
- Aubert, M., Diliberto, S., Finizola, A., Chebli, Y., (2008). Double origin of hydrothermal convective flux variations in the Fossa of Vulcano (Italy). Bull. Volcanol. 70, 743-751.
- Barani S., Ferretti G., Massa M., Spallarossa D. (2007). The waveform similarity approach to identify dependent events in instrumental seismic catalogues. Geophys J Int 168:100-108
- Barberi F., Ferrara G., Keller J., Innocenti F., Villari L. (1974). Evolution of the Aeolian arc volcanism. Earth Planet Sci Lett 21:269-276
- Barberi F., Gandino, A., Gioncada, A., La Torre, P., Sbrana, A., Zenucchini, C., (1994). The deep structure of the Eolian arc (Filicudi-Panarea-Vulcano sector) in light of gravity, magnetic and volcanological data: J. Volcanol. Geotherm. Res. 61, 189–206.
- Barberi F., Navarro JM, Rosi M., Santacroce R., Sbrana A. (1988). Explosive interaction of magma with ground water: insights from xenoliths and geothermal drillings. Rend Soc Ital Mineral Petr 43:901-926
- Barberi F., Neri G., Valenza M., Villari L. (1991). 1987–1990 unrest at Vulcano. Acta Vulcanol 1:95-106
- Battaglia J., Got L., Okubo P. (2003). Location of long-period events below Kilauea Volcano using seismic amplitudes and accurate relative relocation. J Geophys Res 108:2553. doi:10.1029/2003JB002517
- Beccaluva, L., Gabbianelli, G., Lucchini, F., Rossi, P.L., Savelli, C., (1985). Petrology and K/Ar ages of volcanic dredged from the Eolian seamounts: Implications for geodynamic evolution of the Southern Tyhrrenian basin. Earth Planet. Sci. Lett., 74, 187–208.
- Billi, A., Barberi, G., Faccenna, C., Neri, G., Pepe, F., Sulli, A., (2006). Tectonics and seismicity of the Tindari Fault System, southern Italy: crustal

deformations at the transition between ongoing contractional and extensional domains located above the edge of a subducting slab. Tectonics 25, doi:10.1029/2004TC001763.

- Blanco-Montenegro, I., De Ritis, R., Chiappini, M., (2006). Imaging and modelling the subsurface structure of volcanic calderas with high-resolution aeromagnetic data at Vulcano (Aeolian Islands, Italy). Bull. Volcanol. 69, 643-659.
- Blot C (1971) Etude Sismologique de Vulcano. Cahiers Orstom Ser Geophys 11:32 pp
- Bonaccorso, A., Falzone, G., and Gambino, S. (1999). An Investigation into Shallow Borehole Tiltmeters, Geophys. Res. Lett. 26, 1637-1640.
- Bonfanti, P., Diliberto, I.S., and Madonia, P. (2004). Surface temperature surveys for surveillance of volcanic activity, 32nd IGC Florence 2004, Session "T11.06 - Geochemical surveillance of volcanic and seismic active areas".
- Bonforte A., Gambino, S., Neri, M., (2009). Intrusion of eccentric dikes: The case of the 2001 eruption and its role in the dynamics of Mt. Etna volcano. Tectonophysics, 471, 78-86.
- Bonforte A., Guglielmino F. (2008). Transpressive strain on the Lipari–Vulcano volcanic complex and dynamics of the "La Fossa" cone (Aeolian Islands, Sicily) revealed by GPS surveys on a dense network. Tectonophysics. 457, 64-70 doi:10.1016/j.tecto.2008.05.016
- Boyce AJ, Fulignati P, Sbrana A, Fallick AE (2007). Fluids in early stage hydrothermal alteration of high-sulfidation epithermal systems: A view from the Vulcano active hydrothermal system (Aeolian Islands, Italy). J Volcanol Geotherm Res 166:76-90
- Bukumirovic, T., Italiano, F., Nuccio, P.M., (1997). The evolution of a dynamic geological system: the support of a GIS for geochemical measurements at the fumarole field of Vulcano, Italy. J. Volcanol. Geotherm. Res. 79, 253-263.
- Caliro, S., Chiodini, G., Galluzzo, D., Granieri, D., La Rocca, M., Saccorotti, G., and Ventura, G. (2005). Recent activity of Nisyros volcano

(Greece) inferred from structural, geochemical and seismological data, Bull. Volcanol. 67, 358–369.

- Cannata, A., Diliberto, S., Alparone, S., Gambino, S., Gresta, S., Liotta, M., Madonia, P., Milluzzo, V., Aliotta, M., Montalto, P. (2011) Multiparametric approach in investigating hydrothermal systems: the case of study of Vulcano (Aeolian Islands, Italy). Pure and Applied Geophysics, doi:10.1007/s00024-011-0297-z
- Cannata A., Hellweg M., Di Grazia G., Ford S., Alparone S., Gresta S., Montalto P., Patanè D. (2009). Long Period and Very Long Period events at Mt. Etna volcano: characteristics, variability and causality, and implications for their sources. J Volcanol Geotherm Res 187:227-249. doi:10.1016/j.jvolgeores.2009.09.007
- Cannata A., Montalto P., Privitera E., Russo G., (2009). Characterization and location of infrasonic sources in active volcanoes: Mt. Etna, September-November (2007). J. Geophys. Res. 114, B08308, doi:10.1029/2008JB006007.
- Capasso, G., Favara, R., and Inguaggiato, S. (1997). Chemical features and isotopic composition of gaseous manifestations on Vulcano Island (Aeolian Islands, Italy): an interpretative model of fluid circulation, Geochim. Cosmochim. Acta 61, 3425–3440.
- Capasso, G., Favara, R., Francofonte, S., Inguaggiato, S. (1999). Chemical and isotopic variations in fumarolic discharge and thermal waters at Vulcano Island (Aeolian Islands, Italy) during 1996: evidence of resumed activity, J. Volcanol. Geotherm. Res. 88, 167–175.
- Caplan-Auerbach J, Petersen T (2005). Repeating coupled earthquakes at Shishaldin Volcano, Alaska. J Volcanol Geotherm Res 145:151-172
- Carapezza, M., and Granieri, D. (2004). CO_2 soil flux at Vulcano (Italy): comparison between active and passive methods, Appl. Geochem. 19, 73-88.
- Carapezza, M., Nuccio, P.M., and Valenza, M. (1981). Genesis and evolution of the fumaroles of Vulcano (Aeolian Islands, Italy): a geochemical model, Bull. Volcanol. 44, 547-563.

- Carapezza, M.L., Barberi F., Ranaldi M., Ricci T., Tarchini L., Barrancos J. Fischer C., Perez N., Weber K., Di Piazza A., Gattuso A., (2011). Diffuse CO2 soil degassing and CO2 and H2S concentrations in air and related hazards at Vulcano Island (Aeolian arc, Italy), J. Volcanol. Geotherm. Res. (2011), doi:10.1016/j.jvolgeores.2011.06.010
- Carniel, R., Jolis, E.M., and Jones, J. (2010). A geophysical multi-parametric analysis of hydrothermal activity at Dallol, Ethiopia, J. Afr. Earth Sci., doi:10.1016/j.jafrearsci.2010.02.005.
- Castellano, M., Ferrucci, F., Gaudiosi, G., Godano, C., Milano, G., Pino, N.A., Vilardo, G., (1988). Struttura crostale delle aree vulcaniche attive dell'Italia meridionale da indagini di sismica attiva (DSS) e passiva: area vulcanica campana; Isole Eolie meridionali. Mem. Soc. Geol. It. 41, 1299-1305.
- Chiodini G, Cioni M, Marini L, Panichi C (1995). Origin of the fumarolic fluids of Vulcano Island, Italy, and implications for the volcanic surveillance. Bull Volcanol 57:99-110
- Chiodini, G., Cioni, R., Falsaperla, S., Montalto, A., Guidi, M., Marini, L., (1992). Geochemical and seismological investigations at Vulcano (Aeolian Islands) during 1978–1989. J. Geophys. Res. 97, 11025–11032.
- Chiodini, G., Cioni, R., Guidi, M., Marini, L., Raco, B., and Taddeucci, G. (1992). Gas geobarometry in boiling hydrothermal systems: a possible tool to evaluate the hazard of hydrothermal explosions, Acta Vulcanol 2, 99–107.
- Chiodini, G., Cioni, R., Marini, L., (1993). Reactions governing the chemistry of crater fumaroles from Vulcano Island, Italy, and implications for volcanic surveillance. Appl. Geochem. 8, 357-371.
- Chiodini, G., Cioni, R., Marini, L., Panichi, C., (1995). Origin of fumarolic fluids of Vulcano Island, Italy and implications for volcanic surveillance. Bull. Volcanol. 57, 99–110.
- Chouet, B., (1986). Dynamics of a fluid-driven crack in three dimensions by the finite difference method. J Geophys Res 91:13967-13992

- Chouet, B., (1988). Resonance of a fluid-driven crack: radiation properties and implications for the source of long-period events and harmonic tremor. J Geophys Res 93:4375-4400
- Chouet, B., (1996). Long-period volcano seismicity: Its source and use in eruption forecasting. Nature 380, 309-316.
- Chouet, B.A., Page, R.A., Stephens, C.D., Lahr, J.C., and Power, J.A. (1994), Precursory swarms of long-period events at Redoubt Volcano (1989–1990), Alaska: their origin and use as a forecasting tool, J. Volcanol. Geotherm. Res. 62, 95– 135.
- Clocchiatti R, Del Moro A, Gioncada A, Joron JL, Mosbah M, Pinarelli L, Sbrana A (1994) Assessment of a shallow magmatic system: The 1888– 90 eruption, Vulcano Island, Italy. Bull Volcanol 56:466–486
- D'Agostino, N., Selvaggi, G., 2004. Crustal motion along the Eurasia-Nubia

  plate boundary in the Calabrian Arc and Sicily and active extension in the Messina Straits from GPS measurements. J. Geophys. Res. 109, B11402, doi:10.1029/2004JB002998.
- D'Alessandro, A., D'Anna, G., Luzio, D., and Mangano, G. (2009), The INGV's new OBS/H: Analysis of the signals recorded at the Marsili submarine volcano, J. Volcanol. Geotherm. Res. 183, 17–29.
- De Angelis S., (2006). Analyses of unusual long-period earthquakes with extended coda recorded at Katmai National Park, Alaska, USA. Geophys. Res. Lett. 33, L07306, doi:10.1029/2005GL025581.
- De Angelis S., McNutt S.R. (2005). Degassing and hydrothermal activity at Mt. Spurr, Alaska during the summer of 2004 inferred from the complex frequencies of long-period events. Geophys Res Lett 32:L12312. doi:10.1029/2005GL022618
- De Astis, G., Dellino, P., La Volpe, L., Lucchi, F., and Tranne, C.A. (2006), Geological Map of the Island of Vulcano (Aeolian Islands), scale 1:10,000, printed by Litografia Artistica Cartografica, Firenze, Italy.
- De Astis, G., Ventura, G., Vilardo, G., (2003). Geodynamic significance of the Aeolian volcanism (Southern Tyrrhenian Sea, Italy) in light of

structural, seismological and geochemical data. Tectonics 22, 1040, doi:10.1029/2003TC001506.

- De Luca, G., Filippi, L., Patane, G., Scarpa, R., Vinciguerra, S., (1997). Three-dimensional velocity structure and seismicity of Mt. Etna Volcano, Italy. J. Volcanol. Geotherm. Res. 79, 123-138.
- De Rosa, R., Mazzuoli, R., Rossi, P.L., Santacroce, R., Ventura, G., (1989). Nuovi dati ed ipotesi per la ricostruzione della storia eruttiva dell'isola di Salina (Isole Eolie). Boll. GNV, 2, 791-809.
- Del Pezzo E, Martini M (1981). Seismic events under Vulcano-Aeolian Island, Italy. Bull Volcanol 44:521-525
- Dèzes, P., Ziegler, P.A., (2001). European Map of the Mohorovicic discontinuity. In: 2nd EUCOR-URGENT Workshop (Upper Rhine Graben Evolution and Neotectonics), Mt. St. Odile, France.
- Di Liberto, V., Nuccio, P.M., Paonita, A., (2002). Genesis of chlorine and sulphur in fumarolic emissions at Vulcano Island (Italy): assessment of pH and redox conditions in the hydrothermal system. J. Volcanol. Geotherm. Res. 116, 137-150.
- Diaz, J., Gallart, J., and Gaspà, O. (2007). Atypical seismic signals at the Galicia Margin, North Atlantic Ocean, related to the resonance of subsurface fluid-filled cracks, Tectonophysics 433, 1–13.
- Diliberto IS, Alparone S, Lotta M, Madonia P (2007). Relationship between surface temperatures and seismic activity at Vulcano (Eolian Islands). Geophys Res Abstr 9 08553
- Diliberto IS, Gurrieri S, Valenza M (2002). Reletionship between diffuse CO_2 emissions and volcanic activity on the island of Vulcano (Aeolian Islands, Italy) during the period 1984-1994. Bull Volcanol 64:219-228
- Falsaperla S., Neri G. (1986). Contributi sismologici alla sorveglianza vulcanica di Vulcano. Boll GNV:243-254
- Falsaperla S., Neri G., Velardita S., (1985). Struttura della crosta superiore dell'area delle isole Eolie. Rend. Osserv. Geofis. Reggino 29, 103-111 (in Italian).

- Ferrucci, F., Gaudiosi, G., Milano, G., Nercessian, A., Vilardo, G., Luongo, G., (1991). Seismological exploration of Vulcano (Aeolian Islands, southern Tyrrhenian sea): Case history. Acta Vulcanol. 1, 143-152.
- Gabbianelli, G., Romagnoli, C., Rossi, P.L., Calanchi, C., Lucchini, F., (1991). Submarine morphology and tectonics of Vulcano (Aeolian Islands, Southeastern Tyrrhenian Sea). Acta Volcan. 1, 135-141.
- Gambino, S., Milluzzo, V., Scaltrito, A., Scarfì, L. (2012) Relocation and focal mechanisms of earthquakes in the south-central sector of the Aeolian Archipelago: New structural and volcanological insights. Tectonophysics doi:10.1016/j.tecto.2011.12.024.
- Gambino S, Cammarata L, Rapisarda S (2009). High precision locations of long-period events at La Fossa Crater (Vulcano Island, Italy). Annals of Geophysics ()52:137-147
- Gambino S, Campisi O, Falzone G, Ferro A, Guglielmino F, Laudani G, Saraceno B, (2007). Tilt measurements at Vulcano Island. Annals of Geophysics 50:233-247
- Gambino S, Guglielmino F (2008). Ground deformation induced by geothermal processes: A model for La Fossa Crater (Vulcano Island, Italy) j Geophys Res 113: B07402. doi: 10.1029/2007JB005016
- Gambino S, Mostaccio A, Patanè D, Scarfì L, Ursino A, (2004). High-precision locations of the microseismicity preceding the 2002-2003 Mt. Etna eruption. Geophys. Res. Lett., 31, doi: L18604 10.1029/2004GL020499.
- Gasparini, C., Iannaccone, G., Scarpa, R., (1985). Fault plane solutions and seismicity of the Italian Peninsula. Tectonophysics 117, 59–78.
- Ghisetti F, Vezzani L (1982). Different styles of deformation in the Calabrian arc (southern Italy): implications for a seismotectonic zoning. Tectonophysics 85:149-165
- Gil-Cruz F, Chouet B, (1997). Long-period events, the most characteristic seismicity accompanying the emplacement and extrusion of a lava dome in Galeras Volcano, Colombia, in 1991. J Volcanol Geotherm Res 77:121-158
- Gillot, P.Y., (1987). Histoire volcanique des Iles Eoliennes: arc insulaire or complexe orogenique anulaire? Doc Trav. IGAL 11, 35–42.

- Giudicepietro, F., D'Auria, L., Martini, M., Caputo, T., Peluso, R., De Cesare, W., Orazi, M., Scarpato, G., (2009). Changes in the VLP seismic source during the 2007 Stromboli eruption. J. Volcanol. Geotherm. Res. 182, 162-171.
- Gomez, D.M., Torres, R.A., (1997). Unusual low-frequency volcanic seismic events with slowly decaying coda waves observed at Galeras and other volcanoes. J. Volcanol. Geotherm. Res. 77, 173-193.
- Gomez, D.M., Torres, R.A., Seidl, D., Hellweg, M., Rademacher, H., (1999). Tornillo seismic events at Galeras volcano, Colombia: a summary and new information from broadband three-component measurements. Ann. Geofis. 42, 365-378.
- Got, J., Fréchet, J., Klein, F.W., (1994). Deep fault plane geometry inferred from multiplet relative relocation beneath the south flank of Kilauea. J. Geophys R., 99, 15375-15386.
- Gottsmann, J., Carniel, R., Coppo, N., Wooller, L., Hautmann, S., and Rymer, H. (2007). Oscillations in hydrothermal systems as a source of periodic unrest at caldera volcanoes: multiparameter insights from Nisyros, Greece, Geophys. Res. Lett. 34, doi:10.1029/2007gl029594.
- Granieri D, Carapezza ML, Chiodini G, Avino R, Caliro S, Ranaldi M, Ricci T, Tarchini L (2006). Correlated increase in CO_2 fumarolic content and diffuse emission from La Fossa crater (Vulcano, Italy): evidence of volcanic unrest or increasing gas release from a stationary deep magma body? Geophys Res Lett 33:L13316. doi:10.1029/2006GL026460
- Granieri, D., Carapezza, M.L., Chiodini, G., Avino, R., Caliro, S., Ranaldi, M., Ricci, T., and Tarchini, L. (2006). Correlated increase in CO_2 fumarolic content and diffuse emission from La Fossa crater (Vulcano, Italy): evidence of volcanic unrest or increasing gas release from a stationary deep magma body? Geophys. Res. Lett. 33, L13316. DOI 10.1029/2006GL026460.
- Green D, Neuberg J (2006). Waveform classification of volcanic low-frequency earthquake swarms and its implication at Soufrière Hills Volcano, Monserrat. J Volcanol Geotherm Res 153:51-63

- Hagerty M, Benites R (2003). Tornillos beneath Tongariro Volcano, New Zealand. J Volcanol Geotherm Res 125. doi:10.1016/S0377-0273(03)00094-5
- Harris, A.J.L., Carniel, R., and Jones, J. (2005). Identification of variable convectives at Erta‘ Ale Lava Lake, J. Volcanol. Geotherm. Res. 142, 207–223.
- Harris, A.J.L., Lodato, L., Dehn, J., and Spampinato, L. (2009). Thermal characterization of the Vulcano fumarole field, Bull. Volcanol. 71, 441-458.
- Harris, A.J.L., Maciejewski, A.J.H. (2000). Thermal surveys of the Vulcano Fossa fumarole field 1994-1999: evidence for fumarole migration and sealing. J Volcanol Geotherm Res 102:119-147
- Hellweg M (2000). Physical models for the source of Lascar’s harmonic tremor J Volcanol Geotherm Res 101:183-198
- Hellweg M (2003). The polarization of volcanic seismic signals: medium or source? J Volcanol Geotherm Res 128:159-176
- Hill, D.P., and Prejean, S. (2005). Magmatic unrest beneath Mammoth Mountain, California, J. Volcanol. Geotherm. Res. 146, 257-283.
- Hollenstein, Ch., Kahle, H.G., Geiger, A., Jenny, S., Goes, S., Giardini, D., (2003). New GPS constraints on the Africa–Eurasia plate boundary zone in southern Italy. Geophys. Res. Lett. 30, doi:10.1029/2003GL017554.
- Hori S, Fukao Y, Kumazawa M, Furumoto M, Yamamoto A (1989). A new method of spectral analysis and its application to the Earth’s free oscillations: The ‘Sompi’ method. J Geophys Res 94:7535-7553
- Husen, S., Kissling, E., Flueh, E. Asch, G., (1999). Accurate hypocenter determination in the seismogenic zone of the subducting Nazca plate in north Chile using a combined on-offshore network. Geophys. J. Int. 138, 687–701.
- Inguaggiato, S., Mazot, A., Diliberto, I.S., Rowet, D., Vita, F., Capasso, G., Bobrowshj, N., Inguaggiato, C., and Grassa, F. (2008). Preliminary estimate of CO_2 budget discharged from Vulcano island. IAVCEI General Assembly oral presentation 18-25 08 2008 Reykjavik.

- INGV-PA (2006a). Rapporto sul monitoraggio geochimico dei fluidi di Vulcano - Agosto 2006. http://193.206.213.9/intranet/gest_news/uploads/4712ComunicatoVulcano Ago2006.pdf.
- INGV-PA (2006b)- Rapporto mensile sul monitoraggio geochimico dell'Isola di Vulcano – Dicembre 2006. ttp://193.206.213.9/intranet/gest_news/uploads/1272comunicato_vulcano1-2007.pdf.
- Italiano F., Nuccio P.M. (1992). Fumarolic steam output directly measured in fumaroles: Vulcano (Aeolian islands, Italy) between 1983 and 1987. Bull Volcanol 54:623-630
- Italiano F., Pecoraino G., Nuccio P.M. (1998). Steam output from fumaroles of an active volcano: tectonic and magmatic-hydrothermal controls on the degassing system at Vulcano (Aeolian arc), J. Geophys. Res. 103, 29829-29842.
- Jeffreys, H., and Bullen, K.E. (1967). Seismological tables. British association, Gray-Milne Trust.
- Jousset, P., Neuberg, J., Sturton, S., (2003). Modelling the time-dependent frequency content of low-frequency volcanic earthquakes. J. Volcanol. Geotherm. Res. 128, 201–223.
- Julian, B.R., (1994). Volcanic tremor: nonlinear excitation by fluid flow. J. Geophys. Res. 99 (B6), 11859-11877.
- Jurkevics, A., (1988). Polarization analysis of three-component array data. Bull. Seismol. Soc. Am. 78, 1725-1743.
- Keller, J. (1980). The island of Vulcano, Rend. Soc. It. Miner. Petrol. 36, 489-534.
- Kissling, E., (1995). Velest User's Guide. Int. Report, Inst. Geophys., ETH Zurich, 1-26.
- Kissling, E., Ellsworth, W.L., Eberhart-Phillips, D., Kradolfer, U., (1994). Initial reference models in local earthquake tomography. J. Geophys. Res. 99, 19635–19646.
- Kumagai H, Chouet BA (2000). Acoustic properties of a crack containing magmatic or hydrothermal fluids. J Geophys Res 105:25493-25512

- Kumagai H, Chouet BA (2001). The dependence of acoustic properties of a crack on the resonance mode and geometry. Geophys Res Lett 28:3325-3328
- Kumagai H, Chouet BA, (1999). The complex frequencies of long-period seismic events as probes of fluid composition beneath volcanoes. Geophys. J. Int. 138, F7-F12.
- Kumagai H, Chouet BA, Dawson P, (2005). Source process of a long-period event at Kilauea volcano, Hawaii. Geophys. J. Int. 161, 243-254.
- Kumagai H, Chouet BA, Nakano M (2002). Temporal evolution of a hydrothermal system in Kusatsu-Shirane Volcano, Japan, inferred from the complex frequencies of long-period events. J Geophys Res 107:2236. doi:10.1029/2001JB000653
- Kumagai H, Nakano M (2005). Response of a hydrothermal system to magmatic heat inferred from temporal variations in the complex frequencies of long-period events at Kusatsu-Shirane Volcano, Japan. J Volcanol Geotherm Res 147:233-244
- Kumazawa M, Imanishi Y, Fukao Y, Furumoto M, Yamamoto A (1990). A theory of spectral analysis based on the characteristic property of a linear dynamic system. Geophys J Int 101:613-630
- Lahr JC (1989). HYPOELLIPSE/VERSION 2.0: A computer program for determining local earthquake hypocentral parameters, magnitude, and first motion pattern. U.S. Geol. Survey, Open-File Report 89/116, 81 pp.
- Lahr JC, Chouet BA, Stephens CD, Power JA, Page RA (1994). Earthquake classification, location, and error analysis in a volcanic environment: Implications for the magmatic system of the 1989-1990 eruptions at Redoubt Volcano, Alaska. J Volcanol Geotherm Res 62:137-151
- Laigle, M., (1998). Images sismiques de l'Etna à diverses èchelles: Nouveaux éléments sur son comportement et le cadre règional. PhD thesis, University of Paris 7, Paris, 288 pp.
- Lanzafame, G., Bousquet, J.C., (1997). The Maltese escarpment and its extension from Mt. Etna to the Aeolian Islands (Sicily): importance and evolution of a lithosphere discontinuity. Acta Vulcanol. 9, 113–120.

- Latter JH (1971). Near surface seismicity of Vulcano, Aeolian Islands, Sicily. Bull Volcanol 35:117-126
- Lepeltier, C. (1969). A simplified statistical treatment of geochemical data by graphical representation. Econ. Geol. 64, 538–550.
- Lesage P., and Surono (1995). Seismic precursors of the February 10, 1990 eruption of Kelut volcano, Java, J. Volcanol. Geotherm. Res. 65, 135-146.
- Lesage P., Glangeaud F., Mars J. (2002). Applications of autoregressive and time-frequency analysis to the study of volcanic tremor and LP events. J Volcanol Geotherm Res 114:391-417
- Lin CH, Konstantinou KI, Liang WT, Pu HC, Lin YM, You SH, Huang YP (2005). Preliminary analysis of volcanoseismic signals recorded at the Tatun Volcano Group, northern Taiwan. Geophys Res Lett 32:L10313. doi:10.1029/2005GL022861
- Lippitsch, R., White, R., Soosalu, H., (2005). Precise hypocenter relocation of microearthquakes in a high- temperature geothermal field: the Torfajökull central volcano, Iceland. Geophys. J. Int. 160, 371-388.
- Lokmer, I., Saccorotti, G., Di Lieto, B., Bean, C. J., (2008). Temporal evolution of long-period seismicity at Etna Volcano, Italy, and its relationships with the 2004 – 2005 eruption. Earth Planet. Sci. Lett. 266, 205–220.
- Malinverno, A., Ryan, W.B.F., (1986). Extension in the Tyrrhenian Sea and shortening in the Apennines as result of arc migration driven by slab sinking in the lithosphere. Tectonics 5, 227–245.
- Mattia, M., Palano, M., Bruno, V., Cannavò, F., Bonaccorso, A., and Gresta, S. (2008). Tectonic features of the Lipari-Vulcano complex (Aeolian archipelago, Italy) from ten years (1996-2006) of GPS data, Terra Nova 20, 370-377.
- Mazzuoli, R., Tortorici, L., Ventura, G., (1995). Oblique rifting in Salina, Lipari and Vulcano islands (Aeolian Islands, Southern Tyrrhenian Sea, Italy). Terra Nova 7, 444–452.
- McNutt, S.R., (2005). Volcanic seismology. Annu. Rev. Earth Planet. Sci. 32, 461–491.

- Mercalli, G., and Silvestri, O. (1890), Le eruzioni dell'Isola di Vulcano incominciate il 3 agosto 1888 e terminate il 22 marzo 1890, relazione scientifica, Ann. Ufficio Centrale Metereol. Geodin. Ital. 10, 213 pp *(in Italian)*
- Messina A., Langer H. (2011). Pattern recognition of volcanic tremor data on Mt. Etna (Italy) with KKAnalysis — A software program for unsupervised classification. Computers & Geosciences 37, 953–961.
- Michelini A., Lomax A. (2004). The effect of velocity structure errors on double-difference earthquake locations, Geophys. Res. Lett. 31, L09602, doi:10.1029/2004GL019682.
- Miller, S.A., Collettini, C., Chiaraluce, L., Cocco, M., Barchi, M., Boris, J., and Kraus, P. (2004). Aftershock driven by a high-pressure CO_2 source at depth, Nature 427, 724–727.
- Milluzzo, V., Cannata, A., Alparone, S., Gambino, S., Hellweg, M., Montalto, P., Cammarata, L., Diliberto, I.S., Gresta, S., Liotta, M., and Paonita (2010). A. Tornillos at Vulcano: clues to the dynamics of the hydrothermal system. J. Volcanol. Geotherm. Res., doi: 10.1016/j.jvolgeores.2010.09.022.
- Molina I, Kumagai H, Garcia-Aristizabal A, Nakano M, Mothes P (2008). Source process of very-long-period events accompanying lomg-period signals at Cotopaxi Volcano, Ecuador. J Volcanol Geotherm Res 176:119-133
- Molina I, Kumagai H, Yepes H (2004). Resonances of a volcanic conduit triggered by repetitive injections of an ash-laden gas. Geophys Res Lett 31:L03603. doi:10.1029/2003GL018934
- Montalto A. (1994a). Seismic signals in geothermal areas of active volcanism: a case study from “La Fossa”, Vulcano (Italy). Bull Volcanol 56:220-227
- Montalto A. (1994b). Seismic events at Vulcano (Italy) during 1988-1992. J Volcanol Geotherm Res 60:193-206
- Montalto A. (1996). Signs of potential renewal of eruptive activity at La Fossa (Vulcano, Aeolian Islands). Bull. Volcanol. 57, 483-492.

- Moran, S.C., Zimbelman, D.R., and Malone, S.D. (2000). A model for the magmatic-hydrothermal system at Mount Rainier, Washington, from seismic and geochemical observations. Bull. Volcanol. 61, 425-436.
- Morrissey, M.M., and Chouet, B.A. (1997). A numerical investigation of choked flow dynamics and its application to the triggering mechanism of long-period events at Redoubt Volcano, Alaska, J. Geophys. Res. 102, 7965–7983.
- Nakano M, Kumagai H (2005). Response of a hydrothermal system to magmatic heat inferred from temporal variations in the complex frequencies of long-period events at Kusatsu–Shirane Volcano, Japan. J Volcanol Geotherm Res 147:233-244
- Neri, G., Barberi, G., Oliva, G,. Orecchio, B., (2005). Spatial variations of seismogenic stress orientations in Sicily, south Italy. Phys. Earth Planet. In. 148, 175–191.
- Neri, G., Barberi, G., Orecchio, B., Aloisi, M., (2002). Seismotomography of the crust in the transition zone between the southern Tyrrhenian and Sicilian tectonic domains, Geophys. Res. Lett., 29, 2135, doi:10.1029/2002GL015562.
- Neri, G., Barberi, G., Orecchio, B., Mostaccio, A., (2003). Seismic strain and seismogenic stress regimes in the crust of the southern Tyrrhenian region. Earth Planet. Sci. Lett. 213, 97–112.
- Neuberg, J., Pointer, T., (2000). Effects of volcano topography on seismic broad-band waveforms. Geophys. J. Int. 143, 239–248.
- Nishi, Y., Sherburn, S., Scott, B., and Sugihara, M. (1996). High-frequency earthquakes at White Island volcano, New Zealand: insights into the shallow structure of a volcano-hydrothermal system, J. Volcanol. Geotherm. Res. 772, 183-197.
- Nuccio, P.M., Paonita, A., (2001). Magmatic degassing of multicomponent vapors and assessment of magma depth: application to Vulcano Island (Italy). Earth Planet. Sci. Lett. 193, 467-481.
- Nuccio, P.M., Paonita, A., Sortino, F., (1999). Geochemical model of mixing between magmatic and hydrothermal gases: the case of Vulcano Island (Italy). Earth Planet. Sci. Lett. 167, 321-333.

- Ohminato T, Chouet BA, Dawson PB, Kedar S (1998). Waveform inversion of very-long-period impulsive signals associated with magmatic injection beneath Kilauea Volcano, Hawaii. J Geophys Res 103:23839-23862
- Okada, H., Nishimura, Y., Miyamachi, H., Mori, H., and Ishihara, K. (1990). Geophysical significance of the 1988–1989 explosive eruptions of Mt. Tokachi, Hokkaido, Japan, Bull. Volcanol. Soc. Japan 35, 175–203.
- Paonita, A., Favara, R., Nuccio, P.M., and Sortino, F. (2002). Genesis of fumarolic emissions as inferred by isotope mass balances: CO_2 and water at Vulcano Island, Italy, Geochim. Cosmochim. Acta 66, 759-772.
- Patanè, D., Di Grazia, G., Cannata, A., Montalto, P., Boschi, E., (2008). The shallow magma pathway geometry at Mt. Etna volcano. Geochem. Geophys. Geosyst. 9, doi:10.1029/2008GC002131.
- Peccerillo A., Frezzotti, M.L., De Astis, G., Ventura, G., (2006). Modeling the magma plumbing system of Vulcano (Aeolian Islands, Italy) by integrated fluid inclusion geo-barometry, petrology and geophysics. Geology 34, 17-20.
- Petersen, T. (2007). Swarms of repeating long-period earthquakes at Shishaldin Volcano, Alaska, 2001–2004, J. Volcanol. Geotherm. Res. 166, 177-192.
- Pondrelli, S., Piromallo, C., Serpelloni, E., (2004). Convergence vs. retreat in Southern Tyrrhenian Sea: insights from kinematics. Geophys. Res. Lett. 31, 6. doi:10.1029/2003GL019223.
- Pondrelli, S., Salimbeni, S., Ekström, G., Morelli, A., Gasperini, P., Vannucci, G., (2006). The Italian CMT dataset from 1977 to the present. Phys. Earth Planet. Inter. 159, 286–303.
- Rapisarda, S., Alparone, S., Cammarata, L., Cannata, A., Contrafatto, D., Ferrari, F., Manni, M., Marturano, M., Milluzzo, V., Platania, P., Scuderi, L., Torrisi, O., Zuccarello, L., Gambino, S. (2009) Installazione di 5 stazioni digitali a larga-banda sull'isola di vulcano: un contributo alla conoscenza della sismicità superficiale della fossa. Quaderni di Geofisica, 67.

- Reasenberg, P., Oppenheimer, D., (1985). FPFIT, FPPLOT, and FPPAGE: FORTRAN computer programs for calculating and displaying fault plane solutions. U.S. Geol. Surv. Open File Rep. 85/739, 109 pp.
- Revil, A., et al., (2008). Inner structure of La Fossa di Vulcano (Vulcano Island, southern Tyrrhenian Sea, Italy) revealed by high-resolution electric resistivity tomography coupled with self-potential, temperature, and CO2 diffuse degassing measurements, J. Geophys. Res. 113, B07207, doi:10.1029/2007JB005394.
- Richter, C. F., (1958). Elementary Seismology, W. H. Freeman, San Francisco, pp. 135-149.
- Richter, G., Wassermann, J., Zimmer, M., and Ohrnberger, M. (2004). Correlation of seismic activity and fumarole temperature at the Mt. Merapi volcano (Indonesia) in 2000, J. Volcanol. Geotherm. Res. 135, 331-342.
- Scarfì L., Langer H., Scaltrito A. (2005). Relocation of microearthquake swarms in the Peloritani mountains – implications on the interpretation of seismotectonic patterns in NE Sicily, Italy. Geophys. J. Int. 163, 225–237, doi: 10.1111/j.1365-246X.2005.02720.x.
- Scarfì L., Langer H., Scaltrito A. (2009). Seismicity, seismotectonics and crustal velocity structure of the Messina Strait (Italy). Phys. Earth Planet. In., 177, 65-78,doi:10.1016/j.pepi.2009.07.010
- Scarpa, R., and Gasparini, P. (1996). A review of volcano geophysics and volcano-monitoring methods. In Monitoring and mitigation of volcano hazards (eds. Scarpa, Tilling) (Springer, 1996), pp. 3-22.
- Seidl, D., Hellweg, M., (2003). Parameterization of multichromatic tornillo signals observed at Galeras Volcano (Colombia). J. Volcanol. Geotherm. Res. 125, 171-189.
- Shapiro, S.A., Patzig, R., Rothert, E., and Rindschwentner, J. (2003). Triggering of seismicity by porepressure perturbations: permeability related signature of the phenomenon, Pure Appl. Geophys. 160, 1051–1066.
- Shepherd, J.B., and Sigurdsson, H. (1978). The Soufriere crater lake as a calorimeter, Nature 271, 344–345.

- Shimozuru, D., Kagiyama, T., (1989). Some significant features of pre-eruption volcanic earthquakes. In: Latter, J. (Ed.), Volcanic Hazards. Springer, Berlin, pp. 504-512.
- Sturton, S., (2003). Modelling volcanic earthquakes and tremor. Unpublished PhD Thesis, University of Leeds.
- Sturton, S., Neuberg, J., (2006). The effects of conduit length and acoustic velocity on conduit resonance: Implications for low-frequency events. J. Volcanol. Geotherm. Res. 151, 319-339.
- Thurber, C. H., (1993). Local earthquake tomography: Velocity and VP/VS theory, in: Iyer, H.M., Hirahara, K., (Eds.), Seismic Tomography: Theory and Practice, Chapman and Hall, New York, pp. 563– 583.
- Tilling, R.I. (2008). The critical role of volcano monitoring in risk reduction, Adv. Geosci. 14, 3-11.
- Todesco, M., Rinaldi, A.P., and Bonafede, M. (2010). Modeling of unrest signals in heterogeneous hydrothermal systems, J. Geophys. Res. doi:10.1029/2010JB007474.
- Torres, R., Gomez, D., Narvaez, L., (1996). Unusual seismic signals associated with the activity at Galeras volcano, Colombia, from July 1992 to September 1994. Ann. Geofis. 39, 299-310.
- Triastuty, H., Iguchi, M., Tameguri, T., (2006). Source mechanism of monochromatic and low-frequency events at Papandayan volcano, West Java, Indonesia. Indonesian J. Physics 17, 63-72.
- Triastuty, H., Iguchi, M., Tameguri, T., (2009). Temporal change of characteristics of shallow volcano-tectonic earthquakes associated with increase in volcanic activity at Kuchinoerabujima volcano, Japan. J. Volcanol. Geotherm. Res. 187, 1-12.
- Varley, N., Arámbula-Mendoza, R., Reyes-Dávila, G., Stevenson, J., and Harwood, J. (2010). Long-period seismicity during magma movement at Volcán de Colima, Bull. Volcanol., doi: 10.1007/s00445-010-0390-7.
- Ventura, G., (1994). Tectonics, structural evolution and caldera formation on Vulcano Island (Aeolian Archipelago, Southern Tyrrhenian Sea). J. Volcanol. Geotherm. Res. 60, 207-224.

- Ventura, G., Vilardo, G., Milano, G., and Pino, N.A. (1999). Relationships among crustal structure, volcanism and strike-slip tectonics in the Lipari-Vulcano volcanic complex (Aeolian Islands, Southern Tyrrhenian Sea, Italy), Phys. Earth Planet. Inter. 116, 31-52.
- Waldhauser, F., (2001). HypoDD: A computer program to compute double-difference earthquake locations. U.S. Geol. Surv. Open-File Report 01-113.
- Waldhauser, F., Ellsworth, W.L., (2000). A double-difference earthquake location algorithm: Method and application to the northern Hayward fault. Bull. Seism. Soc. Am. 90, 1353-1368.
- Wassermann, J., (2009). Volcano Seismology. In: Bormann, P. (Ed.), New manual of seismological observatory practice. IASPEI.